MODELING INVESTIGATION OF NORTHERN HEMISPHERE EXTRATROPICAL STORM VARIABILITY AND CHANGES IN A WARMING CLIMATE

By

Soumik Basu

RECOMMENDED:

Dr. Uma Bhatt

Dr. Nicole Mölders

Dr. Igor Polyakov

Dr. Xiangdong Zhang
Advisory Committee Chair

Dr. Uma Bhatt
Chair, Department of Atmospheric Sciences

APPROVED:

Dr. Paul Layer
Dean, College of Natural Science and Mathematics

Dr. John Eichelberger
Dean of the Graduate School

Date

MODELING INVESTIGATION OF NORTHERN HEMISPHERE EXTRATROPICAL STORM VARIABILITY AND CHANGES IN A WARMING CLIMATE

A

DISSERTATION

Presented to the Faculty

of the University of Alaska Fairbanks

in Partial Fulfillment of the Requirements

for the Degree of

DOCTOR OF PHILOSOPHY

By

Soumik Basu, B.Sc., M.Sc.

Fairbanks, Alaska

May 2014

Abstract

Extratropical cyclones are fundamental elements for shaping weather patterns, causing fluctuations of temperatures, bringing rain or snow, and carrying winds to impact daily life. The intensity and number of North Hemisphere extratropical cyclones have demonstrated large interannual variability and long-term changes. To understand the variability and changes, we conducted a modeling investigation using the National Center for Atmospheric Research (NCAR)'s Community Atmosphere Model. Specifically, we examined the effects of two surface forcing factors, including sea surface temperature (SST) associated with El Niño and Arctic sea-ice cover, which represent a major source of natural variability and climate changes.

Our modeling investigation indicates that the tropical Pacific SST and Arctic sea ice have significant impacts on Northern Hemisphere mid-latitude and Arctic cyclone activities. The elevated tropical Pacific SST leads to more numerous intense storms over southwestern, southeastern, and northwestern North America, but fewer weaker storms over the northeast. The underlying physical mechanism is enhanced lower tropospheric baroclinicity, which is attributable to a southward shift and an intensification of the subtropical jet. The decreased Arctic sea-ice cover leads to an increased storm activity over the Arctic but a decrease in the mid-latitudes. A corresponding examination of surface climate shows anomalously higher surface air temperature and precipitation when low Arctic sea-ice cover occurs, due to an integrative contribution from an increase in surface sensible and latent heat fluxes and horizontal heat advection. In contrast, reduced

Arctic sea ice weakens storm activity and intensifies anticyclones over Eurasia, giving rise to decreased surface air temperature and precipitation.

Unlike many other parameters, the Arctic sea ice has shown a dramatic decline in addition to interannual fluctuations. We therefore conducted further modeling experiments to identify the role of this long term sea-ice trend on storm activity. The results show that the long-term decline causes a weakening of overall storm activity but an increase in extreme storm events over the Northern Hemisphere. The atmospheric energetic analysis suggests that the increased conversion rate between transient available potential energy and transient kinetic energy is a leading factor in supporting the increased frequency of extreme storms. Over Eurasia, changes in storm activity are mainly governed by the mean kinetic energy of the atmospheric circulation and its conversion to the transient kinetic energy.

Table of Contents

List of Figures

Acknowledgements

First I would like to thank my advisor Xiangdong Zhang for his guidance and suggestions and for teaching me how to conduct research during my stay at University of Alaska Fairbanks (UAF). Also I would like to thank my Graduate Advisory Committee members: Uma S. Bhatt, Igor Polyakov and Nicole Mölders. I would also like to acknowledge University of Alaska Fairbanks for accepting me in their graduate program.

I would like to take this opportunity to thank those who helped me during my process of learning research skills: Peter Bieniek and Paula Moreira for helping me with FORTRAN and NCL codes, teaching me programming and for their valuable suggestions and constant mental support throughout these years of my PhD. I owe thanks to Chas Jones for always helping me with writing and formatting questions.

I also want to thank all the staff of the Arctic Region Super Computing Center (ARSC) for help with running scripts and models in supercomputer. I want to thank Jim Long and Matt Barkdull for helping me with technical and computing support at the International Arctic Research Center.

I would like to acknowledge all the faculty, student and staff of Department of Atmospheric Sciences at UAF and International Arctic Research Center for all their help during my stay at UAF. I thank Richard L. Collins, Kenneth Sassen and Bill Simpson for their guidance in class to finish the required coursework for my PhD. I owe special thanks to Barbara Day for helping me with all the paperwork since the beginning.

I am lucky to have many great friends during my stay here at UAF who constantly motivated me and encouraged me to finish my degree. I thank Abhijit Chatterjee, Bithi De, Bindu Gadamsetty, Cece Borries, Alexander Semenov, Juanxiong He, Vinay Kayetha, Archana Bali, Ipsita Majhi, Santosh Panda, Asish Agrawal, Dee Leelasakultum, Aon Watcharee, John Mayfield, Oliver Dammann, Patrick Joyce, Huy Tran, Tran Trang, Julie Malingowski, Chuhan Lu and Oceana Francis.

My Ph.D. study was supported by the NOAA Grant #NA06OAR4310147, NSF Grant #ARC-1023592 and 1107590, and the Research Theme 3 in the grant to the University of Alaska Fairbanks, International Arctic Research Center, from the Japan Agency for Marine-Earth Science and Technology (JAMSTEC) under the “JAMSTEC and IARC Collaboration Studies". I would like to thank these funding agencies for awarding grant to our group, making it possible for me to complete my Ph.D. degree.

I would also like to thank all my relatives and friends in India and USA who encouraged me to finish my degree with their constant supports and through lengthy phone calls on the weekends. I would like to thank my grandmother Sandhyashree Basu who always supported me and encouraged me to face my difficult times in Fairbanks.

I also owe special thanks from my heart to my “Best Friend”. She guided me towards the completion of my degree through her words of encouragement and provided me mental and emotional support each and every second of my life.

Finally I would like to thank my parents Nilanjan Basu and Swapna Basu and my brother Saptarshi Basu. Without their help and motivation I wouldn't have been able to reach the end of this long academic journey. This PhD was a combined effort of all the people mentioned here without their help this wouldn't have been possible.

Chapter 1 Introduction

1.1 Background: Synoptic and Climatological View of Extratropical Cyclones

Extratropical synoptic-scale cyclonic storms are a fundamental element shaping daily weather patterns and interactively contribute to large-scale general circulation at mid- and high-latitudes. The cyclonic storms generally have a spatial extent ranging from several hundred to a thousand miles with a life cycle spanning from several days to well over a week. The storms typically travel eastward or northeastward following the upper level jet stream pattern. The genesis, development, and decay of storms are prominent features of daily weather charts, which provide key information for weather forecasts.

The extratropical cyclones can bring one or more weather hazards such as rainfall, blizzards, snowfall, freezing rain, and gusty winds that impact our daily life through property damage due to broken trees, snapped power lines (Figure 1.1). It can also cause travel hazards due to icy roads and can result in airport shutdowns. Although these storm activities are limited over mid-latitudes mainly but over the recent years anomalous storm activities are more frequent all over the Northern Hemisphere mid- and high-latitudes [*McCabe et al.,* 2001*; Zhang et al.,* 2004*; Yin,* 2005].

Figure 1.1 Image showing damages due to heavy snowfall, rainfall, freezing rain and gusty winds associated with extratropical cyclones. (source Google image)

Figure 1.2 shows two maps of a super storm developed over the Arctic Ocean on 6th August 2012 and an extreme storm affecting U.S. east coast area on 7th January 2012. The Arctic super storm was formed over north Siberia on 2nd August and then it moved into the Arctic where it intensified with the sea level pressure (SLP) reaching 966 hPa in the center of the cyclone on 6th August (Figure 1.2a). The storm lasted for 13 days and then dissipated over the Canadian Archipelago. The strong winds associated with this super storm played a driving role in the loss of sea ice in the Arctic in 2012 and eventually it was one of the reasons that Arctic sea-ice minimum reached an extreme. Studies have indicated that this storm was greatly influenced by baroclinicity and the presence of a tropopause polar vortex [*Simmonds and Rudeva*, 2012]. The winter storm (Figure 1.1b) was located over the east coast of USA on 7th January. The storm developed

following the onset of an Arctic low pressure system, from Canada, over the continental USA on 4th January (Figure 1.2b). This system later converged with a low pressure system from the Southern Plains on 5th January and due to the combined effect of these two low pressure systems an intense extratropical storm was formed. This storm, with storm center SLP as low as 972 hPa on 7th January, brought gusty winds and heavy snowfall to the cities along the east coast of USA. The cities around Lake Michigan received several inches of extra snowfall due to the lake effect. Thus in this case a cold Arctic air mass converged with a warm air mass from the south and then it developed into an extratropical cyclone supported by vertical wind sheer and baroclinic instability.

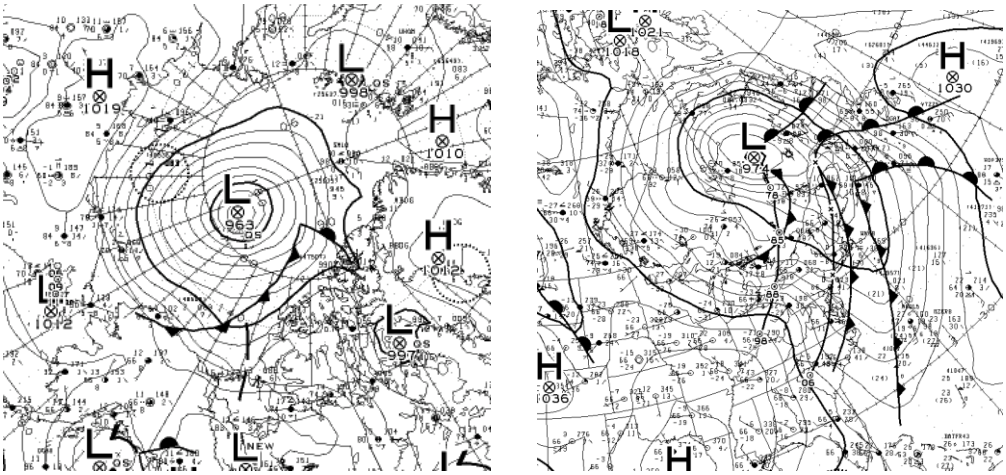

(a) (b)

Figure 1.2 (a) Snapshots showing (a) the super storm that occurred at 18Z August 6, 2012, and (b) the storm that occurred at 00Z January 7, 2014 [adapted from Environment Canada].

Understanding and forecasting individual storms is important. At the same time, it is also scientifically significant to understand integrated climatological features of storms, in particular in a changing climate. Figure 1.3 shows the long-term means of cyclone center count in winter and summer. In climatology the maximum cyclone center count occurred over the North Pacific, North Atlantic, Eurasia and North America [*Zhang et al.*, 2004]. The maps (Figure 1.3) also exhibit a strong seasonality as the meridional temperature gradient plays a prominent role in their formation. Extratropical storms are most common during winter when the strongest meridional temperature gradient exists over the Northern Hemisphere. Hence the peak storm activity occurs during winter over most of the mid-latitude except Eurasia (Figure 1.3a). The storm activity weakens during summer over the entire mid-latitude except Eurasia (Figure 1.3b). Thus storm tracks are commonly known as regions with large synoptic scale baroclinic wave activity [*Blackmon et. al.*, 1977*; Zhang et al.*, 2004] and a prominent seasonal and regional variability of storm activity exists among the storm activity over different geographical regions.

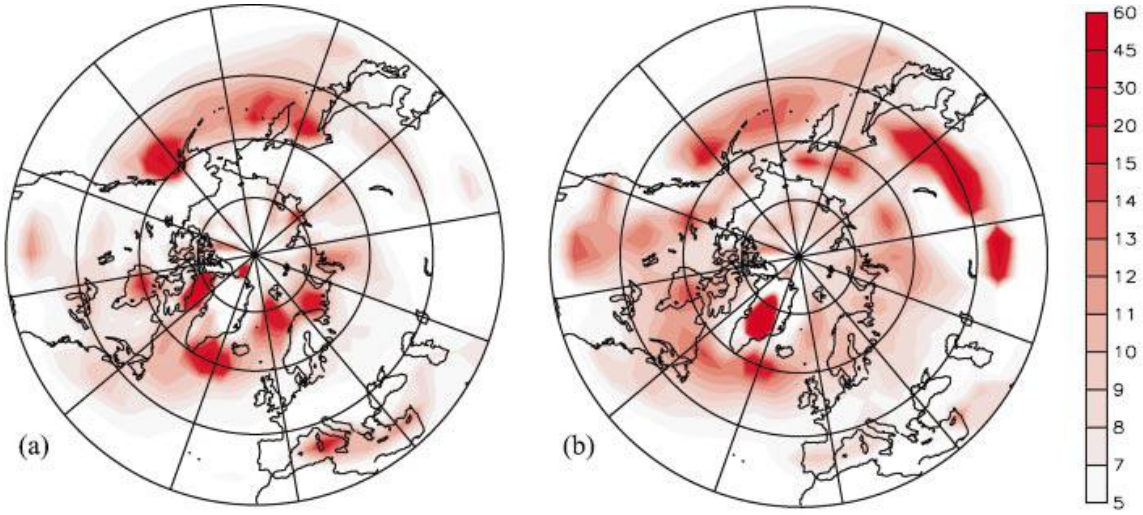

Figure 1.3 The plots showing, long-term mean cyclone center count in (a) winter and (b) summer (unit: counts per 10^5 km^2) [*Zhang et al.*, 2004].

1.2 Motivations for this study: Recent Manifestation of Changes in Storm Activity

Extratropical storms have prominent regional and seasonal structures, and exhibit daily as well as interannual variability [*Hoskins and Hodges*, 2002*; Zhang et al.*, 2004*; Bengtsson et al.*, 2006]. Storm tracks and activities have demonstrated a long-term response to changing climate. Recent studies indicate that northern hemispheric extratropical storm tracks have shifted poleward, and storm activities have intensified in the northern high latitudes and the Arctic. This shift is projected by climate models and observations to continue under global warming scenarios [*McCabe et al.*, 2001*; Zhang et al.*, 2004*; Yin* 2005]. Zhang et al. [2004] further found that storm activities have distinct regional characteristics across different geographic sectors, superimposed on the long-term trend of a poleward-shift (Figure 1.4). What can cause such variability across the geographical regions?

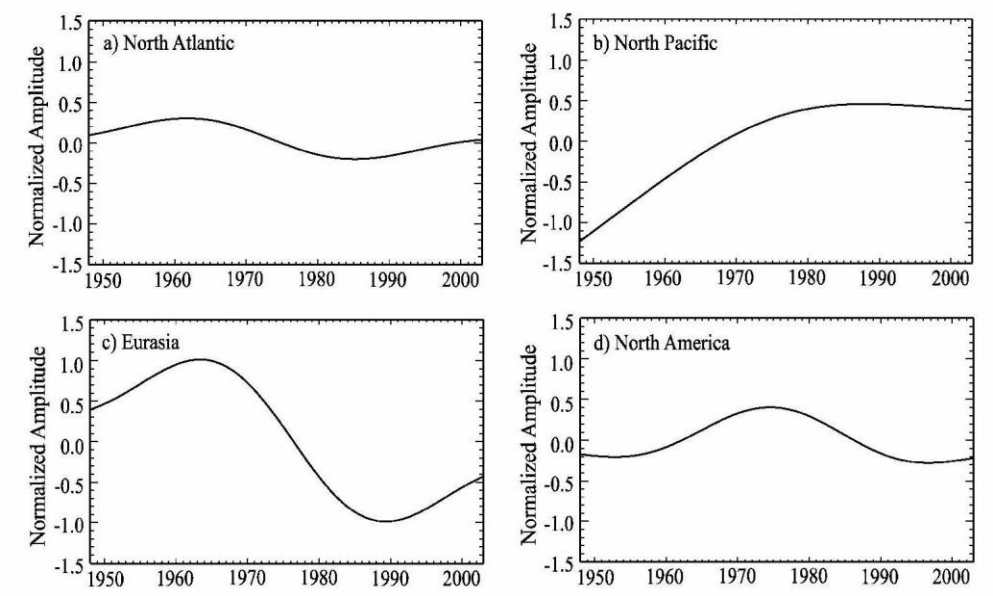

Figure 1.4 Most significant low-frequency variation signals of CAI anomalies (sum of departures of storm center SLP from long term climatological mean SLP at that grid point) as determined by the MTM spectral analysis in the four midlatitude sectors: (a) the North Atlantic, (b) the North Pacific, (c) Eurasia, and (d) North America. The signals in (a)–(c) are significant at the 99% level and the signal in (d) is significant at the 95% level. From [*Zhang et al., 2004*].

Apart from the changes in general circulation due to the warming climate the variability in storm activities can be caused by anomalous surface boundary forcing such as anomalous sea surface temperatures (SST) and Arctic sea ice. El Niño is a prominent interannual mode of SST variability over the eastern and central tropical Pacific and it has many consequences for global weather. The interannual variability of El Niño is shown in Figure 1.5 in terms of niño3 index. There have been several studies showing the

direct and indirect effects of elevated tropical Pacific SST on atmospheric circulation and storm tracks. A PNA-like pattern with intense low pressure over Aleutian Islands has been found to persist during El Niño years [*Wallace et al.,* 1981*, Renwick et al.,* 1996]. The Pacific/ North American teleconnection pattern (PNA) occurs over the Northern Hemisphere extratropics is one of the most prominent modes of low-frequency variability. Elevated tropical Pacific SST impacts the Hadley Cell and Walker circulations. It has been found that the jet streams and the storm tracks are displaced southward and extended eastward over the eastern Pacific Ocean when tropical Pacific SST increases during El Niño [*Trenberth and Hurrell,* 1993*; Hoerling,* 1994*; Straus and Shukla,* 1997*; Zhang and Held,* 1999*; Orlanski,* 1998*;* 2005*; Eichler and Higgins,* 2006*; Compo,* 2010].

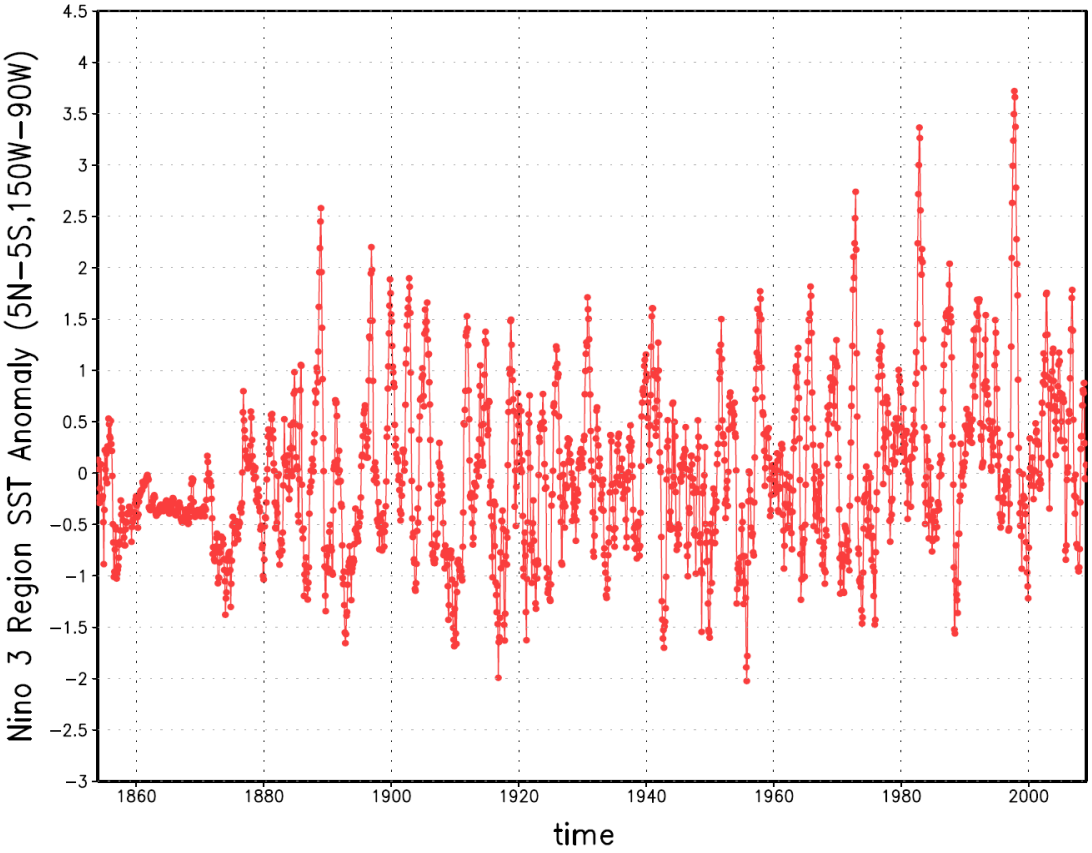

Figure 1.5 Plot showing Niño 3 Index time series from 1850-2009 plotted from NOAA Extended Reconstructed Sea Surface Temperature (SST) v2.

Sea ice plays an important role in the global climate system. It interacts with the ocean and atmosphere through highly complex dynamical processes. The albedo of ice is higher than open water so that area of ice has a dramatic impact on the high-latitude radiation budget. A better understanding of the impact of sea ice on the atmosphere is crucial for

understanding the global climate system. Since the advent of satellites equipped with passive microwave radiometers for monitoring the Arctic sea ice there are well documented record of sea-ice extent, concentration. In the Arctic the maximum sea-ice extent and concentration occur typically in March and the minimum occurs in September. Over the recent decades due to a warming climate, Arctic sea ice is decaying rapidly [*Comiso,* 2003] (Figure 1.6). The growth and decay of Arctic sea ice affects the atmospheric general circulation and global weather pattern [e.g. *Zhang et al.,* 2008*; Graversen et al.,* 2010*; Overland and Wang,* 2010]. From General Circulation Model (GCM) experiments it has been shown that increased open water due to decreased sea ice causes increased surface fluxes of latent and sensible heat [*Alexander et al.,* 2004*; Magnusdottir et al.,* 2004*; Bhatt et al.,* 2008]. Warming of the Arctic causes a decline of sea ice and sea-ice extent anomalies are correlated with atmospheric pressure anomalies over the Arctic [*Herman and Johnson,* 1978]. Due to the dynamical processes, the consequences of changes in Arctic sea ice are not limited to the Arctic only but they have implications on synoptic weather patterns over low and mid-latitudes. It can also influence multiyear oscillations such as Arctic Oscillation and North Atlantic Oscillation [*Balmaseda et al.,* 2010].

However, there has been a gap in our knowledge about relative contribution, of the changes in tropical Pacific SST associated with the El Niño events or changes in Arctic sea ice due to warming climate, on Northern Hemispherical storm activities. Arctic sea ice displays both interannual variability and a long-term trend. The effect of these two components on extratropical storms has also not been investigated. In this thesis, we

present research results on the response of extratropical storms to anomalous surface boundary forcing from SST and Arctic sea ice.

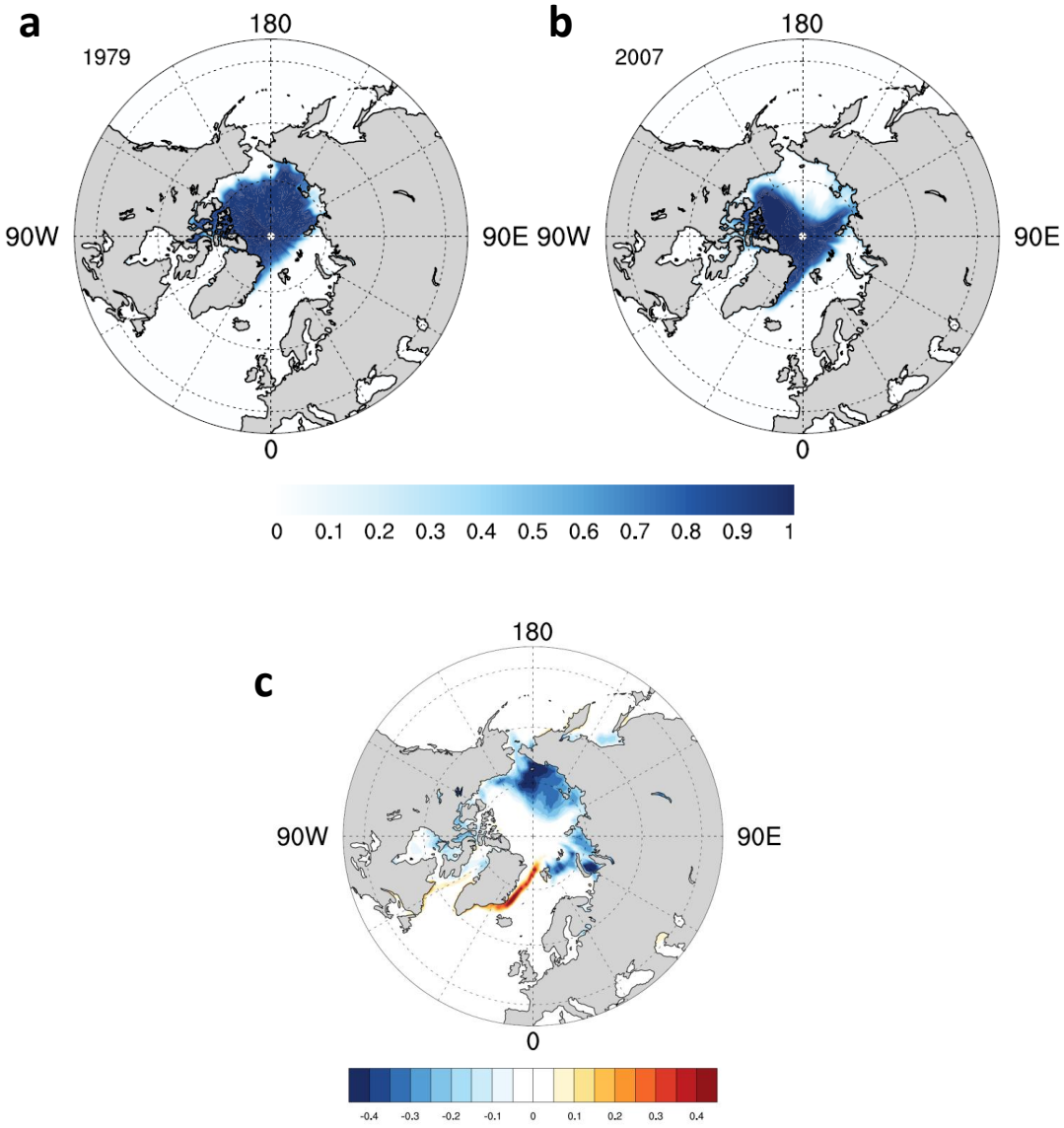

Figure 1.6 (a) Plots showing Arctic sea-ice fraction in September 1979; (b) Arctic sea-ice fraction in September 2007 and (c) differences between September 1979 Arctic sea ice and September 2007 Arctic sea ice (Shea/Hurrell sea ice dataset for CAM).

1.3 Scientific Questions, Hypotheses, and Objectives

In this study, we address the following scientific questions:

1) What is the response of North American storm track to elevated Tropical Pacific SST?

2) What is the response of the Northern Hemispheric storm tracks to changes in Arctic sea ice and what are the corresponding changes in surface climate?

3) What is the difference in response of the Northern Hemisphere storm tracks to long-term trend of Arctic sea ice and interannual variability of Arctic sea ice?

To answer these questions, we hypothesize that change in tropical Pacific SSTs causes a redistribution of air temperature. This changed air temperature creates temperature gradient and can cause a southward shifted jet stream which enhances the baroclinic instability of the atmosphere. The enhanced baroclinic instability can cause more numerous and more intense extratropical storms over the southern part of North America. Another hypothesis is that rapid loss of Arctic sea ice due to global warming creates larger areas of open water over the Arctic, open water thus absorbing more heat and can causing redistribution of gradient of air temperature in the overlying atmosphere. This redistributed temperature gradient can cause changes in atmospheric circulation resulting in more storms moving over the high latitudes and Arctic (Figure 1.7).

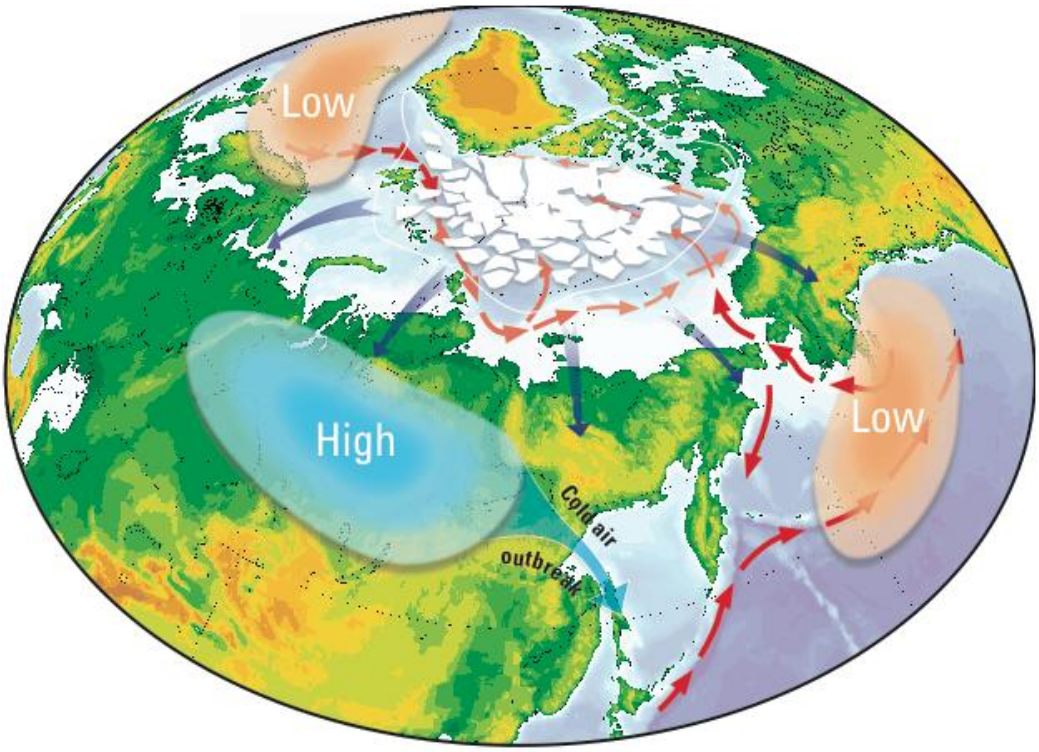

Figure 1.7 Schematic diagram shows the impact of Arctic sea ice on weather events across the mid- and high-latitude (Igor Polyakov personal communication).

Through testing the hypotheses and answering the scientific questions described above, we aim to better understanding the pathway and underlying physical processes by which the anomalous tropical Pacific SST and Arctic sea ice impact variability of and changes in Northern Hemisphere mid- and high-latitude storm activity in a warming climate. The outcome from this study would have important implications for improving predictive capability and assessment of extreme events associated with the changing climate and evaluating climate changes impacts on environment and ecosystem.

1.4 Research Approaches

In order to test our hypothesis several modeling experiments were performed with the National Center for Atmospheric Research Community Atmosphere Model (CAM) version 3.1_p2 (CAM3.1_p2) [*Collins et al*., 2006, *Hurrell et al*., 2006]. CAM is the atmospheric components of the Community Climate System Model 3.1 (CCSM3.0). A horizontal resolution of approximately 1.4°x 1.4° [*Collins et al.,* 2006] with 26 vertical levels and an Eulerian spectral dynamical core with triangular truncation at 85 wave numbers was used in this study. When running CAM3.1 only the Community Atmosphere Model (CAM) and the Community Land Model (CLM) components were interactive. The ocean and ice were specified using monthly values. The Community Land Model (CLM3) has similar horizontal resolution to that of CAM3.1. The surface boundary conditions dataset was developed at NCAR [*Hurrell et al.* , 2008]. This dataset is a merged product based on the monthly mean Hadley Centre sea ice and SST dataset version 1 (HadISST1) and version 2 of the National Oceanic and Atmospheric Administration (NOAA) weekly optimum interpolation (OI) SST analysis were merged to produce this dataset.

In this research a series of modeling experiments were conducted. A Lagrangian approach [*Zhang et al.*, 2004] was used to identify and track each storm with time and then we linked those changes to the general circulation. A storm identification and tracking algorithm was used for the study. The algorithm first identifies a grid point which has lower sea level pressure (SLP) than the surrounding eight grid points. The SLP gradients between that grid point and the surrounding grid points have to be ≥ 15 hPa. If

there is another such point within a 1200 km radius it is considered as the same cyclone. Also, if the location of the cyclone is within 600 km of its previous 6 hourly location it is a new location for that cyclone otherwise it will be considered as a new cyclone generated. Also, the overall life time of the system has to be greater than 12 hours.

In this thesis we want to do an integrated evaluation of relative contribution of SST and Arctic sea ice on Northern Hemisphere storm activities. Surface boundary forcings such as elevated tropical Pacific SST or Arctic sea ice can generate different responses in the storm activity over mid-latitude and the Arctic. As a result we studied the response of the extratropical storms to tropical Pacific SST anomaly and to the changes in Arctic sea ice, separately. We also studied the response of the storms to the long term declining trend of Arctic sea ice to better understand the contribution of Arctic sea ice. Thus these three different modeling experiments complement each other and help advance understanding of the relative contribution of two biggest natural forcings i.e. SST and Arctic sea ice.

The thesis is organized as follows. Chapter 2 presents the modeling study on response of North American extratropical storms to the elevated tropical Pacific SST. Chapter 3 of the thesis presents a modeling study on the response of the extratropical storms to reduced Arctic sea ice and discusses the corresponding changes in surface climate induced by the changes in storm activity. Chapter 4 discusses a modeling investigation on the response of the extratropical storms to the long term trend forcing of Arctic sea ice. Chapter 5 presents the overall conclusion of the thesis is discussed.

References

Alexander, M. A., U. S. Bhatt, J. Walsh, M. Timlin, and J. Miller (2004), The atmospheric response to realistic Arctic sea ice anomalies in an AGCM during winter, *J. Clim.*, 17, 890–905.

Balmaseda, M. A., L. Ferranti, F. Molteni and T. N. Palmer (2010), Impact of 2007 and 2008 Arctic ice anomalies on the atmospheric circulation: Implications for long-range predictions, *Quart. J. Roy. Meteor. Society*, 136(652), 1655-1664.

Bengtsson, L., K. I. Hodges and E. Roeckner (2006), Storm tracks and Climate Change, *J. Clim.*, 19, 3518-3542.

Bhatt, U. S., M. A. Alexander, C. Deser, J. E. Walsh, J. S. Miller, M. S. Timlin, J. Scott and R. A. Tomas (2008), The atmospheric response to realistic reduced summer Arctic sea ice anomalies, Arctic Sea-ice decline: Observations, Projections, Mechanisms, and Implications, *Geophys. Mono. Series*, 180, 91-110.

Blackmon, M. L., J. M. Wallace, N. Lau, S. L. Mullen (1977), An Observational Study of the Northern Hemisphere Wintertime Circulation, *J. Atmos. Sci.*, 34, 1040–1053.

Collins, W. D., P. J. Rasch, B. A. Boville, J. J. Hack, J. R. McCaa, D. L. Williamson, B. P. Briegleb, C. M. Bitz, S.J. Lin and M. Zhang (2006), The Formulation and Atmospheric Simulation of the Community Atmosphere Model Version 3 (CAM3). *J. Clim.*, 19, 2144-2161.

Comiso, J. C. (2003), Warming Trends in the Arctic from Clear Sky Satellite Observations, *J. Clim.*, *16*, 3498-3510.

Compo, G. P. (2010), Removing ENSO related variation from climate record, *J. Clim.*, 23, 1957-1978.

Eichler, T. and W. Higgins (2006), Climatology and ENSO-related variability of North American extratropical cyclone activity, *J. Clim.*, 19, 2076-2093.

Graversen, R. G., T. Mauritsen, S. Drijfhout, M. Tjernstrom and S. Martensson (2010), Warm winds from the Pacific caused extensive Arctic sea ice melt in summer 2007. *Clim. Dyn.*, 36, 2103-2112.

Herman, G. F. and W. T. Johnson (1978), The Sensitivity of the General Circulation to Arctic Sea ice Boundaries: A Numerical Experiment, *Mon. Wea. Rev*., 106, 1649-1664.

Hoerling, M. P. (1994), Organization of Extratropical Transients during El Niño, *J. Clim.*, 7(5), 745–766.

Hoskins, B. J. and K. I. Hodges (2002), New Perspective on the Northern Hemisphere Winter Storm Tracks, *J. Atmos. Sci.*, 59, 1041-1061.

Hurrell, J. W., J. J. Hack, A. S. Phillips, J. Caron and J. Yin (2006), The Dynamical Simulation of the Community Atmosphere Model Version 3 (CAM3), *J. Clim.*, 19, 2162-2183.

Hurrell, J. W., J. J. Hack, D. Shea, J. M. Caron and J. Rosinski (2008), A New Sea Surface Temperature and Sea ice Boundary Dataset for the Community Atmosphere Model, *J. Clim.*, 21.

McCabe, G. J., M. P. Clark and M. C. Serreze (2001), Trends in Northern Hemisphere Surface Cyclone Frequency and Intensity, *J. Clim.*, 14(12), 2763-2768.

Magnusdottir, G., C. Deser, and R. Saravanan (2004): The effects of North Atlantic SST and sea ice anomalies on the winter circulation in CCM3, Part I: Main features and storm-track characteristics of the response, *J. Clim.*, 17, 857-876.

Orlanski, I., 1998: Poleward Deflection of Storm Tracks, *J. Atmos. Sci.*, 55, 2577–2602.

Orlanski, I. (2005), A New Look at the Pacific Storm Track Variability: Sensitivity to Tropical SSTs and to Upstream Seeding, *J. Atmos. Sci.*, 62, 1367-1390.

Overland, J. E., and M. Wang (2010), Large-scale atmospheric circulation changes are associated with the recent loss of Arctic sea ice, *Tellus, 62A (2010)* (1).

Renwick, J. A., J. M. Wallace (1996), Relationships between North Pacific Wintertime Blocking, El Niño, and the PNA Pattern, *Mon. Wea. Rev.*, 124, 2071–2076.

Simmonds, I., and I. Rudeva (2012), The great Arctic cyclone of August 2012, *Geophys. Res. Lett*., 39, L23709.

Straus, D. M. and J. Shukla (1997), Variations of Midlatitude Transient Dynamics Associated with ENSO. *J. Atmos. Sci.*, 54(7), 777–790.

Trenberth, K. E. and J. W. Hurrell (1993), Decadal atmosphere - ocean variations in the Pacific, *Clim. Dyn.*, 9, 303-319.

Wallace, J. M., D. S. Gutzler (1981), Teleconnections in the Geopotential Height Field during the Northern Hemisphere Winter, *Mon. Wea. Rev.*, 109, 784–812.

Yin, J. H. (2005), A consistent poleward shift of the storm tracks in simulations of 21st century climate. *Geophys. Res. Lett*., 32, L18701.

Zhang, X., A. Sorteberg, J. Zhang, R. d. Gerdes and a. J. C. Comiso (2008), Recent radical shifts of atmospheric circulations and rapid changes in Arctic climate system. *Geophys. Res. Lett*., 35, L22701.

Zhang, X., J. E. Walsh, J. Zhang, U. S. Bhatt and M. Ikeda (2004), Climatology and Interannual Variability of Arctic Cyclone Activity: 1948–2002, *J Clim.*, 17, 2300-2317.

Zhang, Y. and I. M. Held (1999), A Linear Stochastic Model of a GCM's Midlatitude Storm Tracks, *J. Atmos.Sci*., 56(19), 3416–3435.

Chapter 2 North American Winter-Spring Storms: Modeling Investigation on Tropical Pacific Sea Surface Temperature Impacts[1]

Abstract

An increased frequency and intensity of winter and spring storms have recently manifested over a broad area of North America—along the east coast of the U.S. especially, though global mean storm tracks are suggested to shift northward. To understand these changes, we have conducted atmospheric model experiments, examining the response of North American storm activity to the elevated tropical Pacific sea surface temperature (SST) associated with El Niño. The results indicate that, when tropical Pacific SST increases, there are more numerous intense storms over southwestern, southeastern, and northwestern North America, but fewer weaker storms over the northeast. Transient eddy analysis of the general circulation demonstrates consistent changes, suggesting systematic changes from large-scale general circulation to synoptic-scale storms. These changes can be attributed to enhanced lower tropospheric baroclinicity, to which the southward shift and an intensification of extratropical jet streams make a major contribution.

[1] S. Basu., X. Zhang, I. Polyakov and U. S. Bhatt (2013). North American winter-spring storms: Modeling investigation on tropical Pacific sea surface temperature impacts. Published in Geophysical Research Letters **40**(19): 5228-5233.

2.1 Introduction

Extratropical synoptic-scale cyclonic storms are a fundamental element of daily weather patterns and interactively contribute to large-scale general atmospheric circulation at middle and high latitudes. They can bring blizzards, snowfall, and gusty winds that impact daily life through infrastructure damage and property loss. Storm activities have prominent regional and seasonal structures, and exhibit daily to interannual variability [*Hoskins and Hodges.,* 2002; *Zhang et al.,* 2004; *Bengtsson et al.,* 2006]. Storm tracks and activities have also demonstrated a long-term response to changing climate. Recent studies indicate that northern hemisphere extratropical storm tracks have shifted poleward and storm activities have intensified in the northern high latitudes and Arctic, and this shift is projected by climate models to continue under global warming scenarios [*McCabe et al.,* 2001; *Zhang et al.,* 2004; *Yin,* 2005]. Zhang et al. [2004] further found that storm activities have distinct regional characteristics across different geographic sectors, superimposed on the long-term trend of a poleward-shift. The variability of storm activity over North America has exhibited a quasi-decadal oscillation [*Zhang et al.,* 2004]. The recently observed intensification of storm activities in North America, in particular along the east coast, would be a manifestation of this regional behavior.

To improve our understanding of such regional variability and changes in storm activities over North America, we have conducted modeling investigations that examine a number of potential forcing factors. One of these factors is the elevated tropical Pacific sea surface temperature (SST) associated with El Niño. Direct and indirect effects of tropical Pacific SST anomalies upon atmospheric circulation and storm tracks have been

investigated in several studies. It has been found that jet streams and storm tracks are displaced southward and extended eastward over the eastern Pacific Ocean when tropical Pacific SST increases during El Niño [*Trenberth and Hurrell,* 1993; *Hoerling,* 1994; *Straus and Shukla,* 1997; *Zhang and Held,* 1999; *Orlanski,* 2005; *Eichler and Higgins,* 2006; *Compo,* 2010]. However, effects of tropical Pacific SST anomalies on storms over the entire North American continent, in particular on recently intensified winter-spring storm activities affecting the east coast, under a climate experiencing accelerated warming have not yet been fully understood. We will address this problem in this study.

2.2 Model experiment design and data analysis methods

We employed the National Center for Atmospheric Research (NCAR) Community Atmosphere Model (CAM) version 3.1.p2 [*Collins et al.,* 2006; *Hurrell et al.,* 2006]. It was configured at a resolution of T85 (approximately 1.4° for both latitude and longitude), with 26 vertical levels. We conducted two groups of modeling experiments in order to isolate the impacts of elevated tropical Pacific SST on North American storm track dynamics and storm activity: Control Experiments (ConExp) and Sensitivity Experiments (SenExp), which have different surface boundary conditions, defined by SST and sea-ice concentration data sets [*Hurrell et al.,* 2008]. To obtain robust results, we performed 60 ensemble runs for each group.

In ConExp, SST and sea-ice concentration are prescribed using their long-term climatological monthly means from 1981-2001 at each grid point over the global ocean. In SenExp, we constructed elevated tropical Pacific SST using SST data from 1997-98,

when a strong El Niño occurred. In particular, we first calculated monthly SST anomalies at each grid point for 1997-98. Then positive SST anomalies were added to the climatological SST at each grid point over the tropical Pacific region between 10°S and 10°N and from 165°W to 80°W, throughout the simulation time period. The maximum tropical Pacific SST anomaly occurs in December and then gradually decays with time (Figure 2.1). Climatological monthly SST data was specified for grid points outside this tropical Pacific region. Climatological sea-ice concentration was specified at the sea ice covered grid points in both the Northern and Southern hemispheres.

All ensemble runs for both ConExp and SenExp were carried out from November 1 to May 31, with six-hourly output of selected variables. We allowed one month for the model to spin up, and we used model results from December to the following May. To analyze storm activities in both experiments, we applied a storm identification and tracking algorithm [*Zhang et al.*, 2004] to the six-hourly sea level pressure (SLP) outputs from each model ensemble. This algorithm identifies a low SLP center, which should have a minimum SLP gradient of at least 0.15 hPa per hundred kilometers with surrounding grid points and should survive for more than 12 hours. More details about this algorithm and its application for investigating Northern Hemisphere storm track variability and changes can be found in *Zhang et al.* [2004]. In addition, considering the distinct geographical features and greater climatological storm activity near the coasts, we divided the North American continent into four sub-regions in this study (Figure 2.2).

2.3 Results

2.3.1 Changes in North American storm activity

The storm identification and tracking algorithm provides parameters that describe various aspects of storm activity, including duration or lifetime, central location, and central SLP, for each individual storm occurring over the study area. By using the data sets of these parameters from each ensemble run of ConExp and SenExp, we derived the number of storm trajectories, mean storm duration, and mean storm intensity for each sub-region in both winter (December-February) and spring (March-May). Following *Zhang et al.* [2004], storm trajectory is defined from the time of storm generation until dissipation within the study area, or from the time when the storm enters the study area until the time it leaves the study area. Mean duration for each sub-region is the average duration for the total number of storm trajectories within the study area. The storm intensity for individual storms was calculated as the difference between the storm's central SLP and the monthly mean SLP at the corresponding location. Mean intensity for each sub-region was obtained by averaging storm intensities over their duration and over all storm trajectories.

We conducted a statistical analysis for all 60 ensembles in both ConExp and SenExp. Probability Density Functions (PDFs) of the number of trajectories, mean intensity, and mean duration exhibit various differences in climate features of storm activity between ConExp and SenExp, over each of the sub-regions and during both winter and spring (Figure 2.3). In both ConExp and SenExp, the number of storm trajectories shows a Gaussian distribution over the sub-regions in winter and spring, except for a bimodal distribution over southwestern North America (SWNA) during winter. Noticeable

seasonality is present in the PDFs for both groups of experiments. In ConExp, the peak frequency generally increases and shifts to a higher number of trajectories from winter to spring over SWNA and southeastern North America (SENA), suggesting more numerous storms in spring in these two sub-regions. An increase and a decrease in peak frequency occur for the trajectories over northwestern North America (NWNA) and northeastern North America (NENA), respectively.

Comparison between ConExp and SenExp indicates noticeable changes in the numbers of storm trajectories when tropical Pacific SST increases. In addition to significant increases based on the Student's t-test, peak frequencies over SWNA and SENA also shift toward a higher number of storm trajectories, from 51 ± 6 and 62 ± 6 to 57 ± 7 and 69 ± 6 during winter (Figure 2.3a-b). Peak frequencies show a slight decrease in spring, and no obvious shift occurs within these two sub-regions. In NWNA, peak frequencies exhibit a shift to a higher number of trajectories in both winter and spring (Figure 2.3c). However, a decrease occurs in the NENA region (Figure 2.3d). Note that interconnections may exist in storm frequencies between the sub-regions, though the analysis here mainly focuses on storm activities in each sub-region. For example, storms, that are generated in or travel to the western U.S., may continually enter the eastern U.S. So, the increased number of storm trajectories in the western U.S. may also contribute to the increase in the eastern U.S.

Climatologically, storm intensity is generally characterized by a narrow, Gaussian-like distribution in all sub-regions and in both winter and spring, according to the simulations

in ConExp (Figure 2.3e-h). Storms are stronger in winter and get weaker in spring in most sub-regions, except for an opposite seasonal variation in NENA. The PDFs of intensity show a similar distribution in SenExp. However, when comparing intensities between ConExp and SenExp, we can readily find significant intensification of storms over most sub-regions, with maximum frequency shifting from a mean intensity of 12.21 ± 0.95 (8.17 ± 0.68) to 17.33 ± 0.61 (10.35 ± 0.23) hPa over SWNA; 14.59 ± 0.72 (11.56 ± 0.93) to 17.65 ± 0.52 (14.11 ± 0.49) hPa over SENA; and 24.15 ± 0.96 (21.90 ± 0.86) to 28.13 ± 1.01 (23.43 ± 0.60) hPa over NWNA in winter (spring). Similar to its seasonal variation, storm intensity noticeably decreases over NENA in winter and spring with increased tropical Pacific SST.

Storms generally have longer duration over the western half of the North American continent than the eastern half, as characterized by their PDFs in Figure 2.3i-l. In response to increased tropical Pacific SST, SWNA storms show a decrease in durations from 38.71 ± 5.59 (33.43 ± 2.72) to 31.22 ± 4.05 (31.22 ± 2.47) hours in winter (spring), as shown by the comparison of peak frequencies of PDFs between ConExp and SenExp. In contrast, storms over SENA exhibit prolonged mean durations, from 30.23 ± 3.02 (34.66 ± 3.14) to 34.48 ± 3.0 (37.51 ± 3.86) hours in winter (spring). Nevertheless, no obvious changes are found in storm durations over NWNA and NENA in SenExp. It is worth mentioning that the duration depends on moving speed of storms within each sub-region. So, storms can carry the same moving features from one sub-region to another, impacting mean durations in two study areas.

Statistical analysis across all ensembles of ConExp and SenExp indicates systematic changes in different aspects of storm activity over North America. When tropical Pacific SST increases, there are more numerous, more intense storms over SWNA, SENA, and NWNA, i.e., the entire U.S. continent, as well as western Canada and Alaska. The storms over SENA, i.e. the eastern U.S., demonstrate longer duration or lifetime than their climatology. To better understand the physical processes and mechanisms behind these changes, we will further examine these synoptic-scale storm activities in the context of the large-scale atmospheric general circulation in the following section.

2.3.2 Perspective from large-scale circulation and associated physical mechanisms

In the above analysis, we employed a Lagrangian approach to identify and track each storm. To link detected storm activities to the atmospheric general circulation, we conducted further analysis by using an Eulerian method to represent overall storm activities at each grid point. Specifically, we computed transient eddy kinetic energy (EKE, KJ/m^2) at each grid point at 775 hPa, defined as

$$EKE = \frac{1}{2}(u'^2 + v'^2) \qquad (2.1)$$

where u´ and v´ are high pass ($\leq$ 6 days) filtered data for a consistency with the analysis above using the Lagrangian approach that used 6-hourly based data. Considering upstream origins of storms impacting North America, our computation and analysis area extends to include the western North Pacific. Figure 2.4a-d shows the EKE from the two groups of simulations, ConExp and SenExp, for winter and spring, respectively.

In climatology simulated by ConExp, large EKE occurs from the middle and eastern North Pacific to the Bering Strait and the interior Alaska in winter. Maximum EKE appears over the Aleutian Islands. Another large wintertime EKE area includes most of the North American continent east of the Rocky Mountains and the North Atlantic coast. These large EKE distributions are in good agreement with climatological winter storm tracks [e.g., *Zhang et al.* 2004; *Bengtsson et al.*, 2006]. EKE also demonstrates seasonal variations, showing considerable decreases from winter to spring (comparing Figure 2.4a vs. b), consistent with the storm intensity analysis shown in the previous sections.

Changes in EKE forced by the increased tropical Pacific SST can be easily identified when comparing simulations between ConExp and SenExp (Figure 2.4). The Aleutian maximum of EKE is dramatically shifted southeastward, to the northeastern North Pacific, in both winter and spring, in spite of large seasonal differences in their magnitude. These changes also exhibit an increase in storm activities along the west coast and extending to the Rocky Mountains. Another pronounced increase occurs from the middle U.S. to the east coast, in particular for the spring season. Each of these EKE changes corresponds well to the intensity changes shown by the PDFs in Figure 2.3e-h.

Why do changes occur in the EKE or storm activities in response to increased tropical Pacific SST forcing? To answer this question, we quantitatively examined the Eady Growth Rate Maximum (EGRM, day^{-1}) at 775 hPa for each ensemble of the ConExp and SenExp. The EGRM is given by *Hoskins and Valdes* [1990] as

$$EGRM = 0.31f\,|\frac{\partial\, u}{\partial z}|N^{-1} \qquad (2.2)$$

Where f is the Coriolis parameter, N the Brunt Väisälä Frequency, and **U** the horizontal wind vector. EGRM depends on vertical wind sheer and atmospheric static stability, and is usually calculated at the lower levels of the atmosphere, where major baroclinic development occurs. It measures the intensity of atmospheric baroclinic instability, which is the principle mechanism supporting extratropical storm development.

Climatological wintertime EGRM for ConExp demonstrates large values mainly over three areas, including the North Pacific, the west coast and Rocky Mountains of the U.S., and the east coast of the U.S. (the contours in Figure 2.4a), suggesting strong baroclinicity in these areas for storm generation and development. In spring, climatological EGRM considerably decreases (Figure 2.4b). Although the primary spatial structures of EGRM in SenExp are very similar to those of ConExp, differences can be found in a comparison between Figure 2.4e and f. An increase in EGRM occurs in SenExp over the eastern North Pacific and along the U.S. west coast, from southeastern Alaska to California, in both winter and spring. This increase also occurs over the area from the southeastern U.S. and the Gulf of Mexico to the east coast in both seasons. In spring, the increase in EGRM extends considerably northward to the central and eastern United States. A decrease occurs from the lee side of the Rocky Mountains to the east coast of Canada. These changes in EGRM are consistent with and provide dynamic support for the spatial shift of storm tracks identified by the tracking algorithm and transient eddy analysis described above.

Vertical wind shear is a primary contributor to the EGRM and its changes. We therefore analyzed the vertical structure of the zonal wind averaged between 180^{o} - 310^{o} longitude in both SenExp and ConExp for both winter and spring (Figure 2.5). The results indicate a strengthening and southward shifting of the subtropical jet stream, particularly in winter, when the tropical Pacific SST increases in SenExp compared to its climatology in ConExp. The changes in the jet stream identified here are consistent with previous findings that elevated tropical Pacific SST can force an intensified and southward contracted Hadley Cell over the eastern Pacific [e.g., *Lu et al.*, 2008]. The changed jet stream between 25°N and 40°N can result in an increase in EGRM further southward than its climatology and, in turn, supports the intensified and southward shifted storm tracks found above. In addition, the jet stream favors storms developing on its south side, due to the associated large upper-level divergence. When further examining large-scale circulation, we found that the difference of 500 hPa geopotential height between SenExp and ConExp shows a PNA-like pattern (not shown), with intensified low pressure systems over the Aleutian Islands and the southeastern U.S. and anomalous high pressures over the northeastern U.S. and eastern Canada. The northwest-to-southeast aliened background steering flow favors storms to propagate to the southeastern U.S.

2.4 Concluding remarks

An increased frequency of intense storms has been observed in North America, in particular along the east coast area. We have employed the community atmospheric model NCAR CAM 3.1 to conduct two groups of modeling experiments. Statistics derived by a storm identification and tracking algorithm [a Lagrangian approach; *Zhang*

et al., 2004] show a distinct seasonality and significant changes in storm activities. In climatology, the number of storm trajectories increases, though intensity decreases from winter to spring over southwestern, southeastern, and northwestern North America. There is also an increase in the number of storm trajectories, though little change in intensity during winter and spring in northeastern North America. When tropical Pacific SST increases, model experiments suggest a significantly increased number and intensity of storms over the Southwest, Southeast, and Northwest, i.e., the entire U.S., as well as western Canada and Alaska, during winter and spring. However, less and weaker storms occur over northeastern North America in both seasons. This suggests a southward shift of storm tracks over the eastern U.S. Meanwhile, storms over southeastern North America, i.e. the eastern U.S., demonstrate a longer duration or lifetime than their climatology.

To better understand these changes in storm activities, we investigated, for the first time, the linkage between surface storms identified by the Lagrangian approach and transient eddies in general circulation computed by Eulerian approach and measured by EKE. Changes in surface storm tracks and activity over North America are consistent with those in EKE, which are attributed to changed baroclinicity. When tropical Pacific SST increases, maximum EGRM shifts southeastward from the Aleutian Islands to western North America, particularly in winter. Considerably increased EGRM occurs from southeastern Alaska and western Canada to California. EGRM also increases substantially from the southern U.S. to the east coast, with the largest increase in spring. The southward shift and intensification of the subtropical jet stream favors an increase in

vertical wind shear in the lower troposphere to the south of the climatological jet stream, contributing to increasing baroclinicity, enhancing air mass divergence, and, in turn, supporting surface storm development and strengthening. Meanwhile, the PNA-like pattern and associated northwest-to-southeast aliened background flow favors storms to propagate to the southeast U.S.

An increase in storm events in a warming climate has significant implications for human society and the natural environment. Recent observations have shown an increasing tendency of frequency and intensity of El Niño (e.g., *Cobb et al., 2013*), although there are still uncertainties in climate model projections in a future warming climate [e.g., *Collins et al.,* 2010]. Results from this study would help improve understanding, enhance predictive capability, and reduce future projection uncertainties of storm events over North America under the scenario of a changed El Niño, induced by global warming forcing, which is important for policy decision-making processes.

Acknowledgements

We are grateful to the editor and the anonymous reviewer for their constructive comments and suggestions, which improved content and presentation of this paper. We thank Dr. Nicole Mölders for serving on Soumik Basu's advisory committee and providing valuable suggestions and comments. We also thank NCAR for making CAM available and the Arctic Region Supercomputing Center for providing computational resources. This study is supported by the NOAA Grant #NA06OAR4310147 and the Grant to the University of Alaska Fairbanks, International Arctic Research Center from the Japan Agency for Marine-Earth Science and Technology (JAMSTEC) under the "JAMSTEC and IARC Collaboration Studies".

References

Bengtsson, L., K. I. Hodges, and E. Roeckner (2006), Storm tracks and climate change, *J. Clim.*, *19*, 3518-3542.

Cobb, K. M., N. Westphal, H. R. Sayani, J. T. Watson, E. Di Lorenzo, H. Cheng, R. L. Edwards, and C. D. Charles (2013), Highly variable El Niño-Southern Oscillation throughout the holocene, *Science*, 339, 67-70, doi: 10.1126/science.1228246.

Collins, W. D., P. J. Rasch, B. A. Boville, J. J. Hack, J. R. McCaa, D. L. Williamson, B. P. Briegleb, C. M. Bitz, S.-J. Lin, and M. Zhang (2006), The formulation and atmospheric simulation of the Community Atmosphere Model Version 3 (CAM3), *J. Clim.*, *19*, 2144-2161.

Collins, M., Soon-Il An, W. Cai, A. Ganachaud, E. Guilyardi, F. Jin, M. Jochum, M. Lengaigne, S. Power, A. Timmermann, G. Vecchi & A. Wittenberg et al. (2010), The impact of global warming on the tropical Pacific Ocean and El Niño, *Nature Geoscience*, 3, 391-397, doi: 10.1038/ngeo868.

Compo, G. P. (2010), Removing ENSO related variation from climate record, *J. Clim.*, *23*, 1957-1978.

Eichler, T., and W. Higgins (2006), Climatology and ENSO-related variability of North American extratropical cyclone activity, *J. Clim.*, *19*, 2076-2093.

Hoerling, M. P. (1994), Organization of extratropical transients during El Niño, *J. Clim.*, *7*, 745–766.

Hoskins, B. J., and P. J. Valdes (1990), On the existence of storm tracks, *J. Atmos. Sci.*, *47*, 1854-1864.

Hoskins, B. J., and K. I. Hodges (2002), New perspective on the Northern Hemisphere winter storm tracks, *J. Atmos. Sci., 59*, 1041-1061.

Hurrell, J. W., J. J. Hack, A. S. Phillips, J. Caron, and J. Yin (2006), The dynamical simulation of the Community Atmosphere Model Version 3 (CAM3), *J. Clim., 19*, 2162-2183.

Hurrell, J. W., J. J. Hack, D. Shea, J. M. Caron, and J. Rosinski (2008), A new sea surface temperature and sea-ice boundary dataset for the Community Atmosphere Model, *J. Clim., 21*.,5145-5152

Lu, J., G. Chen, and D. M. W. Frierson (2008), Response of the zonal mean atmospheric circulation to El Niño versus global warming, *J. Clim., 21*, 5835-5851.

McCabe, G. J., M. P. Clark, and M. C. Serreze (2001), Trends in Northern Hemisphere surface cyclone frequency and intensity, *J. Clim., 14*, 2763-2768.

Orlanski, I. (2005), A new look at the Pacific storm track variability: Sensitivity to tropical SSTs and to upstream seeding, *J. Atmos. Sci., 62*, 1367-1390.

Straus, D. M., and J. Shukla (1997), Variations of midlatitude transient dynamics associated with ENSO, *J. Atmos. Sci., 54*, 777–790.

Trenberth, K. E., and J. W. Hurrell (1993), Decadal atmosphere - ocean variations in the Pacific, *Clim. Dyn.*, 303-319.

Yin, J. H. (2005), A consistent poleward shift of the storm tracks in simulations of 21st century climate, *Geophys. Res. Lett., 32*, L18,701, doi:10.1029/2005GL023684

Zhang, X., J. E. Walsh, J. Zhang, U. S. Bhatt, and M. Ikeda (2004), Climatology and interannual variability of Arctic cyclone activity: 1948–2002, *J. Clim.*, *17*, 2300-2317.

Zhang, Y., and I. M. Held (1999), A linear stochastic model of a GCM's midlatitude storm tracks, *J. Atmos. Sci.*, *56*, 3416–3435.

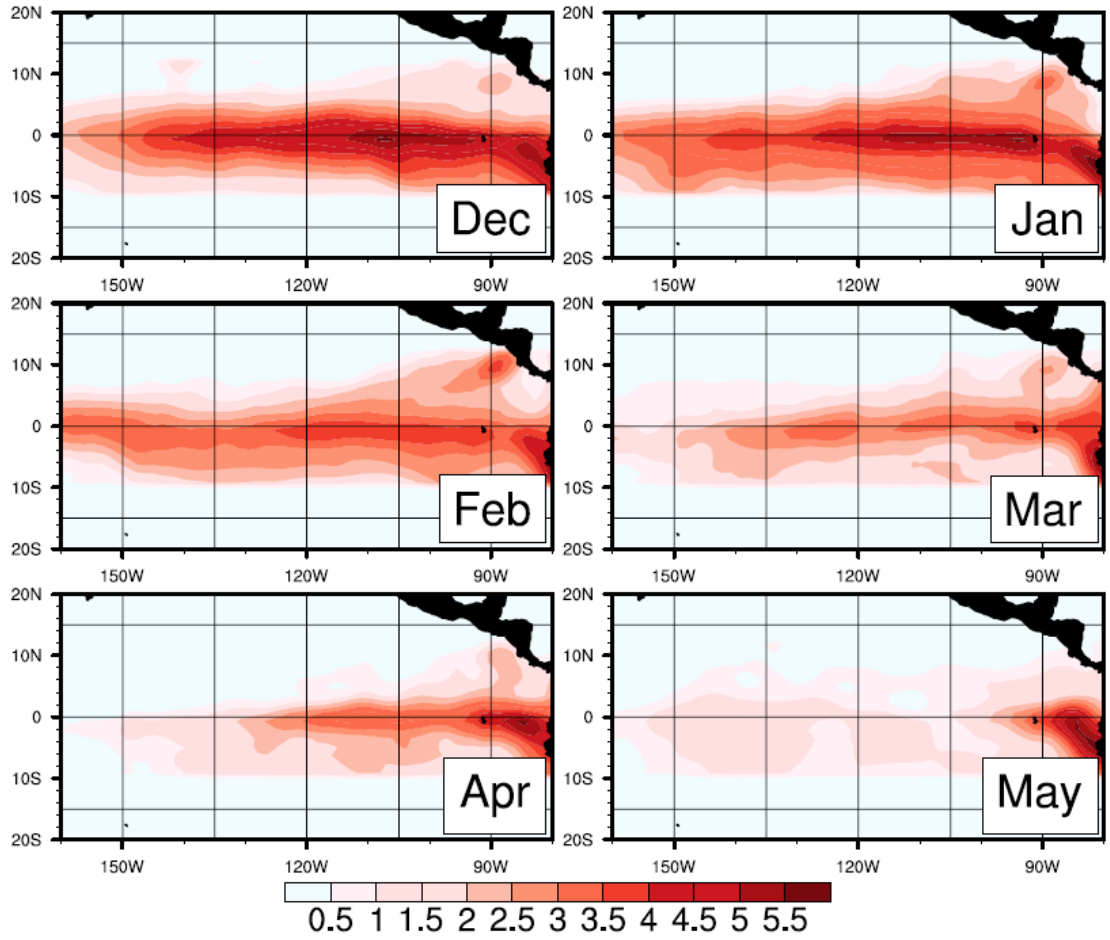

Figure 2.1 Positive SST Anomalies applied to define surface forcing for the sensitivity experiment (SenExp) from December to May.

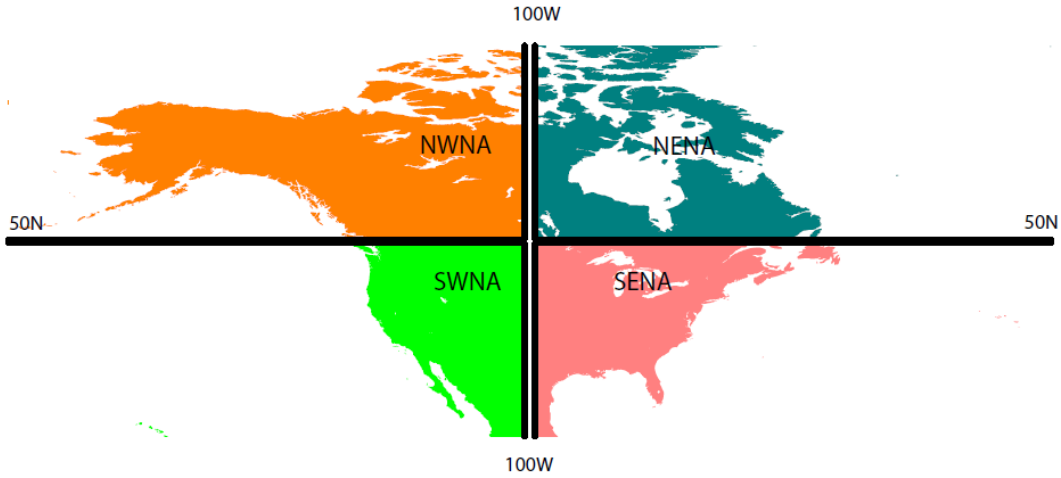

Figure 2.2 The four sub-regions used in this study: SWNA (20ºN-50ºN, western coastline to 100ºW); SENA (20ºN-50ºN, 100ºW to Eastern coastline); NWNA (50ºN-80ºN, western coastline to 100ºW); and NENA (50ºN-80ºN, 100ºW to Eastern coastline).

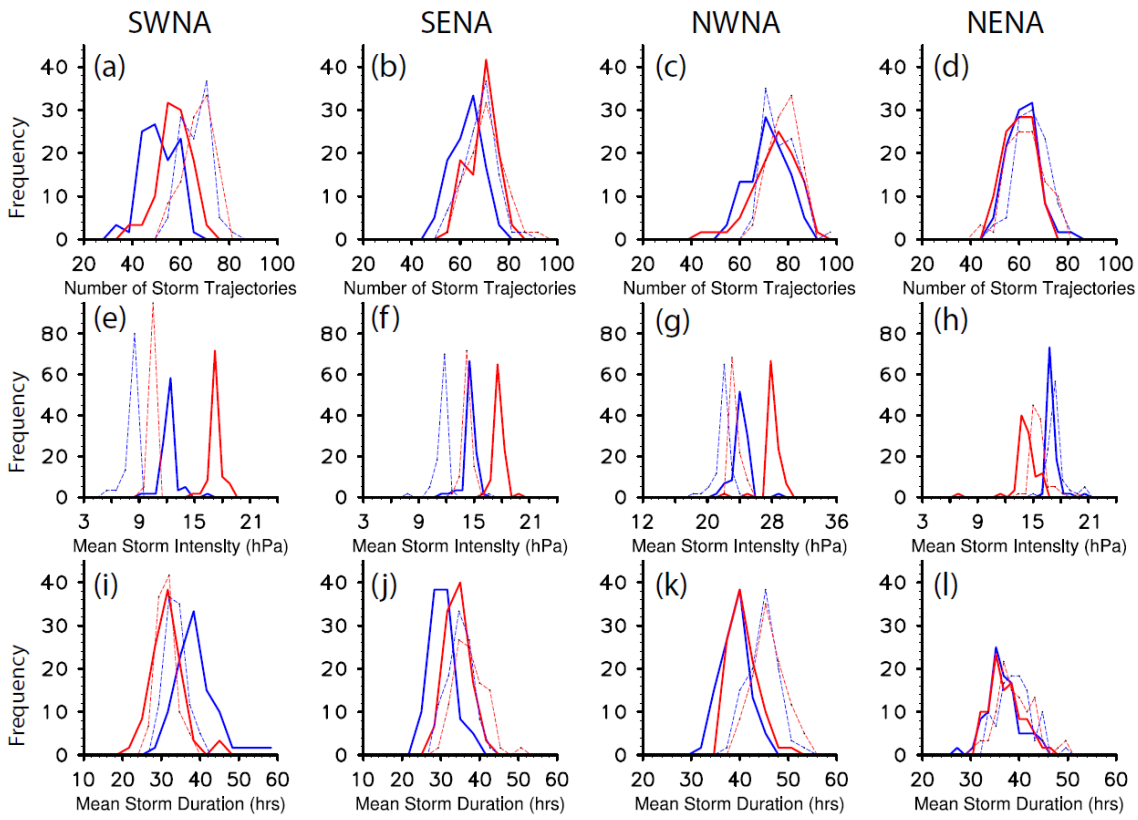

Figure 2.3 Probability Density Functions (PDFs) of the number of storm trajectories (a-d); the mean storm intensity (e-h); and the mean duration (i-l) for the four sub-regions in winter (solid lines) and spring (dashed lines). The blue (red) color represents the results from the ConExp (SenExp).

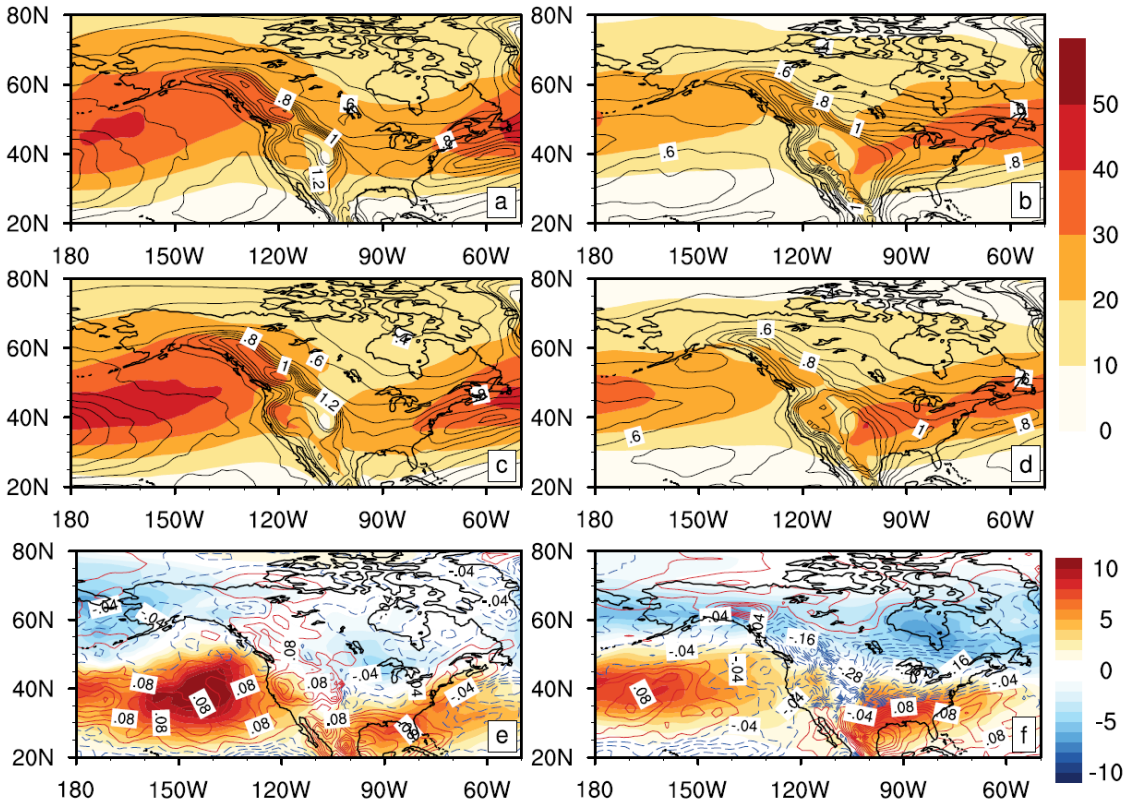

Figure 2.4 Transient Eddy Kinetic Energy (KJ/m^2, shaded) and superimposed Eady Growth Rate Maximum (day^{-1}, contours) at 775 hPa in ConExp for winter (a) and spring (b). (c) and (d) are the same as (a) and (b), but for SenExp. The differences between SenExp and ConExp are displayed in (e) for winter and (f) for spring.

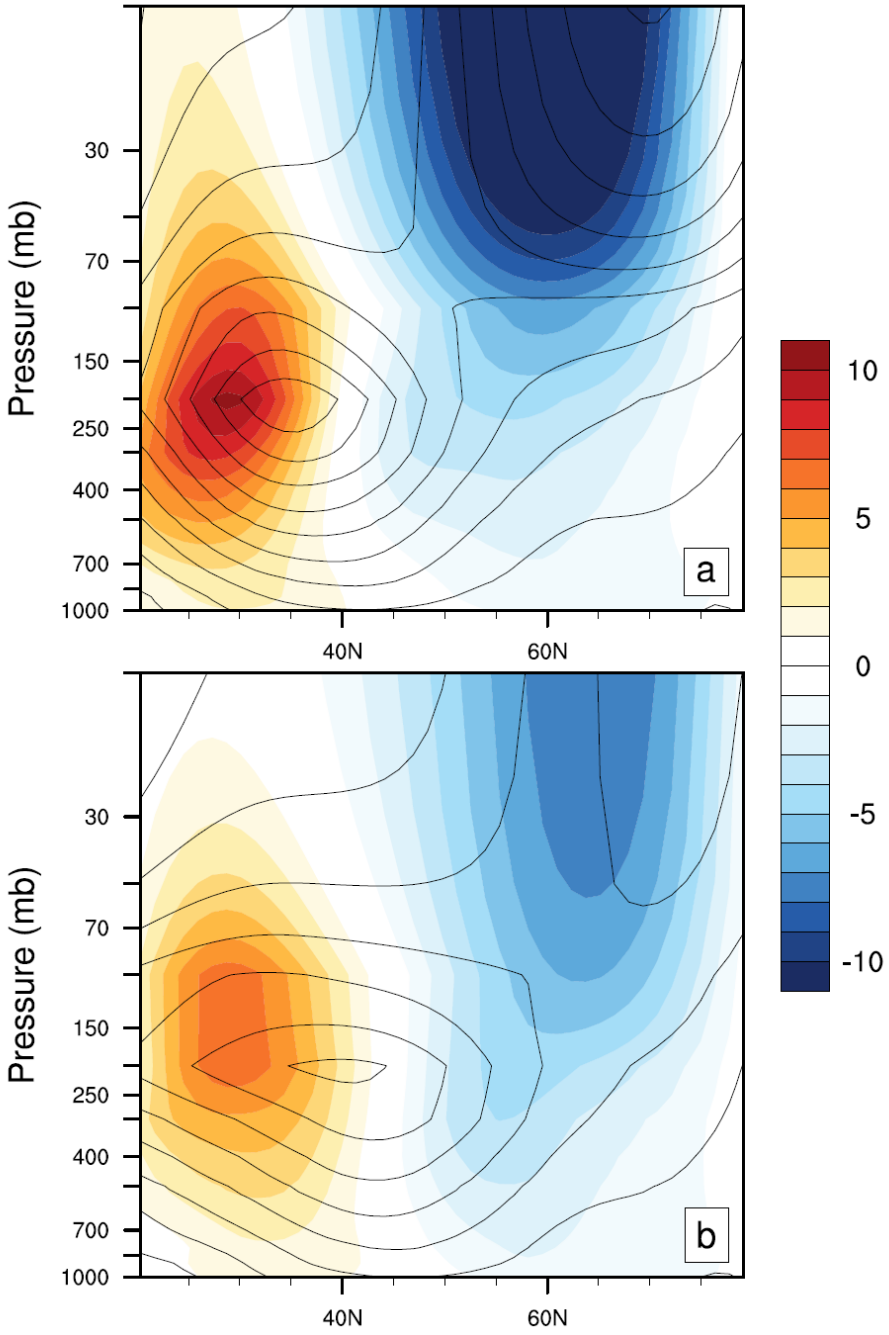

Figure 2.5 Zonally averaged (between 180°-310º) climatological zonal wind (contours) and the differences between SenExp and ConExp (shaded) across the vertical section along 20°N-80°N for winter (a) and spring (b).

Chapter 3 Response of Northern Hemisphere Mid- and High- Latitude Storm Activity to Arctic Sea ice Forcing: A Modeling Investigation[1]

Abstract

Arctic sea ice has exhibited a rapid reduction and large fluctuations during recent decades in conjunction with a warming climate. To identify sea ice impacts on extratropical storm tracks and associated surface climate, we employed the NCAR's Community Atmosphere Model to conduct a suite of modeling experiments, in which is solely forced with observed time-varying sea-ice concentration was prescribe from 1979 to 2008. A storm identification and tracking algorithm was applied for analyzing variability of and changes in storm activities simulated by the model. The results show that reduced sea-ice cover enhances Arctic storm activity and increases warm moist air advection into the Arctic. As a consequence, Arctic surface air temperature (SAT) throughout the year and precipitation in spring, summer and fall seasons increase. By contrast, storm activity weakens and anticyclones strengthen over Eurasia. The strengthened anticyclones lead to a decrease in cloud cover, precipitation and SATs in both fall and winter seasons. These findings also suggest that Arctic sea ice not only impacts local, but also lower latitude weathers and climate.

[1] S. Basu , X. Zhang 2014: Response of Northern Hemisphere Mid and High Latitude Storm Activity to Arctic Sea-ice Forcing: A Modeling Investigation, Journal of Climate, to be submitted to Journal of Climate.

3.1 Introduction

The Arctic has undergone dramatic changes over recent decades in conjunction with a warming climate. There have been many studies showing the impact of warming on Arctic sea ice using observational and modeling data [e.g. *Comiso,* 2003*; Singarayer et al.,* 2006*; Zhang and Walsh,* 2006*; Holland et al.,* 2006*; Bhatt et al.,* 2008*;* 2013*, Polyakov et al.,* 2012]. The Arctic Ocean has lost 40% of its multiyear ice between 2004 and 2009 [*Kwok and Rothrock* 2009]. In 2007, the year with the second lowest sea ice area during the satellite record, the highest mean SAT over the Arctic in the instrumental observations was recorded [*Bekryaev et al*., 2010]. The warming pattern is characterized by lower SAT anomalies in lower latitude regions and higher SAT anomalies over the Arctic, known as Arctic Amplification [e.g. *Alexeev et al*., 2005; *Serreze and Francis,* 2006*; Serreze et al.,* 2009; *Bekryaev et al*., 2010; *Bader et al*., 2011]. Advective transport is among the major causes of enhanced Arctic warming [*Graversen*, 2006; Graversen et al., 2010; *Zhang et al.,* 2008; *Serreze et al*., 2009; *Porter et al*., 2012]. Variations of atmospheric circulation represented by the Arctic Oscillation [*Thompson and Wallace,* 2000] and modulated by the Pacific Decadal Oscillation also influence recent spatial patterns of temperature change [*Mantua and Hare*, 2002]. A number of recent studies also indicate that a spatial transformation of atmospheric circulation, described by the "Arctic Rapid Change Pattern" for the entire Northern Hemisphere [*Zhang et al.*, 2008], or "Arctic Dipole" for the Arctic Ocean [*Overland et al*., 2011], can substantially amplify Arctic warming and sea ice decrease.

Herman and Johnson [1978] performed a global modeling study by imposing pan-Arctic maximum and minimum sea-ice edge variations and found that sea-ice extent anomalies are correlated with atmospheric pressure anomalies. Decreased sea ice also causes increased surface heat fluxes and increase of SAT due to ice-albedo feedback [e.g *Manabe and Stouffer*, 1980; *Curry et al*., 1995; *Bhatt et al*. ,2008]. Although the strongest decay of Arctic sea ice is in summer and fall, the largest surface flux and temperature response was found in winter [*Alexander et al.* 2004; *Deser et al. 2010*; *Bader et al*. 2011]. Petoukhov and Semenov [2010] showed that decreased sea ice in the Barents and Kara seas can change the atmospheric circulation and can cause severe cold events. However, there were not too many attempts to identify the role of Arctic sea ice in variability of and changes in Northern Hemisphere extratropical storm activities and associated surface climate.

Consequences of changes in Arctic sea ice are not limited to the Arctic region only; there is evidence that these changes in Arctic sea ice affect lower latitudes through altering large-scale patterns of variability such as the Arctic Oscillation and the North Atlantic Oscillation or exciting Rossby wave train propagation [*Honda et al.,* 2009*, Balmaseda et al.,* 2010, *Petoukhov and Semenov*, 2010, *Wu and Zhang*, 2010, *Blüthgen et al*., 2012, *Francis and Vavrus*, 2012, *Overland et al*., 2010; 2014]. Dethloff et al. [2006] argued that changes in surface processes impact global climate systems through an atmospheric wave bridge between the Arctic and lower latitudes.

In addition to the changes in the large-scale atmospheric circulation, much attention has been recently paid to extreme weather events in the mid-latitudes, which are generally driven by synoptic weather systems including storms and anticyclones. Observational data analysis and climate model simulations have indicated an overall poleward shift of storm tracks and an intensification of storm activity in northern high latitudes and the Arctic along with a warming climate [e.g. *McCabe et al*., 2001; *Zhang et al.*, 2004; *Yin*, 2005]. However, a close examination also suggests a strong regional and seasonal dependence of the storm activity, which has caused various extreme weather events. Severe cold winters with intensified anticyclones and weakened cyclones have been observed over the mid-latitude (especially Eurasia) in the recent years [*Zhang et al*., 2012].

In this modeling study we investigate changes in extratropical storms in response to the observed Arctic sea ice changes and variability. The corresponding changes in surface climate are also examined. To this end, we adopted a Lagrangian approach [*Zhang et al*., 2004] to study the storm tracks. We first identified and tracked each storm from the 6 hourly sea level pressure (SLP) snapshots from a general circulation model and studied the subsequent changes in storm activities. The changes in storm activities can impact surface climate. Thus, we further examined the changes in surface climate parameters such as SLP, SAT, surface wind, total precipitation and total snowfall over the mid-latitudes and the Arctic.

3.2 Model Experiment Designs and Data Analysis Method

We employed the National Center for Atmospheric Research (NCAR) Community Atmosphere Model (CAM) version 3.1_p2 [*Collins et al*. 2006; *Hurrell et al*., 2006]. For our modeling experiments, we configured the model at T85 resolution (approximately 1.4º in both latitude and longitude) with 26 vertical levels. Monthly SST and sea ice data sets [*Hurrell et al*., 2008] were used as the surface boundary forcings (Figure 3.1). We studied the impact of Arctic sea ice on the mid- and high-latitudes storms over the Northern Hemisphere only; however, the model simulations were global. To construct robust results we conducted five ensembles of our experiment with each ensemble starting from different initial conditions and each ensemble was run from January 1979 to December 2008, saving 6-hourly instantaneous outputs of selected variables.

In our experiments, sea-ice concentration over the Arctic was assigned to their observed values for the period of January 1979 to December 2008. Sea-ice concentration over the Southern Hemisphere was prescribed to its climatological values and SSTs were fixed at their climatological values all over the globe. Bilinear interpolation was used to prescribe SST to the grid cells contiguous to the southern sea-ice edge in the Arctic.

To investigate the extratropical storms, we employed the storm identification and tracking algorithm and applied this algorithm to the 6-houly SLP outputs from each model ensemble. This algorithm first identifies a low SLP center which has at least a minimum SLP gradient of 0.15 hPa with the surrounding grid points and survives for more than 12 hours. More details about this algorithm and its application for investigating

Northern Hemisphere storm tracks can be found in Zhang et al. [2004]. Considering distinct features of climatological storm activity, we divided the Northern Hemisphere continent into two sub-regions in this study: the mid-latitude and the Arctic. The mid-latitude region was further divided into four sub-regions with prominent storm activities: North Atlantic, North Pacific, Eurasia and North America (Figure 3.2).

The storm identification and tracking algorithm provided various parameters describing storm activity, including duration or lifetime, central location, and central SLP for each individual storm occurring over the study area. By using the data sets of these parameters from each ensemble member of our experiment, we obtained the number of storm trajectories, mean storm duration, and mean storm intensity for each sub-region in winter (December-February), spring (March-May), summer (June-August) and fall (September-November). The storm trajectory was defined from the time of storm generation until dissipation within the region or from the time when the storm enters the region until the time it leaves the region. The mean duration for each region was the averaged duration throughout the total number of storm trajectories. The storm intensity for each individual storm was calculated as a difference between the storm's central SLP and the monthly mean SLP at the corresponding location. The mean storm intensity for each region was obtained by averaging storm intensities throughout their duration and over the number of storm trajectories.

3.3 Results

3.3.1 Changes in Storm Activity

In this section, we show that reduced Arctic sea ice resulted in increased storm activity over the Arctic and weakened storm activity over Eurasia in most seasons. In order to study changes in the mean number of storm trajectories, mean intensity and mean duration a composite analysis was performed on all the model's ensembles. A probability density function (PDF) analysis based on the composites of the years with detrended sea-ice extent outside a critical value of ± 0.5 standard deviation (σ) was performed (Figure 3.3). This critical value was chosen in order to maximize the number of years for each composite. We named the composite of the years above positive critical value as Pos and the combined years below the negative critical value as Neg and we will use these acronyms hereafter. To assess statistical significance of the difference in means between the Pos and Neg years, a t-test was applied to the storm and surface climate parameters.

The spatial composite of enhanced below average sea-ice concentration is identified as Neg – Pos and seasonal plots are shown in Figure 3.4. The largest negative sea ice anomalies in winter were over the Bering, Norwegian and Barents seas – i.e., in the marginal ice zone (MIZ). In spring, it was over the Barents and Bering seas. As expected, in summer the ice reduction was the largest of all the seasons and occurred over the largest area in the Arctic Ocean including the Chukchi, Laptev and Barents seas. In fall, ice reduction was most prominent over the Beaufort, Chukchi, Laptev and Barents seas.

The PDFs of mean number of storm trajectories for Pos and Neg years across each geographical region and during each season are shown in Figure 3.5. These PDFs demonstrate that during winter the peak frequency shifted towards a higher number of storms, from 26 to 29 over the North Atlantic (Figure 3.5a) and occurrence of peak frequency increased from 20% to 30% over the North Pacific during winter (Figure 3.5e). In spring a decreased percentage of occurrences of peak frequency from 40% to 30% was found for the North Atlantic region (Figure 3.5b). A slight increase in peak frequency was found over the Arctic. In summer the peak frequency is shifted towards a lesser number of storm trajectories from 36 to 32 over the Arctic (Figure 3.5s) whereas over Eurasia the percentage of occurrence of peak frequency decreased from 46% to 34% (Figure 3.5k). In fall there was a noticeable increase in peak frequency of occurrences from 36% to 60% for the North Atlantic region (Figure 3.5d). Over the North Pacific, the peak frequency increased from 30 to 36 with a decrease in percentage of occurrences of peak frequency from 44% to 30% (Figure 3.5h). Other changes in PDFs were not significant.

In our analysis, we identified the changes in mean storm intensity in response to anomalous Arctic sea ice (Figure 3.6). In winter, a weakening of storms over the Arctic under reduced ice conditions was found as the peak shifted towards weaker intensity of storms from 22 to 16 hPa (Figure 3.6q). In spring, under reduced sea-ice conditions, the peak storm intensity over the North Pacific decreased by 40% from 20 to 12 hPa (Figure 3.6f) and over Eurasia decreased from 15 to 13 hPa (Figure 3.6j). In summer there was a reduction of 23% in the peak from 13 to 10 hPa signifying less intense storms over

Eurasia (Figure 3.6k). In contrast, over the Arctic there has been an increase in frequency of occurrences of the peak storm intensity from 38% to 46% under reduced Arctic sea-ice condition (Figure 3.6s). In fall an increased percentage of occurrences of peak frequency of mean storm intensity from 30% to 46% was simulated over the North Atlantic (figure 3.6d) and increased peak intensity from 13 to 17 hPa was found over the North Pacific (Figure 3.6h). There were many other changes in PDFs but they were not significant.

Figure 3.7 shows the PDF analysis for the mean duration of the storms for each of the regions for Pos and Neg years. Comparing winters of Neg versus Pos illustrates that mean storm duration is longer both over the North Atlantic (30 versus 35 hours) (Figure 3.7a) and the North Pacific (40 versus 44 hours) (Figure 3.7e). In spring, the peak frequency shifted towards shorter duration from 40 to 36 hours, i.e. a 10% decrease in mean duration over Eurasia (Figure 3.7j) and towards longer duration from 40 to 48 hours over the Arctic, a substantial 20% increase (Figure 3.7r). In summer, the percentages of occurrence of peak frequency increased from 30% to 44% over the North Pacific (Figure 3.7g). Over the Arctic percentages of occurrences of peak frequency increased from 32% to 44% (Figure 3.7s). The peak frequency of mean duration shifted towards longer duration from 34 to 40 hours, which is an 18% increase in mean duration over the North Atlantic (Figure 3.7d) and the percentage of occurrences peak frequency increased from 32% to 50% over the North Pacific in fall (Figure 3.7h). The other changes in the PDFs were not significant.

In order to express the overall storm activity over each region during each season we calculated cyclone activity index (CAI) anomaly [Zhang et al. 2004]. CAI is an integrated index which simultaneously characterizes several storm parameters – number of storm trajectories, mean intensity and mean duration. This index was calculated by summing the differences in storm center SLPs and the climatological SLPs at the corresponding grid points, over a region. An increase (decrease) in the CAI anomaly indicates an increase (decrease) in storm activity.

Figure 3.8 shows that in winter over the Arctic, the CAI anomaly decreased from +5 to 0 (Figure 3.8q), which is attributed to a decrease in the mean intensity of the storms. In spring the peak frequency of CAI anomalies decreased from +3 to -4 over the North Pacific (Figure 3.8f). This reduced storm activity was related to decreased storm intensity and duration. Over Eurasia under reduced Arctic sea-ice conditions, CAI anomalies showed an increase of percentage of occurrences of peak frequency from 35% to 50%, with a slight shift in the peak from +1 to -1 (Figure 3.8j). The decreased overall storm activity over Eurasia in spring was primarily caused by a decrease in the mean intensity of the storm. Over the Arctic, the occurrence of peak frequency percentage of CAI anomaly increased from 22% to 27% in spring which was caused by an increased number of storm trajectories and increased mean intensity (Figure 3.8r). In summer, the peak frequency showed a decrease from +1 to -1 over Eurasia with increased percentage of occurrences of peak frequency from 45% to 60% (Figure 3.8k). This prominent summer decrease in overall storm activity over Eurasia was caused by a decrease in number of storm trajectories, mean intensity and mean duration of the storms over Eurasia. The peak

frequency of CAI anomaly showed a slight increase from 0 to +1 over the Arctic that was caused by increased storm intensity and duration of storms (Figure 3.8s). However, due to a large decrease in the number of storm trajectories over the Arctic, the increase in overall storm activity was small. In fall, the peak frequency shifted from -2 to +2 over both the North Atlantic and North Pacific (Figure 3.8d, 3.8h). This increase in storm activity was caused by an increased number of storm trajectories, mean intensity and mean duration. Over the Arctic, in fall the peak frequency increased from -2 to + 2 as well (Figure 3.8t). However, this increase in overall storm activity over the Arctic in fall was caused by an increased number of storm trajectories only.

From our analysis of the PDFs, we conclude that in response to reduced Arctic sea ice there was increased storm activity over the Arctic in spring, summer and fall. This is in contrast to the reduced storm activity over Eurasia. Under reduced Arctic sea-ice conditions we expect that these changes in storm activities are associated with altered surface climate parameters over the mid- and high-latitudes. Thus, in the next section we examined sea level pressure.

3.3.2 Changes in Sea Level Pressure

In the above analysis we employed a Lagrangian approach to identify and track synoptic scale storms. Here we complement this analysis by using an Eulerian method to represent the overall storm activity at each grid point in terms of SLP. The composite mean of SLP for the Pos and Neg years resembles the climatological spatial distribution of SLP (Figure 3.9). In both Pos and Neg years the lowest Northern Hemisphere SLP is over the Aleutian

Islands and Iceland which represents the North Pacific and the North Atlantic storm pathways, respectively. The highest pressure is seen over Eurasia and over the Pacific off the west coast of southern California.

The most striking difference between Pos and Neg years is an increased SLP over the Arctic and Eurasia by ~3 hPa in winter (Figure 3.9). The positive anomaly of SLP is consistent with decreased storm activity under reduced Arctic sea-ice conditions as indicated by a decreased CAI anomaly over the Arctic and Eurasia (Section 3.3.1). The pattern of SLP anomaly in winter with positive anomalies over the Arctic and negative anomalies over North Pacific and North Atlantic is similar to the negative phase of Arctic Oscillation [Thompson and Wallace, 2000]. In spring, Arctic SLP decreased by 1.5 hPa; however there was a large increase of SLP over the North Pacific by 2 hPa. In spring, negative SLP anomalies over the Arctic was caused by the increased storm activity associated with reduced Arctic sea ice. However, there was decreased storm activity over the North Pacific which agrees well with the increased SLP. In summer, reduced sea ice caused decreased SLP over the Arctic by 1.5 hPa consistent with increased storminess. The most prominent feature of the SLP pattern in fall was increased SLP over Eurasia by 1.5 hPa related to decreased storm activity. The weakened storm activity over Eurasia as found from the analysis of CAI anomalies resulted in the intensification of Eurasian anticyclones causing the positive SLP anomaly there. However, a decrease in SLP by ~ 2hPa was found over the Arctic due to increased storm activity there. Thus, reduced Arctic sea ice results in a decrease of SLP over the Arctic during spring, summer and fall and this negative SLP anomaly results from increased storminess over the Arctic,

consistent with the regional Arctic sea-ice anomalies. A prominent increase in SLP was found over Eurasia during most of the seasons. This positive SLP anomaly over Eurasia may also be attributed to the decreased storm activity.

3.3.3 Changes in Cloud Cover

Changes in SLP greatly influence the cloud cover over a region. Therefore in this section we analyzed the vertically integrated total cloud cover. Figure 3.10 demonstrates that in both Pos and Neg years the highest cloud cover was over the regions with greatest storminess i.e. the North Pacific and the North Atlantic. In summer, there was high cloud cover over the Arctic. Figure 3.10 shows the differences between Neg and Pos years, where in winter reduced sea ice leads to decreased cloud cover over the Arctic and Eurasia, which was consistent with decreased storm activity and increased SLP. In spring when sea ice is below normal, total cloud cover over Alaska and the entire Arctic displays positive anomalies. In summer, there was increased cloud cover over the North Pacific and over the Arctic along the coast, which was largely consistent with regional reduction of sea ice. In fall, there was a significant increase in cloud cover the Arctic, which is consistent with the increased regional storminess. Although the changes were small (ranging from -5% to 5%), an increase (decrease) in cloud cover during each season corresponds well to the increase (decrease) in storm activity and the abovementioned changes in regional SLP patterns over these regions. Radiative feedback from the cloud cover plays a driving role in the SAT over a region, thus in the next section we examined spatial changes in SAT due to reduced Arctic sea ice.

3.3.4 Changes in SAT and Surface Wind

Figure 3.11 shows spatial distribution of the SAT and surface wind in Pos and Neg years and the difference between Neg and Pos years for four seasons.

In winter, the most prominent positive SAT anomalies were observed over the Bering, Greenland and Barents seas regions i.e. the MIZ which has the largest sea-ice anomalies. The strongest negative winter SAT anomaly was found over Eurasia extending into the Arctic. An anticyclonic wind anomaly suggesting intensification of anticyclones over Eurasia and the Arctic was found which is consistent with the increased SLP and decreased storminess there. However, strong positive SAT anomalies over the MIZ do not necessarily result in strong regionally averaged SAT anomalies as shown by the PDF analysis (Figure 3.12): according to this analysis, the changes over the Arctic were not notable. At the same time, the PDF analysis demonstrates a decreased percentage of occurrences of peak frequency of regionally averaged SAT from 42% to 30% over Eurasia in winter.

In spring, a large wide-spread warming caused by reduced Arctic sea ice was found over the entire Arctic and the northern part of Eurasia and North America. From the PDF analysis, it was found that reduced Arctic sea ice caused the peak frequency of area averaged SAT to shift towards higher SATs from -16 to -12 °C over the Arctic and from 4 to 5 °C over the North Pacific. A prominent change in the PDFs for North America, North Atlantic and Eurasia was also found, consistent with the warming under reduced Arctic sea-ice conditions in spring. The percentage of occurrences of peak frequency of

area averaged SAT increased from 45% to 70% over the North Atlantic, 50% to 65% over Eurasia and from 40% to 60% over the North America. A cyclonic wind anomaly was found over the Arctic in association with the increased storminess and a corresponding decreased SLP. Anticyclonic wind anomalies related to the positive SLP anomalies shown in Figure 3.9 over Eurasia and the North Pacific were found. These anomalies suggest an intensification of anticyclones over Eurasia and North Pacific and enhanced warming.

In summer, the SAT changes showed a broad pattern of modest cooling over the Arctic, northern North America and Eurasia. Weak positive anomalies of SAT were found over the western part of Europe and continental USA. An increased peak frequency from 13 to 15 °C was found over the North Atlantic and increased percentage of occurrences of peak frequency from 70% to 90% over North America shown by the PDF analysis confirmed that moderate warming was found in the spatial SAT anomalies under reduced Arctic sea-ice cover in summer.

In fall there was a positive SAT anomaly over the Arctic in the MIZ region along with a cyclonic wind anomaly due to increased storminess. From the PDF analysis it was found that percentage of occurrences of peak frequency of area averaged SAT over the Arctic increased from 60% to 80%. However, a cooling pattern extended over the continents during fall under reduced Arctic sea ice. PDF analysis further demonstrated that there was a shift in the peak frequency towards lower SATs from 10 to 9 °C over the North Pacific and from 4 to 2 °C over Eurasia.

Similar composite analysis was performed on monthly global SATs from ERA Interim datasets in order to compare our prominent changes in SAT with the observations (Figure 3.13). In the comparison it was found that our findings of SAT anomalies in response to reduced Arctic sea ice were consistent with the observed SAT anomalies. A similar warming pattern persists over the Arctic in spring and fall, while a similar cooling pattern occurs over the Arctic in winter and summer. We found a cooling in contrast to the warming over the mid-latitude in fall. But it is to be noted that our study excludes the effect of time varying SST and southern hemisphere sea ice.

3.3.5 Changes in Total Precipitation Rate and Total Snowfall Rate

Figure 3.14 showing Neg and Pos differences suggest that in winter the total precipitation and total snowfall decreased over Eurasia by 0.1 to 0.2 mm/day which was consistent with the earlier discussions of a strengthening of the high pressure and decreased storm activity. We also found a notable increase in total precipitation over the Western Europe.

In spring, with below normal sea ice, the total precipitation and snowfall is higher over Alaska, Northern Canada and the Arctic ranging from 0.05 to 0.2 mm/day due to increased storm activity. The PDF analysis (Figure 3.15) showed that the percentages of occurrences of peak frequency of total precipitation increased from 70% to 80% over the Arctic. There is decreased precipitation and snowfall over Eurasia by 0.1 to 0.2 mm/day that corresponds to reduced storm activity there. There is another prominent decrease in total precipitation over the North Pacific by 0.05 to 0.2 mm/day. These anomalies in spatial distribution were also reveled by the PDF analysis as the percentage of

occurrences of peak frequency of total precipitation decreased from 75% to 55% over the North Pacific and 80% to 60% over Eurasia. The decrease in precipitation over Eurasia and the North Pacific were associated with an intensification of anticyclones due to reduced storm activity.

In summer under reduced sea ice, there is an increase in total precipitation over the entire Arctic by 0.05 to 0.25 mm/day. The increased total precipitation corresponds well to increased storminess over the Arctic and also agrees with the negative Arctic SLP anomaly and cyclonic wind anomaly. From the PDF analysis it was found that under reduced sea-ice conditions in summer the percentages of occurrences of peak frequency of total precipitation increases from 50% to 60% over the Arctic. This increased precipitation was due to increased storminess over the Arctic. Over Eurasia the peak frequency of total precipitation shifted towards lower precipitation from 2.3 to 1.8 mm/day, which denotes dry summer. The storm activity over Eurasia weakened, which resulted in a decreased precipitation.

In fall there is a noticeable increase in total precipitation over the Arctic by 0.05 to 0.25 mm/day corresponding to an increased storminess and a negative SLP anomaly over the Arctic. A prominent increase in total precipitation was observed over the United Kingdom and Western Europe by 0.2 to 0.25 mm/day in fall. The PDF analysis showed that in fall peak frequency of total precipitation increases from 3 to 4 mm/day over the North Atlantic and shifted from 1.8 to 2.4 mm/day over the Arctic. In contrast with that

there was a decreased total precipitation over the Alaska, the northern Eurasia and North America.

3.4 Discussion

In the previous sections we have shown that reduced Arctic sea ice caused substantial anomalies in storm activity and surface climate parameters. The relationship between reduced sea ice, the storm activities and their effect on surface climate is summarized in a graphic for each season (Figure 3.21).

In winter (Figure 3.21a) the negative Arctic sea-ice anomalies were most prominent over the MIZ in the Bering, Barents and Norwegian seas. A positive SAT anomaly, increased cloud cover and total precipitation were also found over the MIZ, as (we hypothesize) a result of anomalous surface sensible and latent heat fluxes (Figure 3.18 - 3.19). Decreased storm activity, associated with increased SLP, anticyclonic wind anomalies and decreased total precipitation were found over the central Arctic and Eurasia. Enhanced outgoing longwave radiation (LW) (Figure 3.17) resulted from intensified anticyclone over eastern Eurasia which extends into the central Arctic and weakened advections (Figure 3.20) caused by anomalous south western winds are plausible candidates to explain lower SAT over these regions.

The negative anomalies of Arctic sea ice *in spring* (Figure 3.21 b) mainly occurred over the MIZ in the Bering and Barents seas. Reduced sea ice resulted in dramatic warming over the Arctic and (to a lesser degree) mid-latitudes - one of the most pronounced changes found in our experiments. There were prominent positive SAT anomalies located

over the Barents Sea which extends into Eastern Eurasian continent and over the MIZs extending into western Arctic. There was a decreased storminess associated with increased SLP, less clouds which resulted in enhanced shortwave (SW) heating (Figure 3.16) over the continental mid-latitude regions. The land-ocean temperature contrast was manifested through an increased storm activity, associated with decreased SLP, cyclonic wind anomaly and increased precipitation, over the Arctic. The increased storm activity caused an increased heat advection (Figure 3.20) into the Arctic, through the Bering Strait along eastern coast of Eurasia and through Nordic Seas contributing to the anomalous warming pattern in spring. Anomalous sensible and latent heat fluxes (Figure 3.18-3.19) due to reduced sea ice made a local contribution to these regional warmings over the Arctic.

Summer (Figure 3.21c) had the largest anomaly in Arctic sea ice which occurred over the MIZ in the Chukchi, Laptev and Barents seas. In response to reduced Arctic sea ice we found a contrastingly modest response of SAT in the high- and mid-latitude regions including a slight decrease in SAT over the high latitudes. We also found an increase of storm activity associated with an increased cloud cover and total precipitation over northern North America, northern Eurasia and the Arctic. The increased cloud cover caused a decrease in downward shortwave radiation (Figure 3.16) which is possibly one of the contributors for this negative SAT anomaly over the high-latitudes in summer. In association with the increased storminess decreased SLP and a cyclonic wind anomaly was also found over the Arctic. These synchronous changes of increased precipitation and cooling over the Arctic are consistent with the findings of Bhatt et al. in a modeling

study [2008] and with finding in Bhatt et al. [2013] in an analysis of observational data respectively.

In fall (Figure 3.21d) the most prominent sea-ice anomalies were also located in the MIZ in the Beaufort, Chukchi, Laptev and Barents seas. A remarkable positive SAT anomaly was found over the Arctic MIZ over the Siberian shelf probably due to the enhanced albedo feedback and anomalous longwave, latent and sensible heat fluxes particularly over ice-free water (Figure 3.18-3.19). We found increased storm activity along with a cyclonic wind anomaly, increased cloud cover and total precipitation over the Arctic MIZ. The increased warm air advection associated with increased storminess made further contribution to the warming over the Arctic (Figure 3.20). An anticyclonic wind anomaly and increased SLP in association with decreased storm activity dominated Eurasia. This intensification of anticyclones over Eurasia caused a prominent cooling over the continent due to outgoing longwave radiation (Figure 3.17).

There is a growing number of studies which suggest that storminess has increased over the Arctic in warmer climate that is linked to the loss of sea ice [e.g. *McCabe et al*., 2001; *Zhang et al*., 2004; *Yin*, 2005]. In this study we have demonstrated that in response to reduced Arctic sea ice there is indeed increased storm activity over the Arctic in spring, summer and fall. We have also found that the Arctic is responding with springtime warming in response to reduced sea ice, which is consistent with the findings from previous studies [e.g. *Singarayer et al*., 2006; *Comiso*, 2003; *Bhatt et al.*, 2008; 2013; *Budikov*a, 2009]. The most remarkable finding in our SAT analysis was the cooling over

the Arctic in summer. Some of the previous studies have shown similar cooling pattern over the continental Arctic in summer [*Bhatt et al.,* 2008; 2013] but in this modeling study we identified reduced Arctic sea ice as the reason for such a cooling. We also found that there was increased precipitation over the high latitudes during summer in response to reduced Arctic sea ice. Over the recent years weakening of storm activities over Eurasia, especially in winter, has been observed along with an intensification of anticyclones [*Zhang et al*., 2008, *Overland and Wang,* 2010, *Zhang et al*., 2012]. These changes over Eurasia have caused severe cold events in winter. Many of these previous studies speculated that these changes were caused by Arctic sea ice loss but in this study we have showed that decreased sea ice over the Arctic causes decreased Eurasian storm activity. These authors speculated that these changes were due to the rapid sea-ice decline which affects the overlying atmospheric circulation pattern by exciting stationary Rossby wave train propagation towards Eurasia and East Asia [*Honda et al*. 2009] influencing the cyclones and anticyclones. In correspondence with the recent colder temperatures over Eurasia we have found similar cooling over Eurasia in winter and fall due to reduced sea ice. We note that Cohen and Entekhabi [1999] linked Eurasian cold weather events to increased snow depth; however we have demonstrate that the cooling may be associated to intensified anticyclones over Eurasia along with reduced total snowfall in response to decreased sea ice.

3.5 Conclusions

The increased storminess observed over the Arctic in recent years has been an actively debated topic in the scientific community. In order to understand the response of the

extratropical storms to observed Arctic sea ice we conducted a modeling experiment, using the NCAR Community Atmosphere Model (CAM) version 3.1. A Lagrangian approach, a storm identification and tracking algorithm [*Zhang et al.*, 2004], was used to derive statistics of the 6-hourly based storm activity for a composite analysis corresponding to the years with below and above average sea-ice extent. In this modeling study we identified the sole impacts of sea ice change on storm activity and surface climate parameters like SAT, surface wind, total precipitation, total snowfall and SLP. The new scientific findings obtained in this study are summarized below:

1) Reduced Arctic sea ice causes increased storm activity over the Arctic in spring, summer, and fall.

2) Reduction of Arctic sea ice results in changes in decreased storm activity over Eurasia in all seasons, which is consistent with previous observational data analysis by Zhang et al. [2004; 2012], suggesting this decreases is mainly attributable to Arctic sea ice.

3) A wetter Arctic in spring, summer and fall occurs due to increased storminess in response to reduced Arctic sea ice.

4) A colder-than-normal summer Arctic emerges in the year with less-than-normal sea ice because of increased storminess, precipitation and decreased downward shortwave.

5) Decreased storm activity occurs over Eurasia, result in decreased precipitation and surface air temperature in fall due to increased outgoing longwave radiation under a clear sky resulted from intensified anticyclones.

We note that the present analyses are subject to certain limitations. Understanding the Arctic climate system and its nontrivial relationship with the mid-latitude weather systems driven by many complex physical mechanisms is difficult. At the same time a detailed study of physical mechanisms of changes in surface climate in response to reduced sea ice was beyond the scope of this paper. For example, we did not investigate mechanisms responsible for spring SW radiation anomalies at surface over mid-latitude regions found in the results of our simulations. Climate models are known to have biases compared to observations. A comprehensive evaluation of the model biases of climatology simulated by this model has been done for example, by Collins et al. [2006] and can be found at NCAR's webpage [http://www.cesm.ucar.edu/models/atm-cam]. Time history has certain impacts on climate responses; in our study we have not considered this important aspect of climate change and this is a limitation of the selected method of analysis in addition to important advantages provided by this approach. Also, the sea ice data, derived from satellite measurements, are known to have biases. Thus, due to the impact of biases in both the model and the observational data sets on our results, they are somewhat limited. For example, the climate models have well known uncertainties in the estimation of clouds and we found that in our simulations changes in cloud cover in response to reduced se ice are small, ranging between -5% to +5%. Therefore, the impact of this important climate parameter on simulated surface climate may be underestimated. In the future, improved sea ice and ocean data and improved model physics will help minimize these uncertainties. Adding more ensemble members to the model simulation will help enhance the statistical robustness of our results, especially

our PDF estimates. Note also that in order to identify the response of climate parameters to changes in Arctic sea ice we have fixed SST and Southern Hemisphere sea ice, thus limiting somewhat the impacts of feedback mechanisms on atmospheric variability. Despite these limitations the results we have presented in this study provide insight and contribute towards our understanding of the impact of Arctic sea ice on extratropical storms in the Northern Hemisphere and corresponding changes in surface climate.

Increased storm activities over the Arctic have notable implications for humans and the natural environment. Results from this study will help improve understanding, enhance predictive capability, and reduce uncertainties of future projection of storm events over mid-latitudes and the Arctic Ocean Sector, which is important for advancing policy for decision-making processes.

Acknowledgements

We thank Dr. Uma Bhatt, Dr. Nicole Mölders and Dr. Igor Polyakov for serving on Soumik Basu's advisory committee and providing valuable suggestions and comments. We thank Dr. Peter Bieniek for assisting Soumik Basu with programming and codes. We also thank NCAR for making CAM available for conducting this research, and the Arctic Region Supercomputing Center for providing computational resources. This study is funded by through grants to the University of Alaska Fairbanks, International Arctic Research Center from the Japan Agency for Marine-Earth Science and Technology (JAMSTEC) under the "JAMSTEC and IARC Collaboration Studies" and National Science Foundation (NSF) Grant #ARC-1023592 and 1107590.

References

Alexander, M. A., U. S. Bhatt, J. Walsh, M. Timlin, and J. Miller (2004), The atmospheric response to realistic Arctic sea ice anomalies in an AGCM during winter, J. Clim., 17, 890–905.

Alexeev, V. A., P. L. Langen, and J. R. Bates (2005), Polar amplification of surface warming on an aquaplanet in "ghost forcing" experiments without sea ice feedbacks, *Clim. Dyn., 24*(7-8), 655-666.

Bader, J., M. D. S. Mesquita, K. I. Hodges, N. Keenlyside, S. Østerhus, and M. Miles (2011), A review on Northern Hemisphere sea-ice, storminess and the North Atlantic Oscillation: Observations and projected changes, *Atmos. Res., 101*(4), 809-834.

Balmaseda, M. A., L. Ferranti, F. Molteni and T. N. Palmer (2010), Impact of 2007 and 2008 Arctic ice anomalies on the atmospheric circulation: Implications for long-range predictions, *Quart. J. Roy. Meteor. Soc*., 136(652): 1655-1664.

Bekryaev, Roman V., Igor V. Polyakov, Vladimir A. Alexeev (2010), Role of Polar Amplification in Long-Term Surface Air Temperature Variations and Modern Arctic Warming, *J. Climate*, 23, 3888–3906.

Bhatt, U. S., M. A. Alexander, C. Deser, J. E. Walsh, J. S. Miller, M. S. Timlin, J. Scott and R. A. Tomas (2008), The atmospheric response to realistic reduced summer Arctic sea ice anomalies. Arctic Sea-ice decline: Observations, Projections, Mechanisms, and Implications, *Geophys. Mono. Series*, 180: 91-110.

Bhatt, U.S.; Walker, D.A.; Raynolds, M.K.; Bieniek, P.A.; Epstein, H.E.; Comiso, J.C.; Pinzon, J.E.; Tucker, C.J.; Polyakov, I.V. (2013), Recent Declines in Warming and Vegetation Greening Trends over Pan-Arctic Tundra. *Remote Sens.*, *5*, 4229-4254.

Blüthgen J., Gerdes R. and Werner M. (2012), Atmospheric response to the extreme Arctic sea ice conditions in 2007, *Geophys. Res. Lett*. 39 L02707.

Budikova, D. (2009), Role of Arctic sea ice in global atmospheric circulation: A review, *Global and Planetary Change*, *68*, 149-163.

Cohen, J., and D. Entekhabi (1999), Eurasian snow cover variability and northern hemisphere climate predictability, *Geophys. Res. Lett.*, *26*(3), 345-348.

Collins, W. D., P. J. Rasch, B. A. Boville, J. J. Hack, J. R. McCaa, D. L. Williamson, B. P. Briegleb, C. M. Bitz, S.J. Lin and M. Zhang (2006), The formulation and atmospheric simulation of the Community Atmosphere Model Version 3 (CAM3). *J. Clim.,* 19: 2144-2161.

Comiso, J. C. (2003), Warming Trends in the Arctic from Clear Sky Satellite Observations, *J. Clim*, 16, 3498-3510.

Curry, J. A., J. L. Schramm, and E. E. Ebert (1995), Sea ice-Albedo Climate Feedback Mechanism, *J. Clim.*, 8, 240-247.

Dethloff, K., Rinke, A., Benkel, A., Køltzow, M., Sokolova, E., Kumar, S.S., Handorf, D.,Dorn, W., Rockel, B., von Storch, H., Haugen, J.E., Røed, L.P., Roeckner, E., Christensen, J.H., Stendel, M. (2006), A dynamical link between the Arctic and the global climate system, *Geophys. Res. Lett.* 33, L03703.

Deser, C., R. Tomas, M. Alexander, and D. Lawrence (2010), The Seasonal Atmospheric Response to Projected Arctic Sea ice Loss in the Late Twenty-First Century, *J. Clim.*, *23*, 333-351.

Francis J A and Vavrus S J (2012), Evidence linking Arctic amplification to extreme weather in mid-latitudes, *Geophys. Res. Lett*. 39, L06801.

Graversen, R. G. (2006), Do changes in the midlatitude circulation have any impact on the Arctic SAT trend? , *J. Clim.*, 19(20): 5422-5438.

Graversen, R. G., T. Mauritsen, S. Drijfhout, M. Tjernstrom and S. Martensson (2010), Warm winds from the Pacific caused extensive Arctic sea ice melt in summer 2007, *Clim. Dyn.*, 36, 2103-2112.

Herman, G. F. and W. T. Johnson (1978), The sensitivity of the general circulation to Arctic sea ice boundaries: A Numerical Experiment *Mon. Wea. Rev.*, 106: 1649-1664.

Holland, M. M., Bitz, C. M. and Tremblay, B. (2006) Future abrupt reductions in the summer Arctic sea ice, *Geophys. Res. Lett.* 33, L23503.

Honda M, Inoue J and Yamane S (2009), Influence of low Arctic sea ice minima on anomalously cold Eurasian winters, *Geophys. Res. Lett.*, 36, L08707.

Hurrell, J. W., J. J. Hack, A. S. Phillips, J. Caron and J. Yin (2006), The Dynamical Simulation of the Community Atmosphere Model Version 3 (CAM3), *J. Clim.*, 19: 2162-2183.

Hurrell, J. W., J. J. Hack, D. Shea, J. M. Caron and J. Rosinski (2008), A New Sea Surface Temperature and Sea ice Boundary Dataset for the Community Atmosphere Model, *J. Clim.*, 21, 5145–5153.

Kwok, R., and D. A. Rothrock (2009), Decline in Arctic sea ice thickness from submarine and ICESat records: 1958–2008, *Geophys. Res. Lett*., 36, L15501

Manabe, S., and R. J. Stouffer (1980), Sensitivity of a global climate model to an increase of CO_2 concentration in the atmosphere, *J. Geophys. Res*., 85(C10), 5529–5554.

Mantua, N. J., and S. R. Hare (2002), The Pacific Decadal Oscillation, *J. Ocean., 58*, 35-44.

McCabe, G. J., M. P. Clark and M. C. Serreze (2001), Trends in Northern Hemisphere Surface Cyclone Frequency and Intensity, *J. Clim.*, 14(12): 2763-2768.

Overland, J. E. and M. Wang (2010), Large-scale atmospheric circulation changes are associated with the recent loss of Arctic sea ice, *Tellus*, 62A (2010) (1).

Overland J E, K. R. Wood and M. Wang (2011), Warm Arctic-cold continents: Climate impacts of the newly open Arctic sea, *Polar Res.*, **30,** 15787.

Overland, J. E., M. Wang, J. E. Walsh, and J. C. Stroeve (2014), Future Arctic climate changes: Adaptation and mitigation time scales, *Earth's Future*, 2: 68–74.

Petoukhov V. and V. A. Semenov (2010), A link between reduced Barents–Kara sea ice and cold winter extremes over northern continents, *J. Geophys. Res*., 115, D21111.

Polyakov, Igor V., J. E. Walsh, R. Kwok, (2012), Recent Changes of Arctic Multiyear Sea ice Coverage and the Likely Causes, *Bull. Amer. Meteor. Soc.*, 93, 145–151.

Porter, D. F., J. J. Cassano, and M. C. Serreze (2012), Local and large-scale atmospheric responses to reduced Arctic sea ice and ocean warming in the WRF model, *J. Geophys. Res.* 117, D11115.

Serreze, M. C., A. P. Barrett, J. C. Stroeve, D. N. Kindig, and M. M. Holland (2009), The emergence of surface-based Arctic amplification, *The Cryosphere*, *3*, 11-19.

Serreze, M. C. and Francis, J. A. (2006), The Arctic on the fast track of change, *Weather*, 61: 65–69.

Singarayer, J. S., Bamber, J. L. and Valdes, P. J. (2006), *Twenty-first-century climate impacts from a declining Arctic sea ice cover, J. Clim.*, 19 (7), 1109-1125.

Thompson, D. W. J., and J. M. Wallace (2000), Annular Modes in the Extratropical Circulation. Part I: Month-to-Month Variability, *J. Clim.,13*, 1000-1016.

Wu Q and Zhang X (2010), Observed forcing-feedback processes between Northern Hemisphere atmospheric circulation and Arctic sea ice coverage, *J. Geophys. Res.*, 115, D14119.

Yin, J. H. (2005), A consistent poleward shift of the storm tracks in simulations of 21st century climate, *Geophys. Res.Lett.*, 32, L18701.

Zhang, X. and Walsh, J. E. (2006), Toward a seasonally ice-covered Arctic Ocean: Scenarios from the IPCC AR4 model simulations, *J. Clim.*, 19, 1730-1747.

Zhang, X., C. Lu and Z. Guan (2012), Weakened cyclones, intensified anticyclones and recent extreme cold winter weather events in Eurasia, *Env. Res. Lett.*.,7.

Zhang, X., A. Sorteberg, J. Zhang, R. d. Gerdes and a. J. C. Comiso (2008), Recent radical shifts of atmospheric circulations and rapid changes in Arctic climate system, *Geophys.Res. Lett*., 35, L22701.

Zhang, X., J. E. Walsh, J. Zhang, U. S. Bhatt and M. Ikeda (2004), Climatology and Interannual Variability of Arctic Cyclone Activity: 1948–2002, *J. Clim.*, 17: 2300-2317.

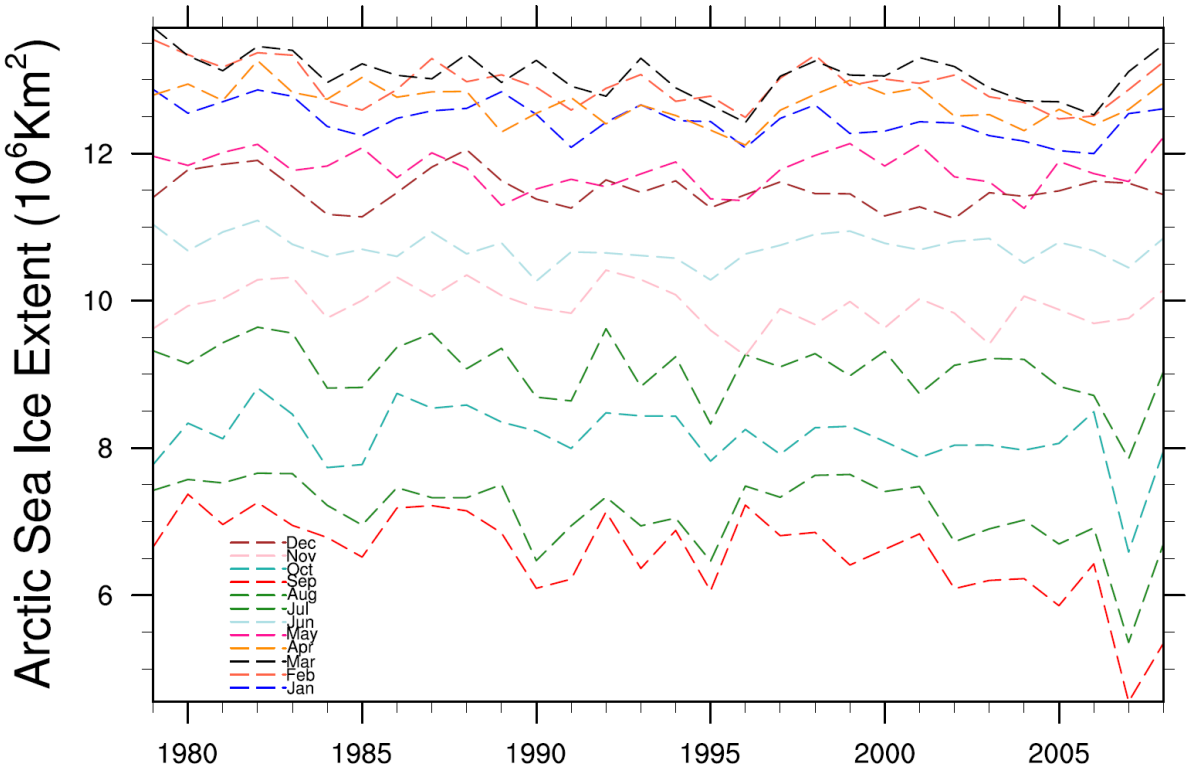

Figure 3.1 Plot showing monthly time series of Arctic sea-ice extent from 1979 to 2008 from monthly sea-ice concentration datasets prepared for CAM (Hurrell et al. 2008).

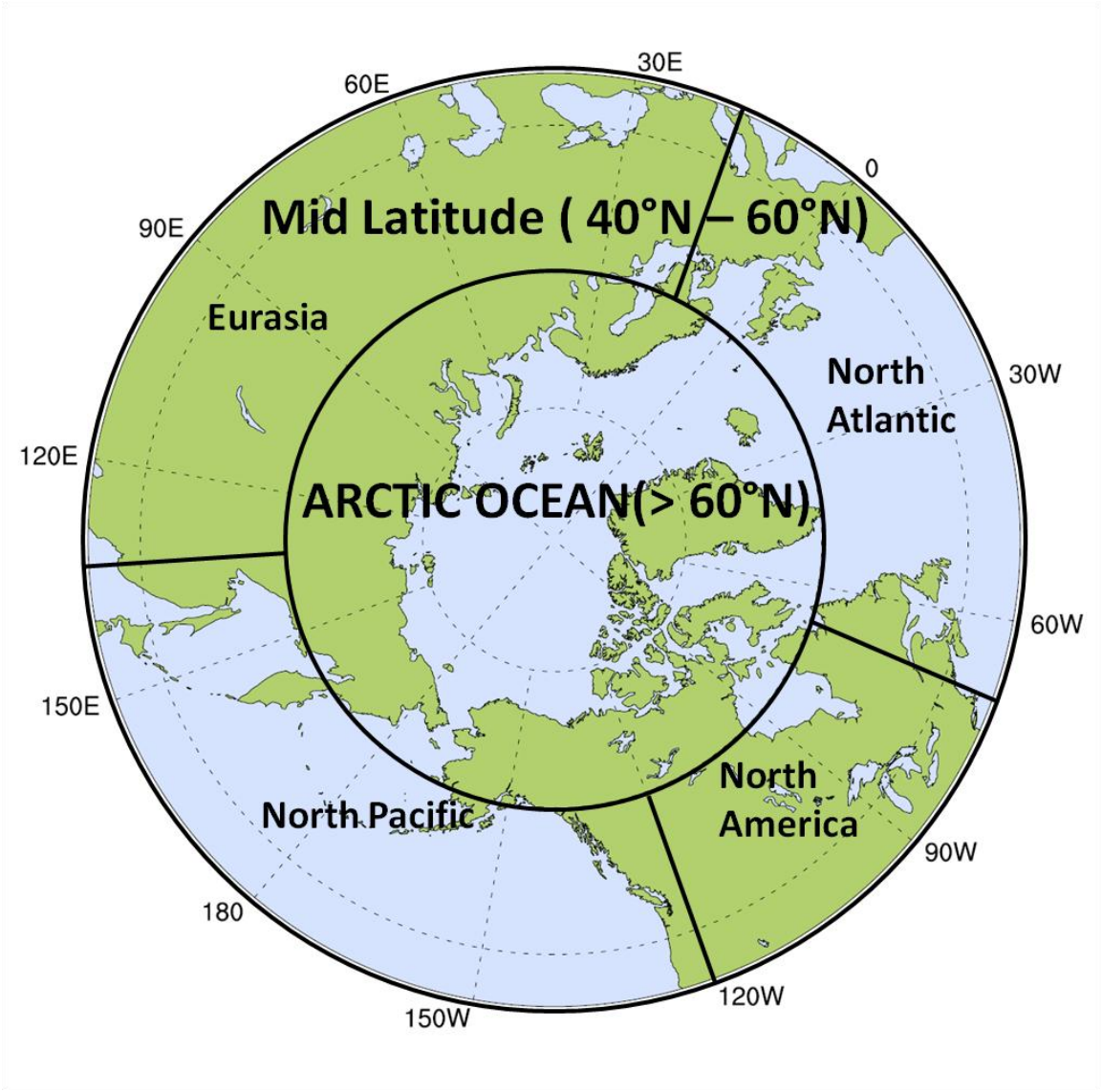

Figure 3.2 Map showing storm track regions over the Northern Hemisphere – mid-latitide (40°N-60°N) and the Arctic (above 60°N). The mid-latitude region is further divided into the North Pacific (140°E-120°W), North America (120°W-70°W), North Atlantic (70°W-20°E) and Eurasia (20°E-140°E) sub-regions.

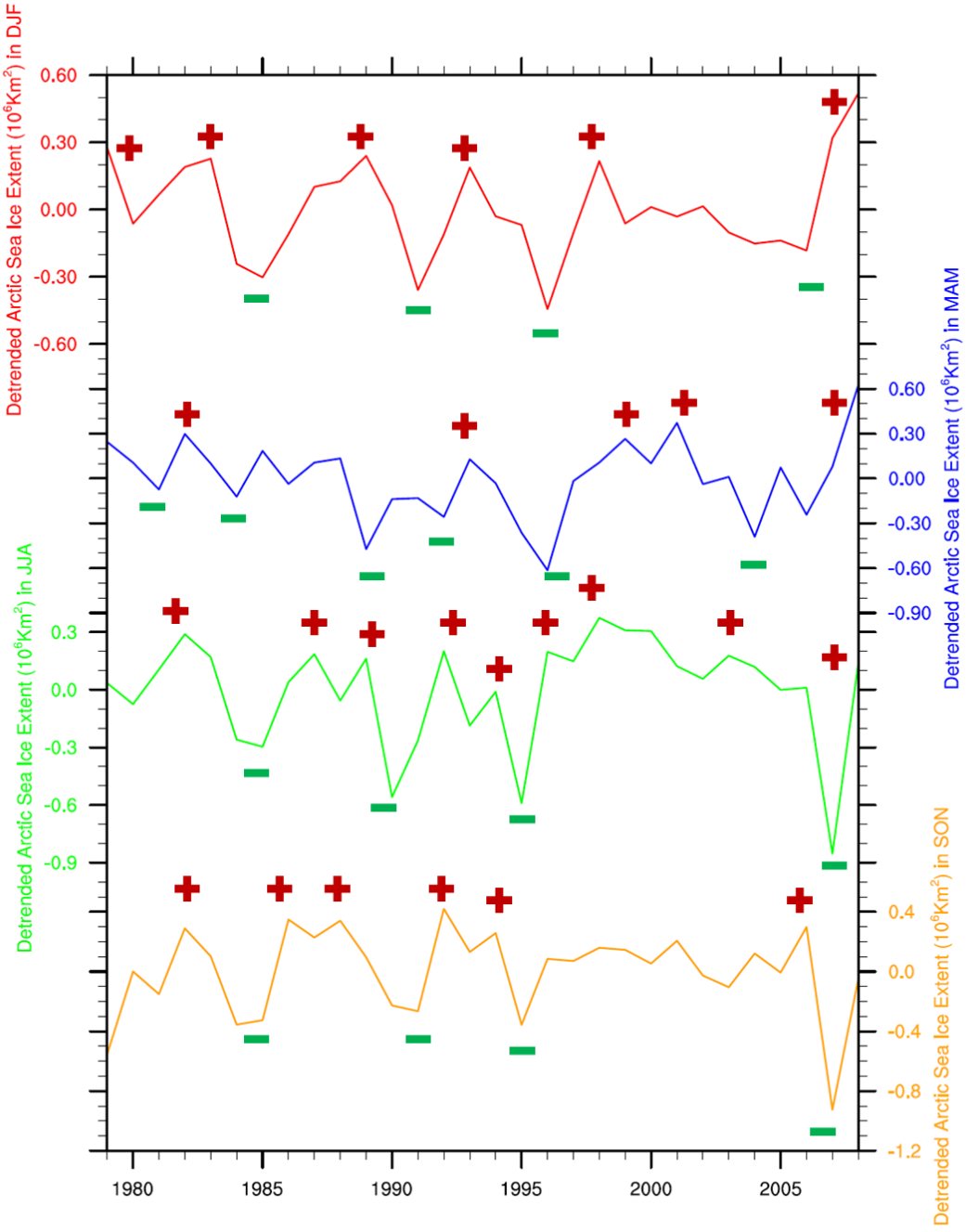

Figure 3.3 Plot shows, detrended Arctic sea ice time series for DJF, MAM, JJA and SON showing the positive and negative extreme (above or below ± 0.5σ) years for the composite analysis.

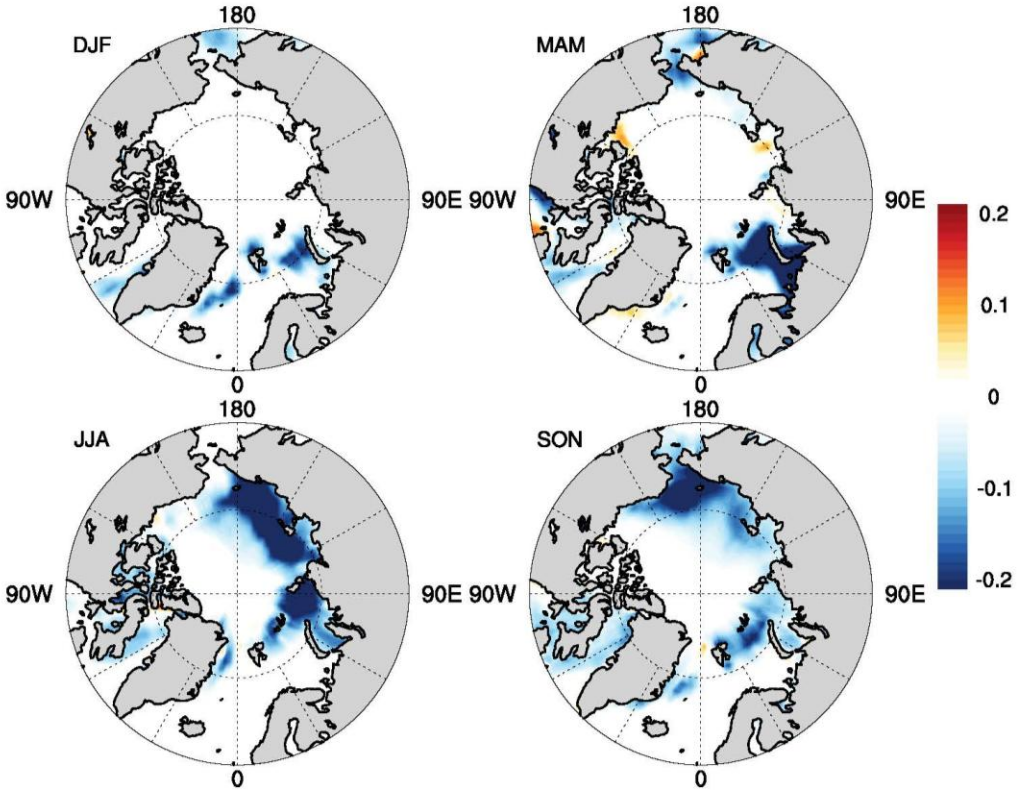

Figure 3.4 Plot showing spatial distribution of Neg - Pos differences in Arctic sea-ice fraction for DJF, MAM, JJA and SON seasons.

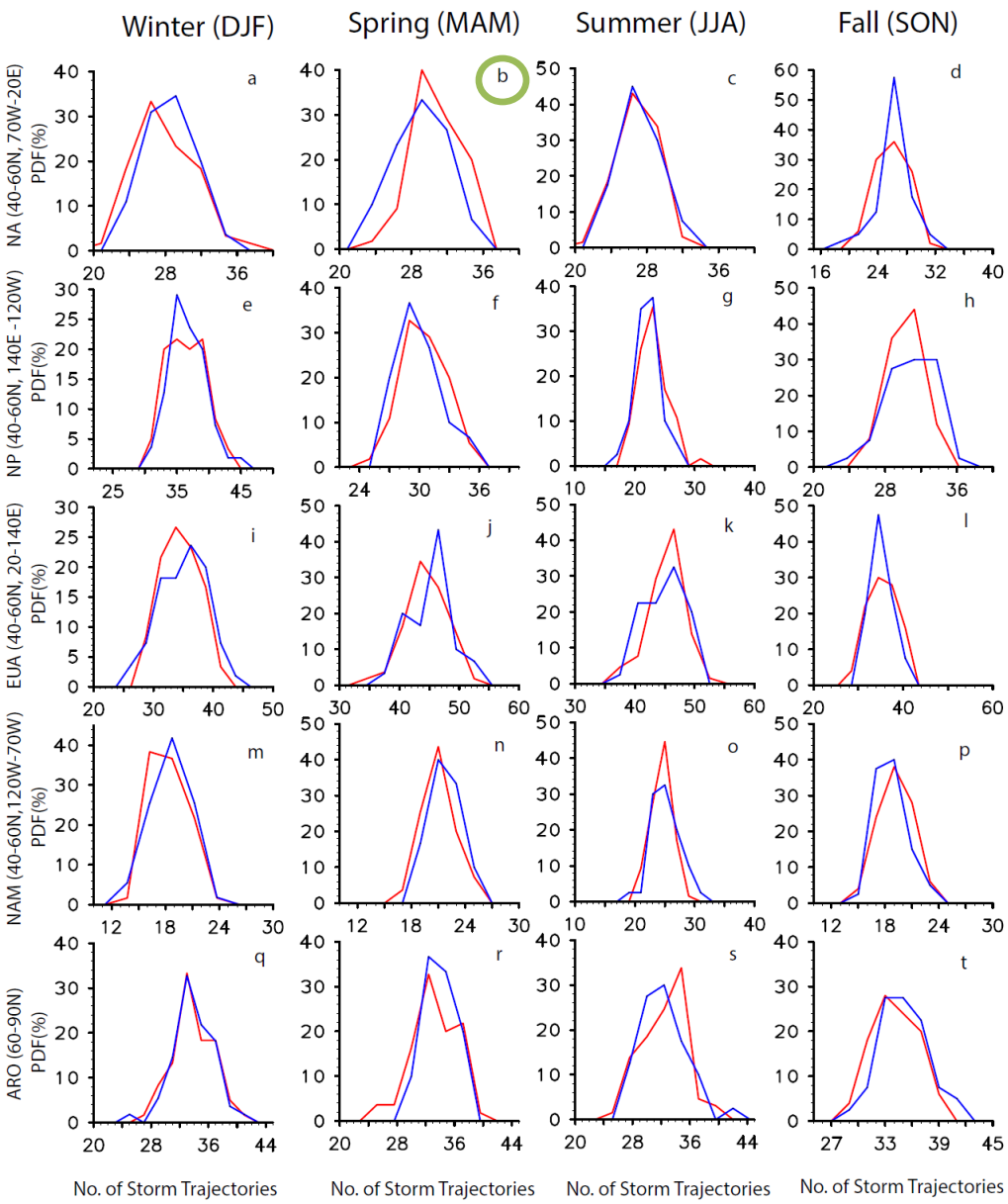

Figure 3.5 Probability Density Function (PDF) of mean number of storm trajectories for winter, spring, summer and fall respectively for the North Atlantic (a-d), North Pacific (e-h), Eurasia (i-l), North America (m-p) and Arctic (q-t) regions. Red lines for Pos (more sea ice years) and blue line for Neg (less sea ice years). Green circles represent statistically significant (> 95%) changes.

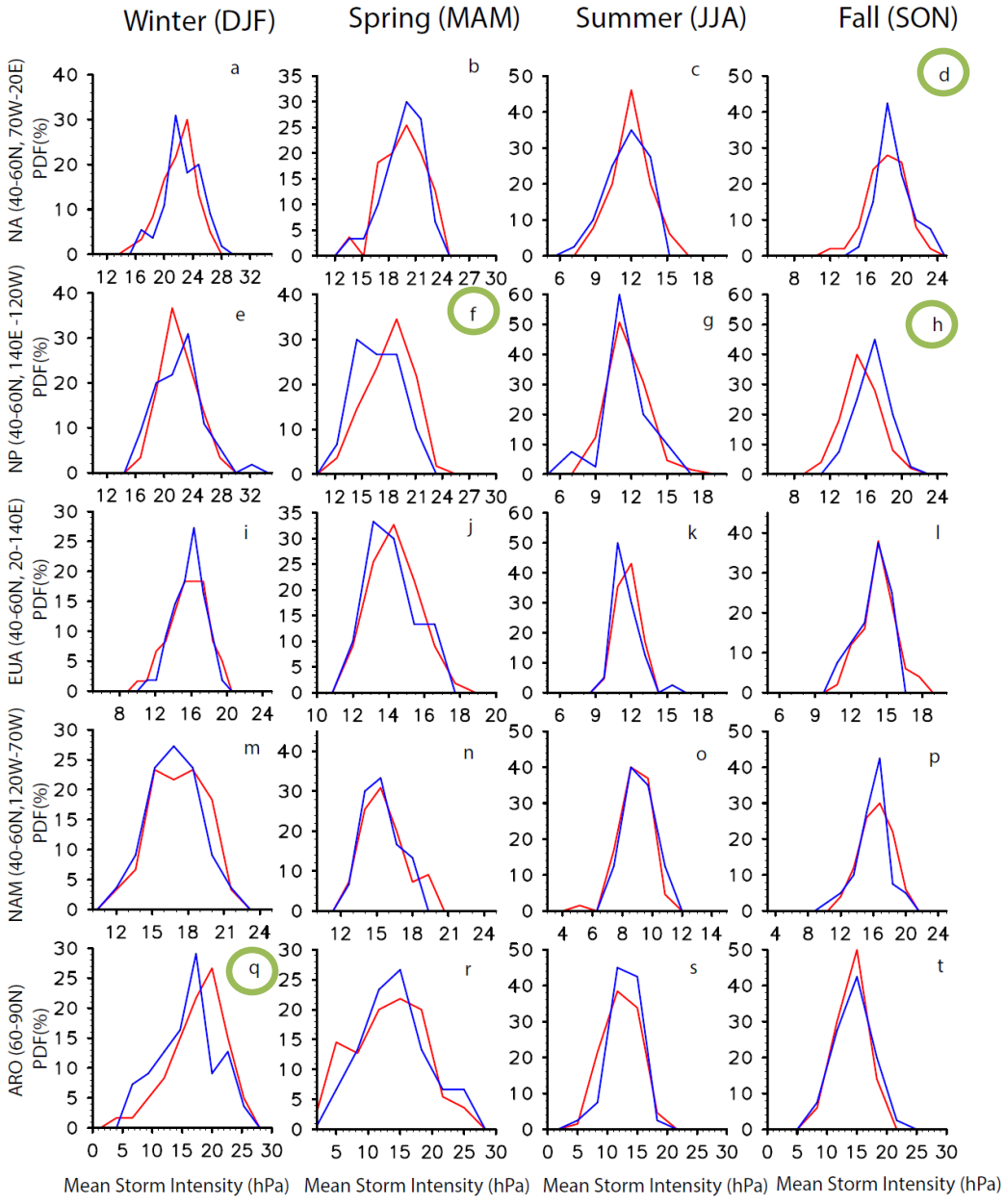

Figure 3.6 PDFs of mean storm intensity for winter, spring, summer and fall respectively for the North Atlantic (a-d), North Pacific (e-h), Eurasia (i-l), North America (m-p) and Arctic (q-t) regions. Red lines for Pos (more sea ice years) and blue line for Neg (less sea ice years). Green circles represent statistically significant (> 95%) changes.

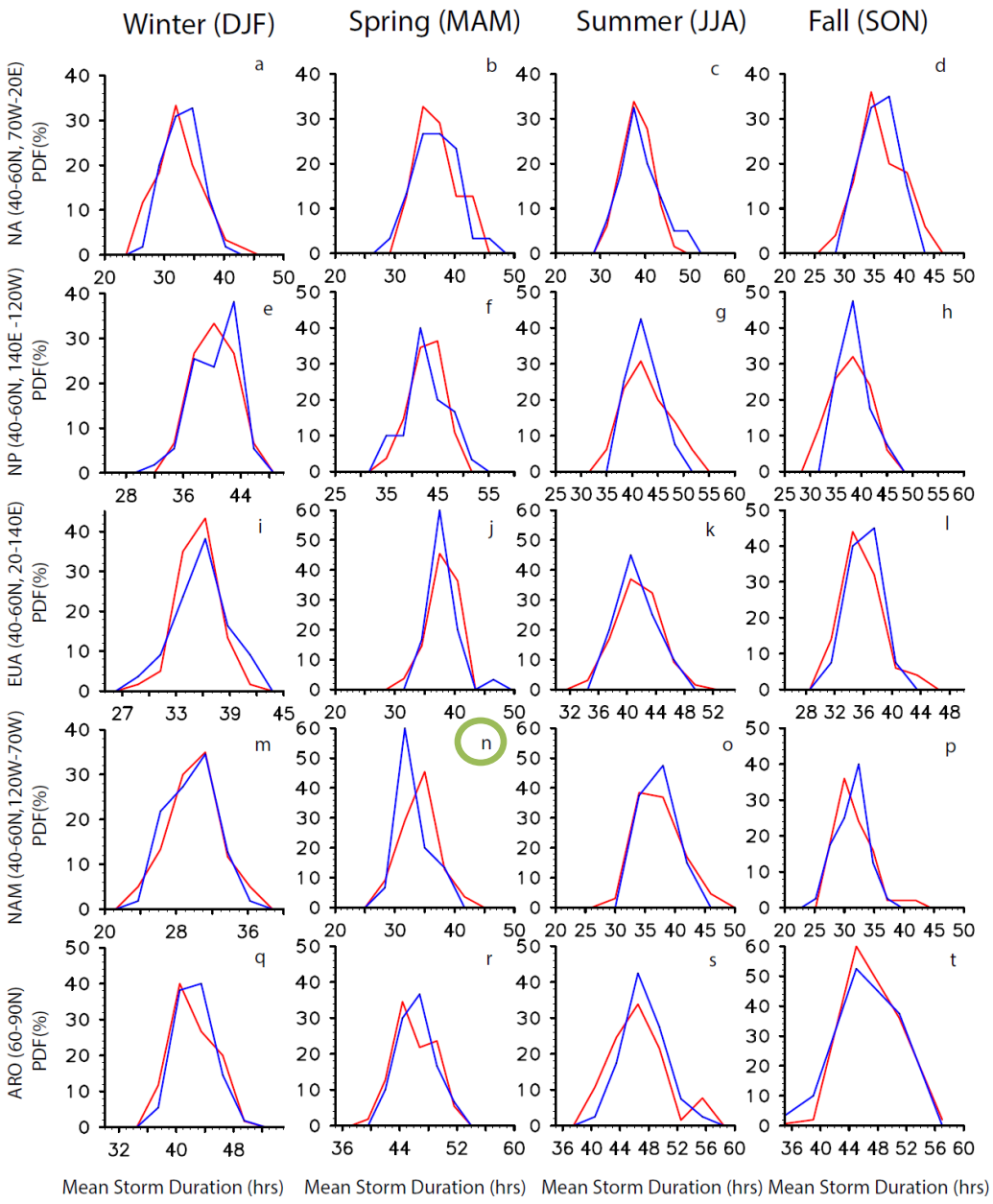

Figure 3.7 PDFs of mean storm duration for winter, spring, summer and fall respectively for the North Atlantic (a-d), North Pacific (e-h), Eurasia (i-l), North America (m-p) and Arctic (q-t) regions. Red lines for Pos (more sea ice years) and blue line for Neg (less sea ice years). Green circles represent statistically significant (> 95%) changes.

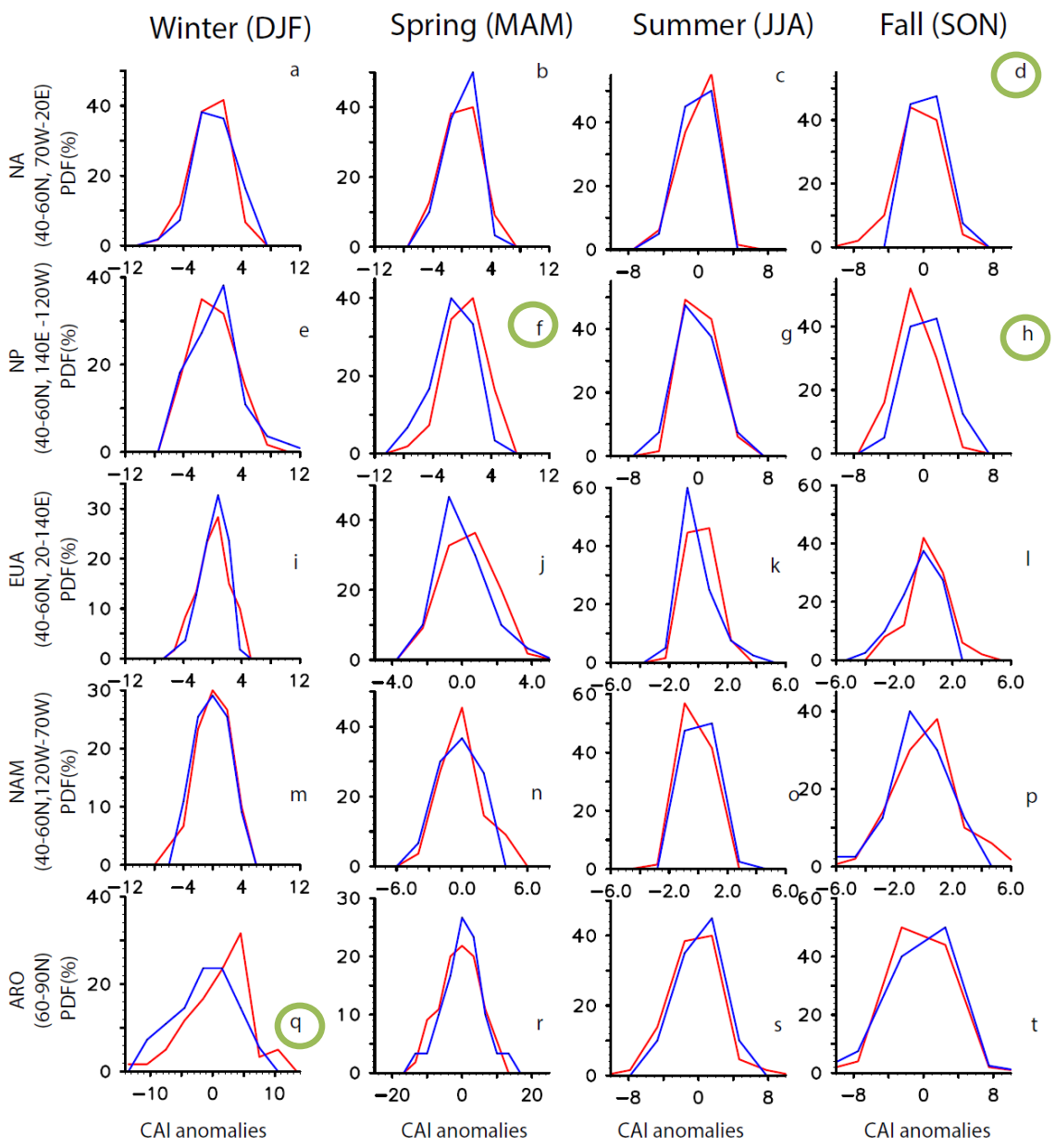

Figure 3.8 PDFs of cyclone activity index anomaly (CAI) for winter, spring, summer and fall respectively for the North Atlantic (a-d), North Pacific (e-h), Eurasia (i-l), North America (m-p) and Arctic (q-t) regions. Red lines for Pos (more sea ice years) and blue line for Neg (less sea ice years). Green circles represent statistically significant (> 95%) changes.

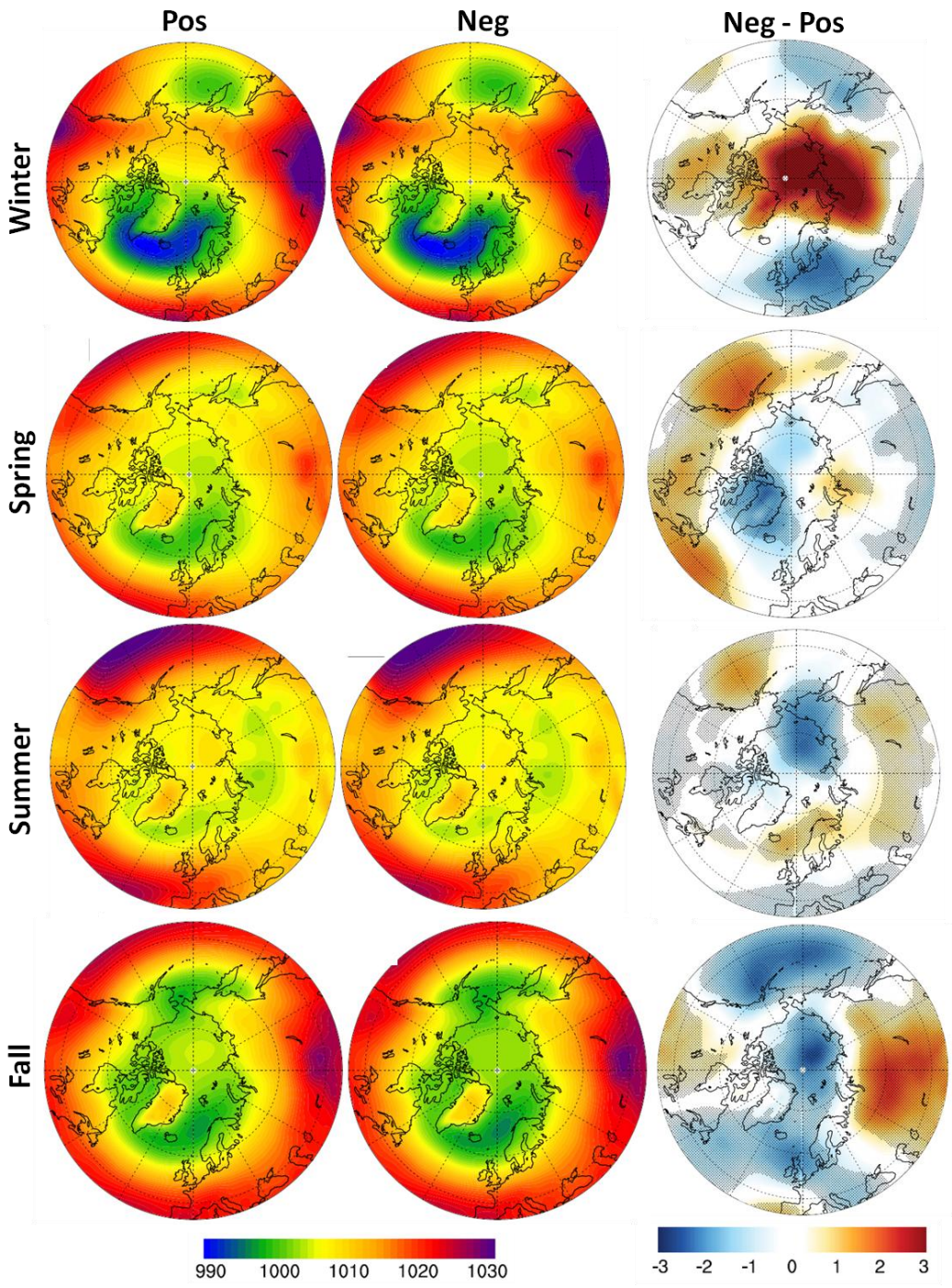

Figure 3.9 Plots showing SLP (hPa) composites for Pos and Neg years and Neg – Pos (Diff) changes during winter, spring, summer and fall. Hatching in the right column panels represents SLP anomalies statistically significant above 95%.

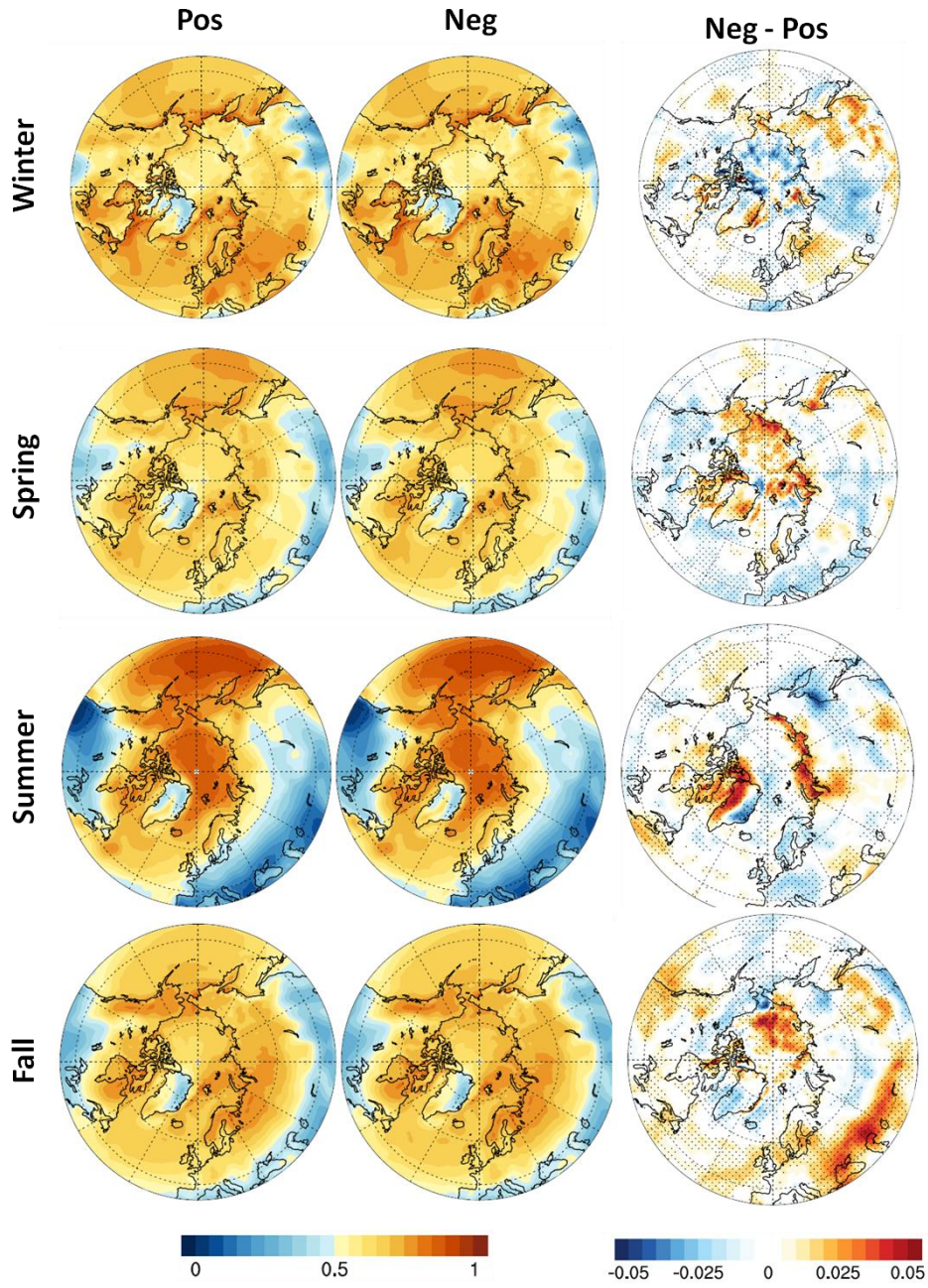

Figure 3.10 Panels showing Vertically integrated total cloud cover composites for Pos and Neg years and Neg – Pos (Diff) changes during winter, spring, summer and fall. Hatching in the right column panels represents cloud cover anomalies statistically significant over 95%.

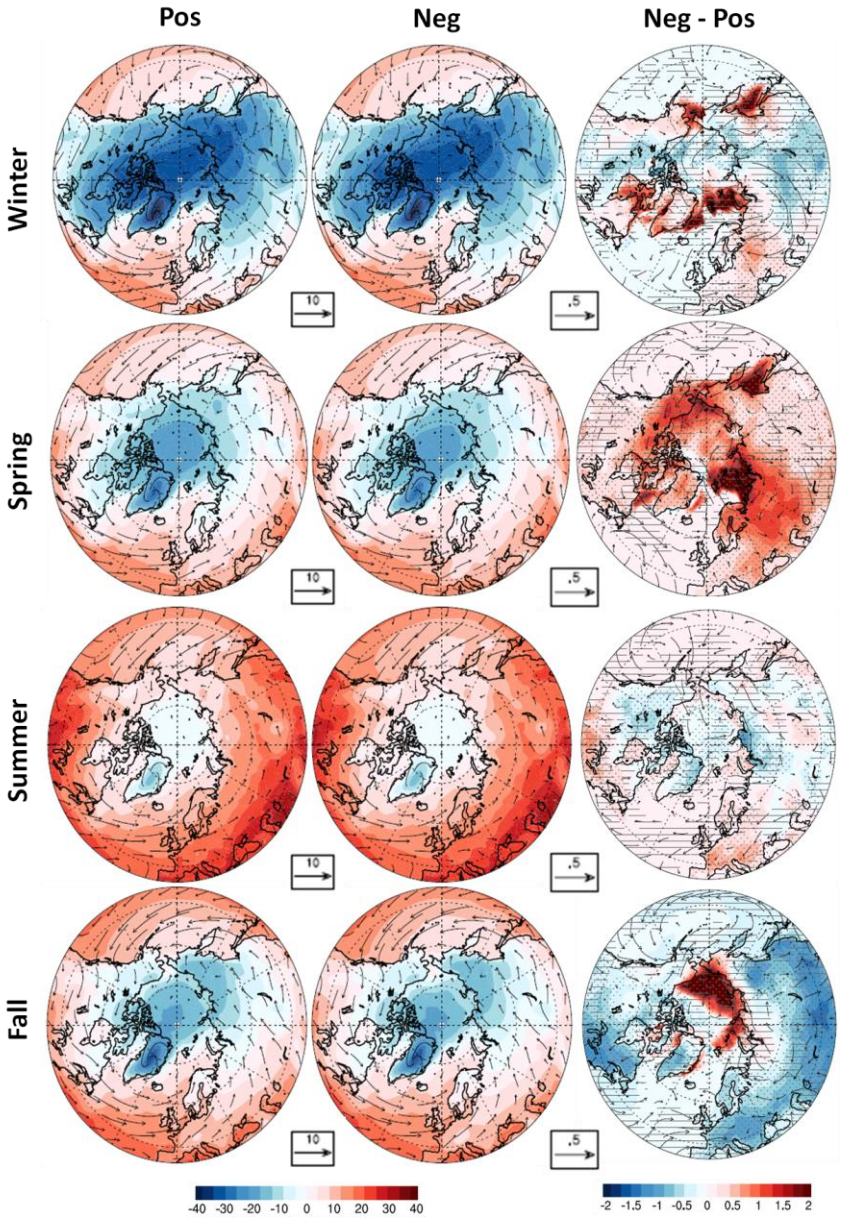

Figure 3.11 Plot shows, SAT (°C, color) and surface wind (m/s, vectors) composites for Pos and Neg years for and Neg – Pos (Diff) changes during winter, spring, summer and fall. Hatching in the right column represents statistically significant SAT anomalies above 95%. Horizontal lines represent statistically significant changes (95%) in surface wind.

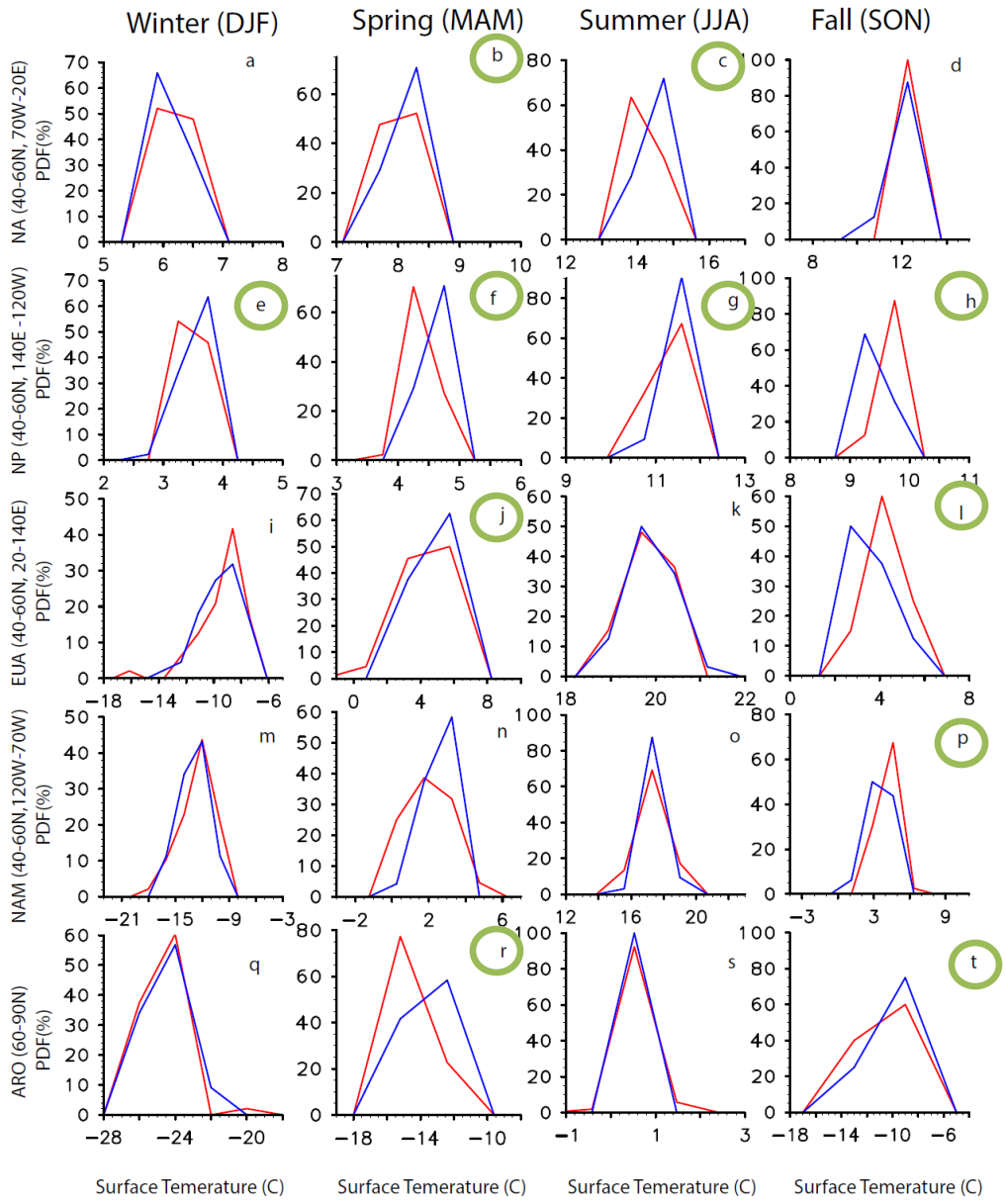

Figure 3.12 PDFs of area-averaged SAT for winter, spring, summer and fall respectively for the North Atlantic (a-d), North Pacific (e-h), Eurasia (i-l), North America (m-p) and Arctic (q-t) regions. Red lines for Pos (more sea ice years) and blue line for Neg (less sea ice years). Green circles represent statistically significant (> 95%) changes.

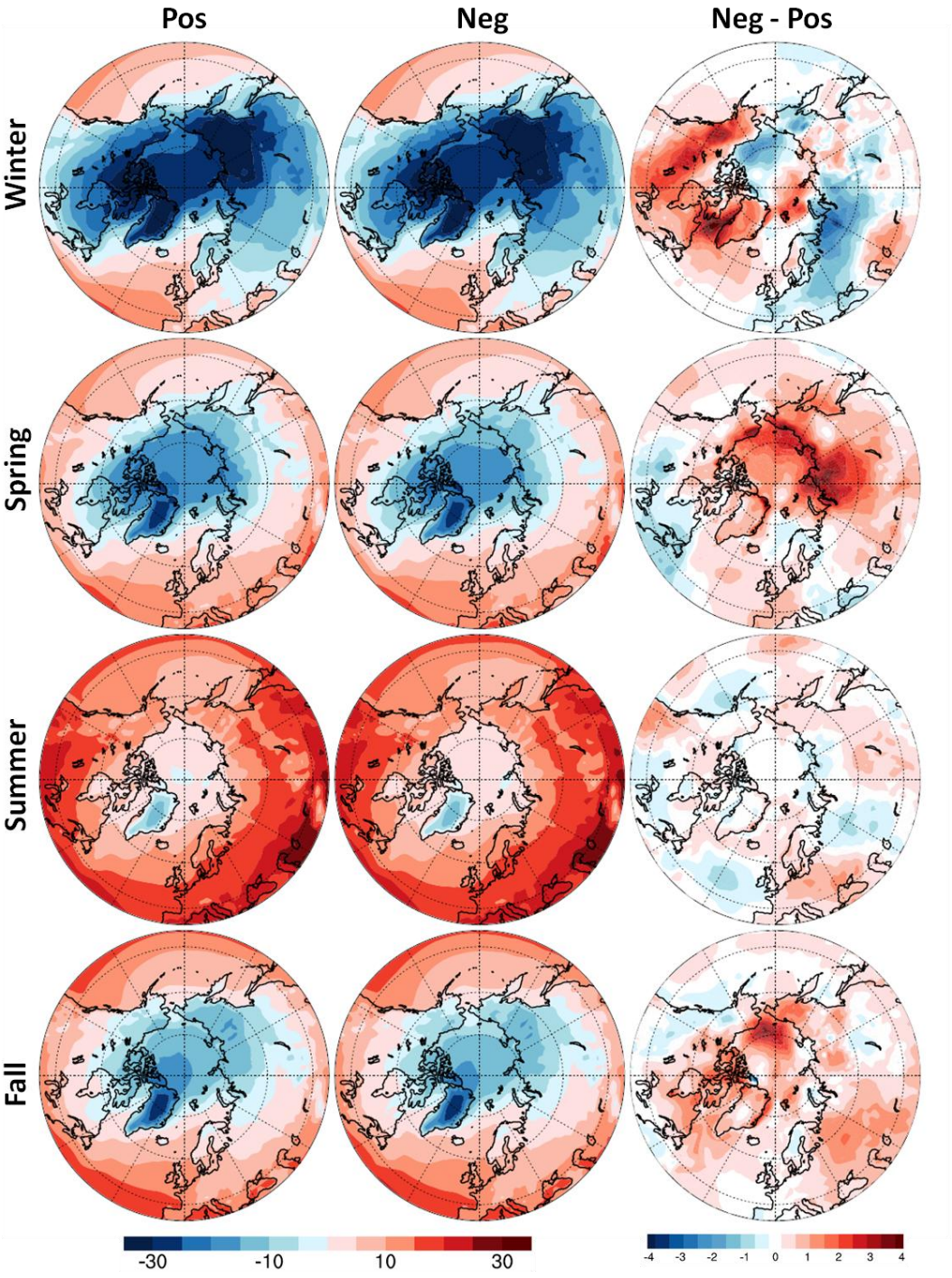

Figure 3.13 Panels showing SAT (°C, color) composites for Pos and Neg years for and Neg – Pos (Diff) changes during winter, spring, summer and fall from ERA interim.

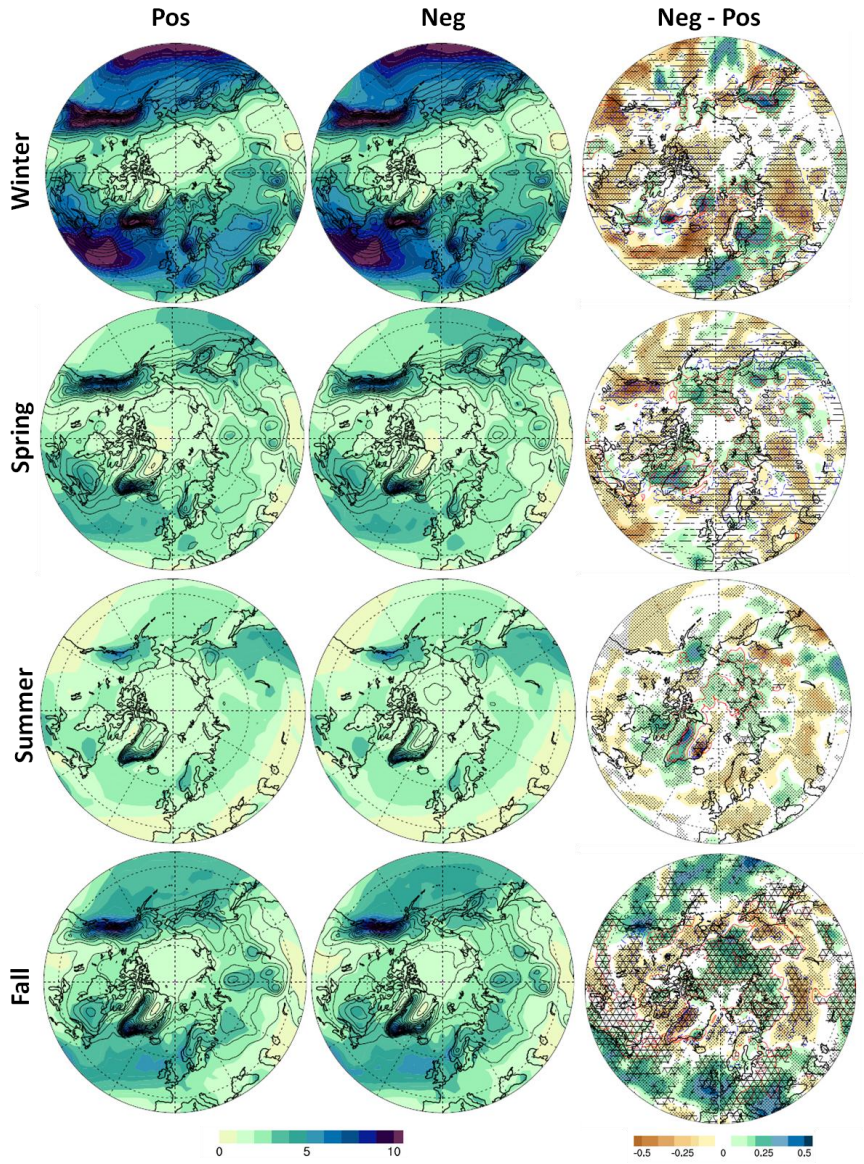

Figure 3.14 Plot shows, total precipitation (mm/day, color) and total snowfall (mm/day, isolines) composites for Pos and Neg years for and Neg – Pos (Diff) changes during winter, spring, summer and fall. Hatching in the right column panels represents statistically significant total precipitation anomalies above 95%. Horizontal lines represent statistically significant changes (95% level or greater) in total snowfall.

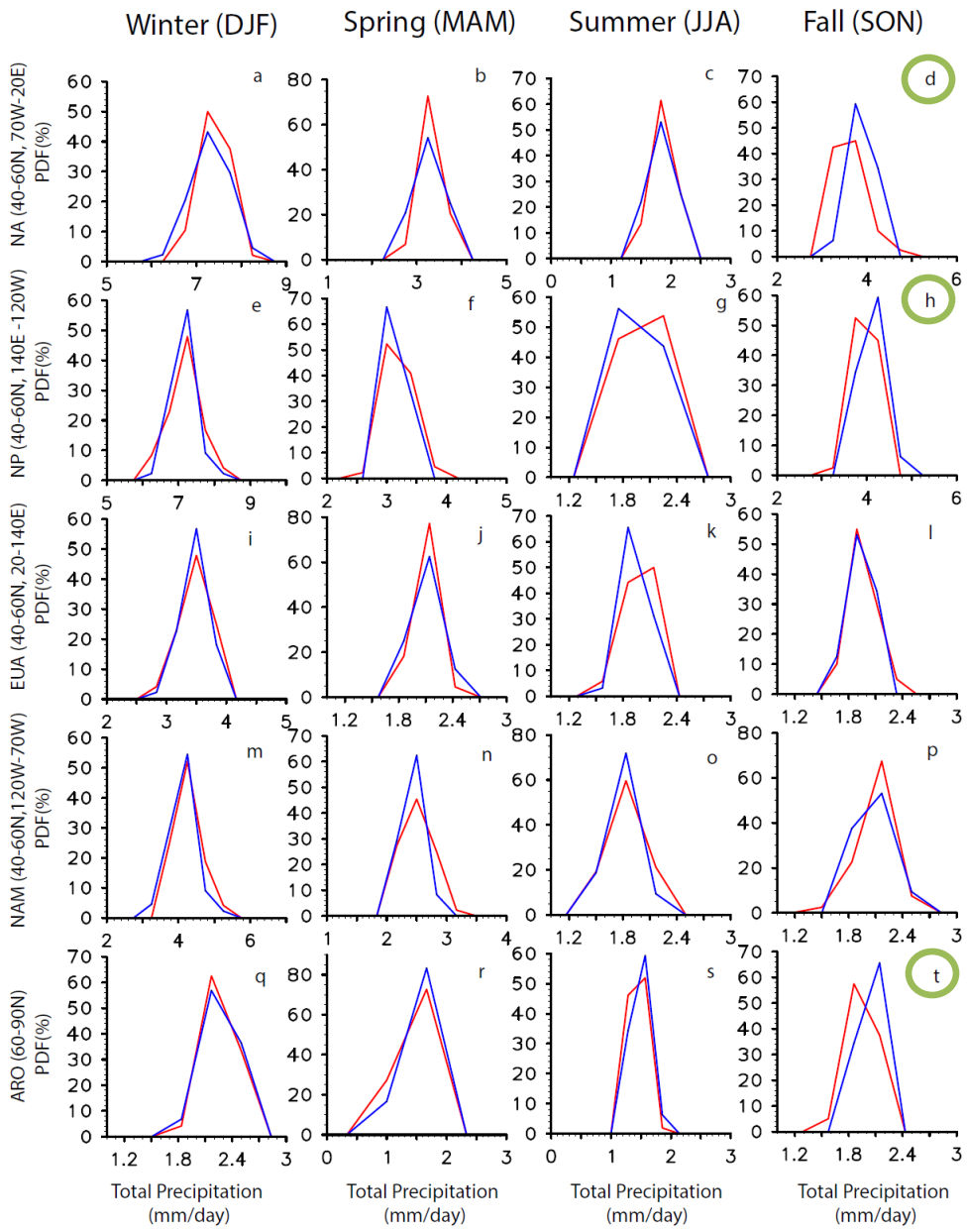

Figure 3.15 PDF of area-averaged total precipitation for winter, spring, summer and fall respectively for the North Atlantic (a-d), North Pacific (e-h), Eurasia (i-l), North America (m-p) and Arctic (q-t) regions. Red lines for Pos (more sea ice years) and blue line for Neg (less sea ice years). Green circles represent statistically significant (> 95%) changes.

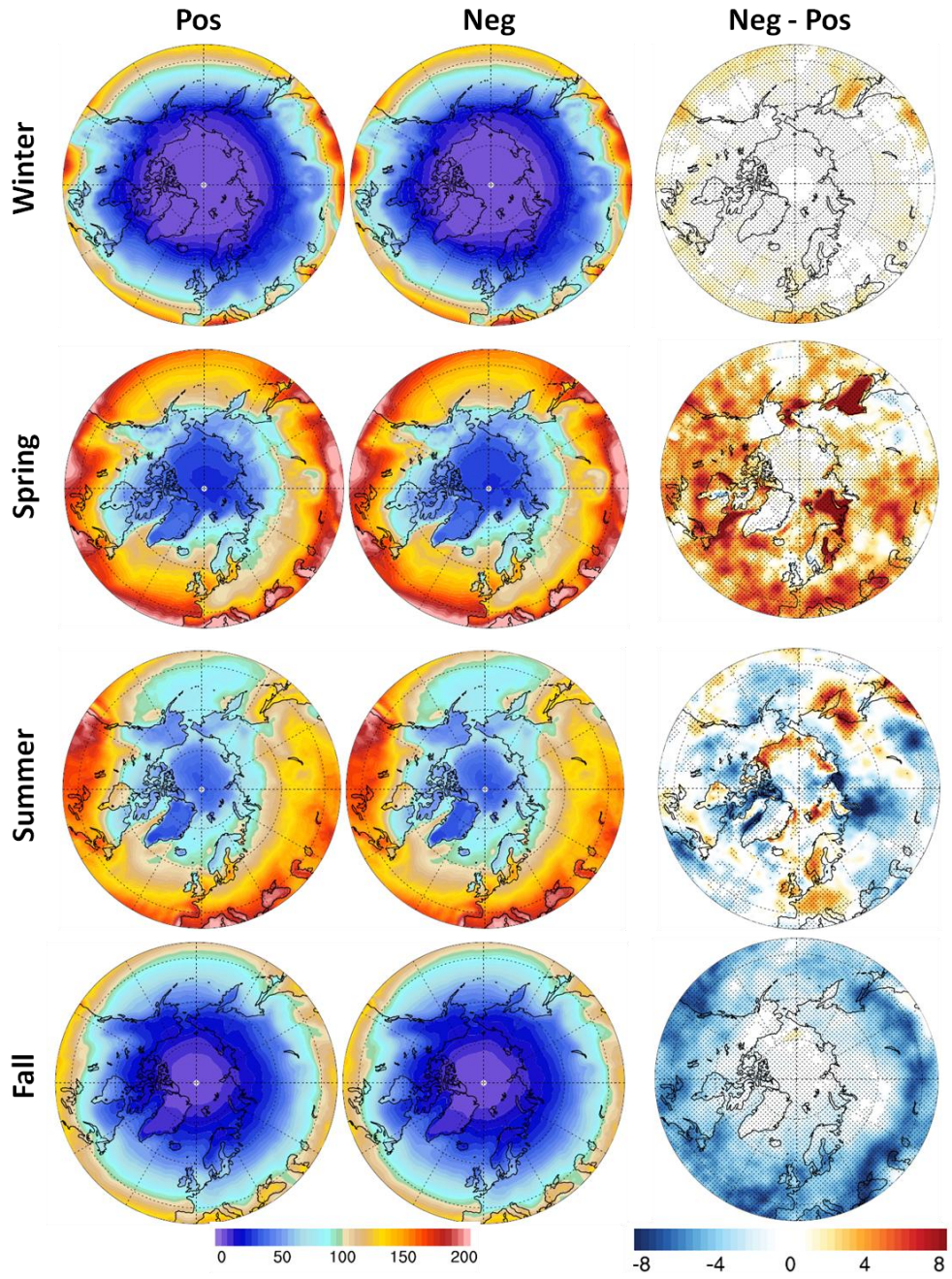

Figure 3.16 Plot shows, net shortwave flux at surface (W/m^2) composites for Pos and Neg years and Neg – Pos (Diff) changes during winter, spring, summer and fall. Hatching in the right column panels represents net SW flux anomalies statistically significant above 95%.

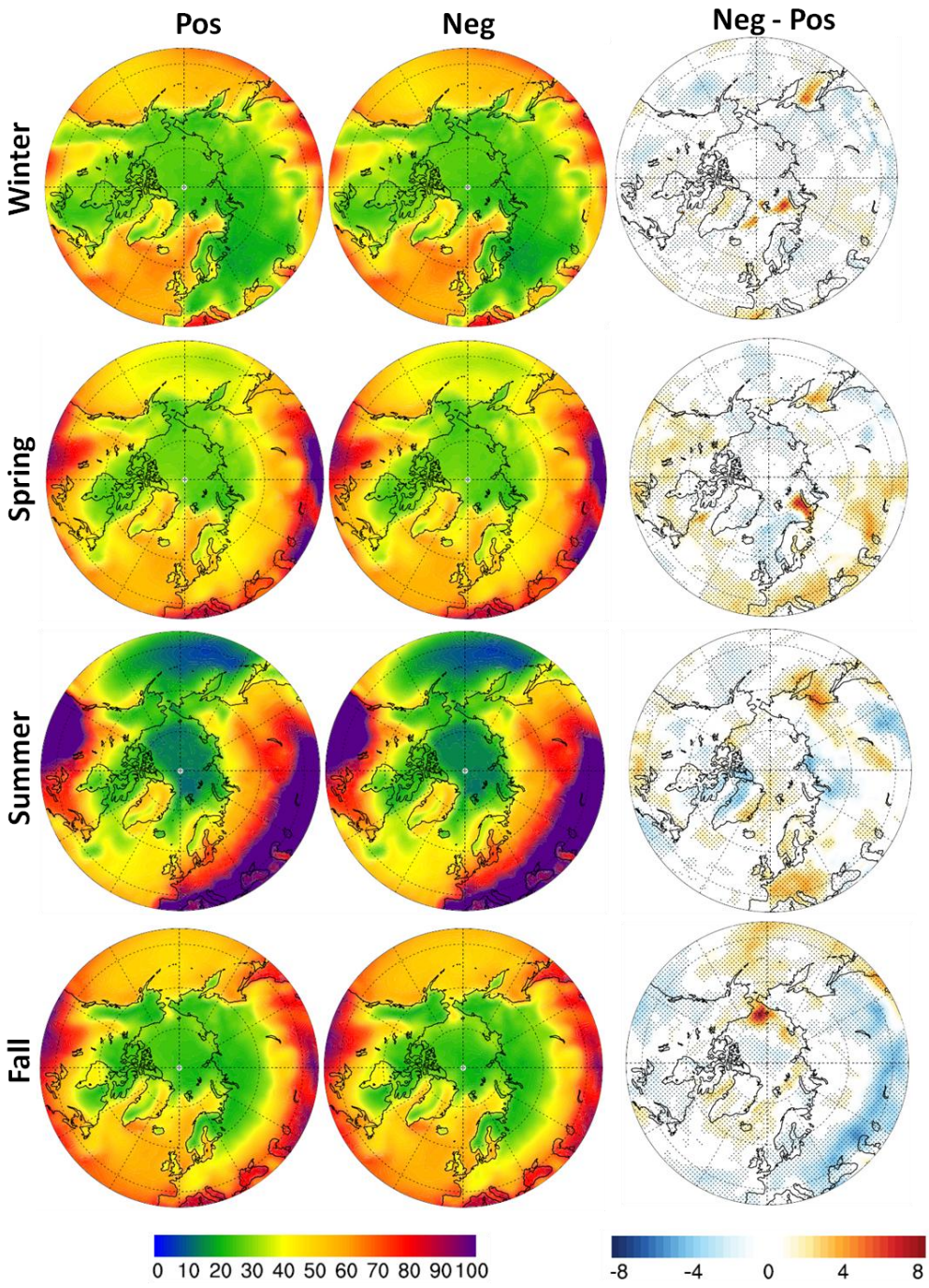

Figure 3.17 Plot showing net longwave at surface (W/m^2) composites for Pos and Neg years and Neg – Pos (Diff) changes during winter, spring, summer and fall. Hatching in the right column panels represents net LW anomalies statistically significant above 95%.

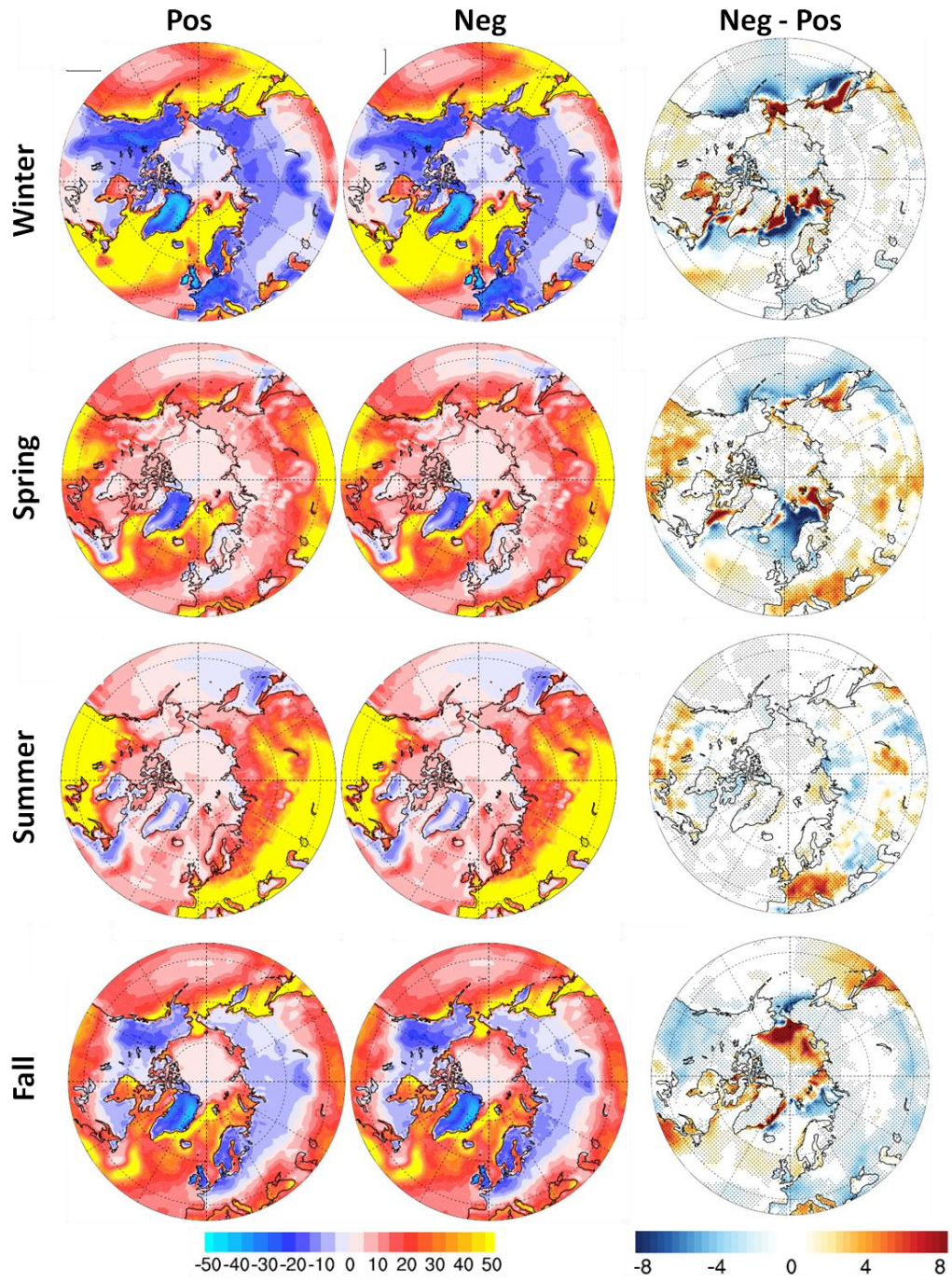

Figure 3.18 Plot shows, sensible heat flux (W/m^2) composites for Pos and Neg years and Neg – Pos (Diff) changes during winter, spring, summer and fall. Hatching in the right column panel represent sensible heat flux anomalies statistically significant above 95%.

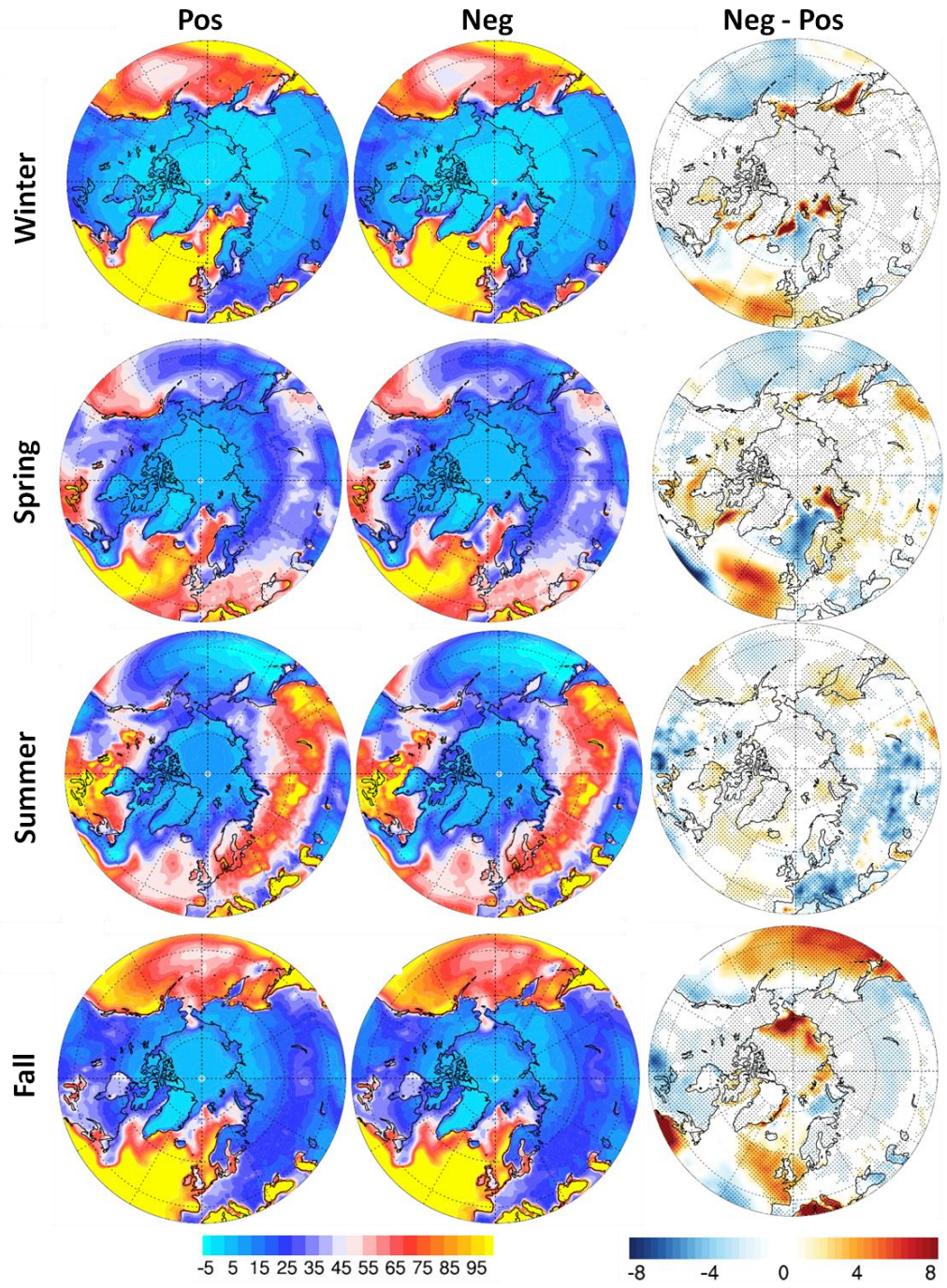

Figure 3.19 Plot shows, latent heat flux (W/m^2) composites for Pos and Neg years and Neg – Pos (Diff) changes during winter, spring, summer and fall. Hatching in the right column panel represent latent heat anomalies statistically significant above 95%.

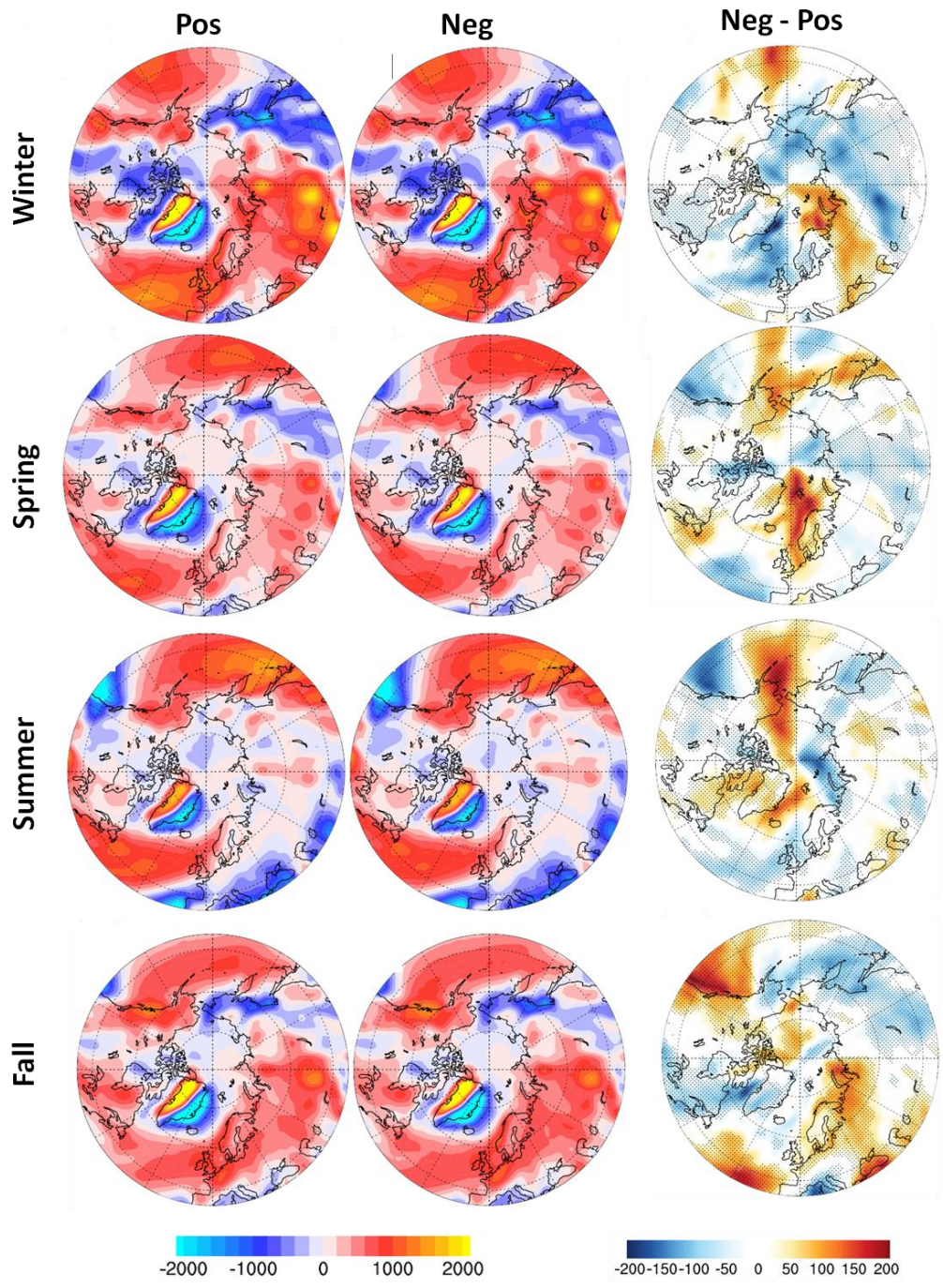

Figure 3.20 Plot showing meridional advection (K m/s) composites for Pos and Neg years and Neg – Pos (Diff) changes during winter, spring, summer and fall. Hatching in the right column panel represent advection anomalies statistically significant above 95%.

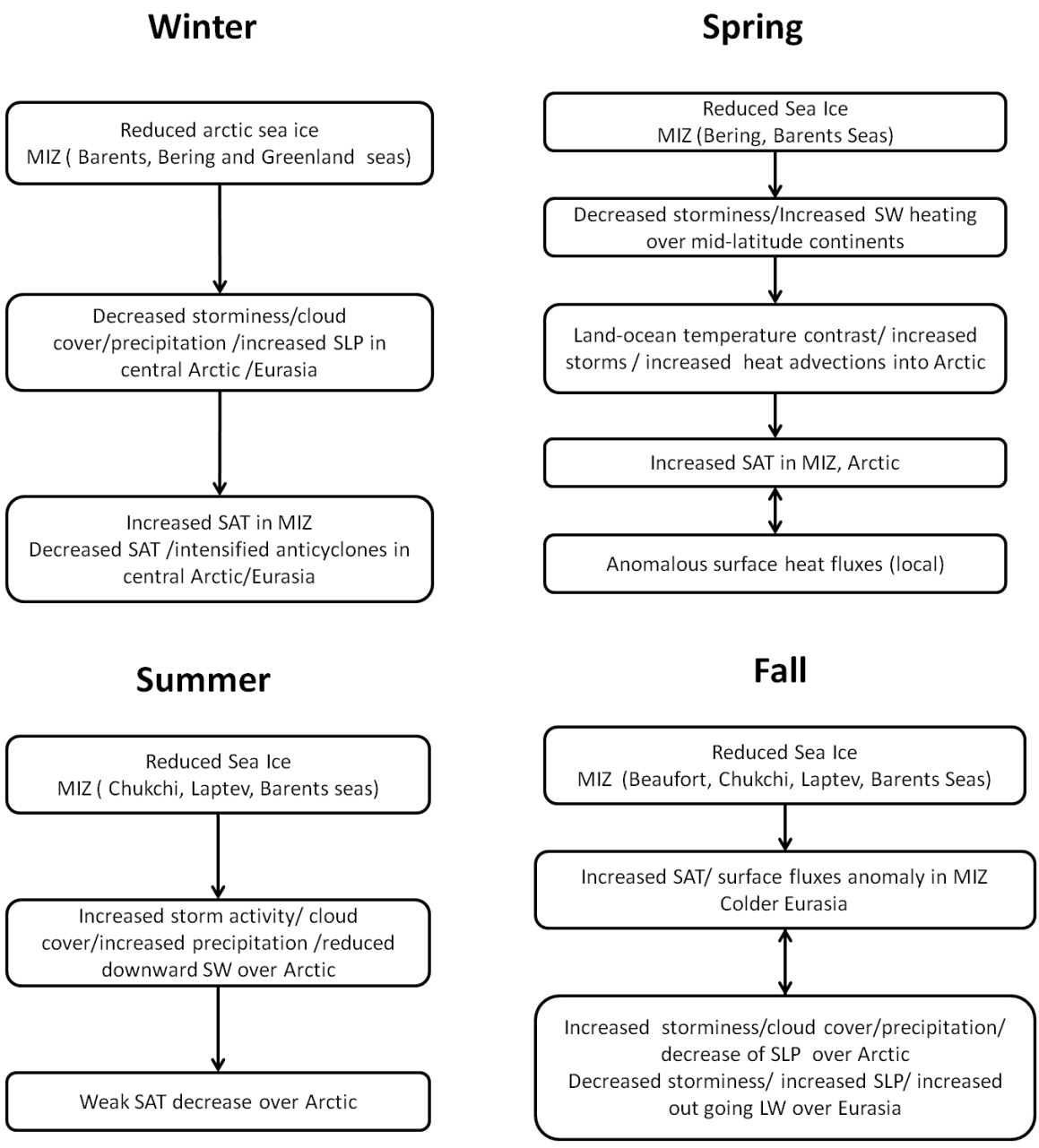

Figure 3.21 Sequence of events linking the reduced Arctic sea ice, storm activities and most prominent surface climate changes.

Chapter 4 Role of Arctic Sea ice Declining Trend in Northern Hemispheric Storm Activity: A Modeling Investigation[1]

Abstract

Arctic sea ice has experienced a significant declining trend under the influence of global warming, in addition to its large interannual fluctuations. To detect the role of this declining trend in Northern Hemisphere extratropical storm activity, we conducted a modeling experiment using NCAR Community Atmosphere Model version 3.1_p2, which is forced by the long term trend of Arctic sea ice, and compare the model results with those forced by the observed sea-ice cover. The model experiments cover a time period from 1979-2008 and were configured at a resolution of T85 (1.4°x1.4°). A storm identification and tracking algorithm was employed to analyze the 6-hourly model output. The results show that declining sea-ice trend causes a weakening of overall storm activity along with an increase in extreme storm events. A diagnostic analysis of the atmospheric energy balance demonstrates a strong regional-dependence of the energy conversion terms in supporting variability of storm activity. The conversion between transient available potential energy and transient eddy kinetic energy plays a dominant role in controlling the storm activity over the Arctic. However Eurasian storm activity was mainly controlled by the mean kinetic energy and its conversion to the transient kinetic energy.

---

[1] S. Basu and X. Zhang, 2014: Role of Arctic Sea-ice Declining Trend in Northern Hemisphere Storm Activity: A Modeling Investigation, Journal of Climate, Draft in revision for submission.

4.1 Introduction

Extratropical storms are an important component of daily weather and are the primary driver of atmospheric heat and energy transfer processes through interactions with the general circulation in mid-latitudes and Arctic. They can also bring weather extremes like blizzards, freezing rain, and wind gusts causing extensive property damage and travel hazards. Integrated storm activities show distinct regional and seasonal distributions and exhibit daily to interannual variability [*Hoskins and Hodges*, 2002; *Zhang et al*., 2004; *Bengtsson et al*., 2006]. Under recent warming climate a poleward shift of the extratropical storms has been observed [*McCabe et al*., 2001; *Zhang et al*., 2004]. Climate model experiments under global warming scenarios have also projected this poleward shift [*Yin*, 2005].

During recent decades, Arctic sea ice has experienced a dramatic decrease with large interannual fluctuation superimposed. A number of studies have detected the impacts of anomalous Arctic sea ice on the atmospheric circulation and associated surface climate [e.g., *Honda et al*., 2009; *Petoukhov and Semenov*, 2010; *Wu and Zhang*, 2010; *Blüthgen et al*., 2012; *Francis and Vavrus*, 2012]. The role of changed atmospheric circulation in sea ice variability and decrease has been also investigated [e.g., *Zhang et al*., 2008; *Graversen et al*., 2010]. Although the atmospheric circulation plays a steering role in development and movement of weather systems, impacts of sea ice on extratropical storms and, in particular, the associated physical mechanisms have not been well understood.

In order to investigate the impacts of changed sea ice on storm dynamics, we analyzed atmospheric energetics in the atmospheric model simulations with specified sea ice. A prominent feature accompanying sea ice loss is warmer temperature of the Arctic surface and lower troposphere [*Comiso*, 2003; *Polyakov et al*., 2012]. The sea ice melt and resulting increase in open water alters the surface energy budget, in particular by increasing the amount of solar energy absorbed by the ocean. The increased open water also causes enhanced surface fluxes of latent heat and sensible heat [*Bhatt et al*., 2008]. Due to the changed sea ice and surface energy balance over the Arctic Ocean, the temperature gradient between the tropics and poles and atmospheric Available Potential Energy (APE) would be also changed. This APE can be partially converted to kinetic energy (KE) through baroclinic processes or convection. Thus the changes in Arctic sea-ice concentration may impact the conversion between APE and KE, and, in turn, storm track dynamics [*Lorenz*, 1954; *Murakami*, 2011; *Murakami et al*., 2011].

The changes in Arctic sea ice include two components: natural variability and long-term trend. In this study, we will investigate impacts of these two components on storm activities by conducting atmospheric model simulations, and explore mechanisms responsible for the fluctuations and changes of storm activity through diagnostic analysis of atmospheric energetics.

4.2 Model Experiment Designs and Data Analysis Method

We employed the National Center for Atmospheric Research (NCAR) Community Atmosphere Model (CAM) version 3.1_p2 [*Collins et al*., 2006; *Hurrell et al.*, 2006]. We configured the model at T85 resolution (approximately 1.4º in both latitude and longitude) with 26 vertical levels. We performed two different groups of modeling experiments which have different surface boundary conditions defined by SST and sea ice datasets [*Hurrell et al*., 2008] - Trend Experiment (Trex) and Control Experiment (Conex). We made an effort to identify the impact of the declining sea-ice trend on the extratropical cyclones over the Northern Hemisphere during winter (DJF) and spring (MAM). To ensure robust results we did five ensemble runs of each experiment with each ensemble consisting of a 30 year model run from January 1979 to December 2008 with the 6-hourly instantaneous outputs of selected variables. We performed Student's t-test on the differences between Trex and Conex to check the statistical significance of our results.

In Conex, sea-ice concentration over the Arctic was assigned to their observed values for the period of January 1979 to December 2008 to capture the reality which includes the effect of long term trend as well as interannual variability. Sea-ice concentration over the Southern Hemisphere was prescribed to their climatological values and sea surface temperature (SST) was fixed at their climatological values all over the globe. In Trex, we first calculated the slope of regression of sea-ice concentration at each grid point and then based on the regression the sea ice at each grid point over the Arctic was linearly prescribed. The SST was fixed at their climatological values all over the globe and sea-

ice concentration in Southern Hemisphere was also maintained at their climatological values.

In order to analyze the storm activities in both the experiments, we applied a storm identification and tracking algorithm and applied this algorithm to the 6-hourly sea level pressure (SLP) outputs from each model ensemble. The principles of this algorithm are to first locate a low SLP center which has at least a minimum SLP gradient of 0.15 hPa with the surrounding grid points and survives for more than 12 hours. A detailed description about this algorithm and its application for investigating Northern Hemisphere storm track variability and changes can be found in Zhang et al. [2004]. Considering distinct features of climatological storm activity, we divided the Northern Hemisphere continent into two sub-regions in this study: Mid-latitude and Arctic. Mid-latitude was further divided into four sub regions with prominent storm activities: North Atlantic, North Pacific, Eurasia and North America (Figure 4.1).

We investigated various parameters describing storm activity, including duration or lifetime, central location, and central SLP from the storm algorithm for each individual storm occurring over the study area. By using the datasets of these parameters from each ensemble member of Conex and Trex, we derived the number of storm trajectories, mean storm duration, and mean storm intensity for each sub-region. Our analysis was limited to two seasons which have maximum extratropical storm activity over Northern Hemisphere - winter (December-February) and spring (March-May). The storm trajectory was defined from the time of storm generation until dissipation within the study area or from the time

when the storm entered the study area until the time it left the study area. The mean duration for each sub-region was the averaged duration throughout the total number of storm trajectories. The storm intensity for an individual storm was calculated as a difference between the storm's central SLP and the monthly mean SLP at the corresponding location. The mean intensity for each sub-region was obtained by averaging storm intensities throughout their duration and over the number of storm trajectories.

4.3 Results

4.3.1 Variability and Changes in Storm Activity over Northern Hemisphere

To study the changes in number of mean trajectories, mean intensity and mean duration a statistical analysis was performed on Conex and Trex (Figure 4.2). The Probability Density Function (PDFs) of the number of trajectories, mean intensity and mean duration showed many changes between Conex and Trex.

The seasonal differences between winter and spring were prominent over the North Atlantic and North Pacific where both the distribution showed a decrease in peak frequency of number of storm trajectories in spring. However, over Eurasia and North America there are more trajectories in spring than winter. Comparing Conex and Trex, many changes were evident. Over the Arctic, in winter Trex showed a bimodal distribution with an increased peak frequency of number of storm trajectories from 34 to 40. But the percentages of occurrence of peak frequency decreased from 44% to 26%. In spring, the peak frequency of the number of storm trajectories shifted towards fewer

numbers of trajectories in Trex from 33 to 26 over the North Atlantic. Over the North Pacific in spring the percentage of occurrences of peak frequency of number of trajectories decreased from 42% to 22%. Over Eurasia, peak frequency of number of trajectories in spring decreased from 48 to 42 and the percentages of occurrences of peak frequency decreased from 40% to 30%.

The PDFs of mean storm intensity showed a seasonal response of the storm activity with stronger storms in winter than the spring over all the regions. However, a comparison of mean storm intensities of Conex and Trex, a decrease in mean storm intensity was found over all the regions, except the Arctic. In winter, over Eurasia, the percentages of occurrences of peak frequency of number of trajectories decreased from 32% to 20%. Over the Arctic, in winter, a bimodal distribution with increased peak frequency of mean storm intensity from 15 hPa to 20 hPa was found. In spring, the percentages of occurrences of peak frequency decreased from 42% to 32% over the Arctic.

Over all the regions storms have a longer duration in spring than winter in both Conex and Trex. In response to the long-term trend forcing the storms over the North Pacific, in winter, showed a decrease in percentages of occurrences of peak frequency of mean duration from 61% to 40%. Over the Arctic, in spring, the percentages of occurrences of peak frequency decreased from 40% to 22%.

In order to express the overall changes in storm activity of Conex and Trex we used an integrated index of storm activity known as the cyclone activity index (CAI) [Zhang et.al, 2004]. This index was calculated by doing a sum of the differences in storm center SLP

and the climatological SLP at that corresponding grid point. For better understanding of the changes we did PDF analysis of the CAI anomaly (Figure 4.3). In climatology, according to Conex, the distribution shows a narrow distribution around zero in winter and spring for all the regions. The PDFs also exhibited seasonality in the storm activity with a weaker storm activity in spring for most of the regions. The comparison between Conex and Trex suggested that in winter, over the North Pacific the peak frequency shifted from -2 to +2 i.e. from a negative CAI anomaly to positive anomaly. Over Eurasia, in winter, the percentage of occurrences of peak frequency of CAI anomaly decreased from 0 to a bimodal distribution with two peaks at -2 and +4. However in spring, the peak frequency of the CAI anomaly shifted from -2 to +2. Over the Arctic, in response to the Arctic sea-ice trend forcing the distribution is bimodal with peaks at -8 and +4 in winter and with peaks at -6 and +6 in spring respectively. Thus, the changes in CAI anomalies, in response to Arctic sea-ice linear trend forcing, indicates a decrease in overall storm activity over the Northern Hemisphere but with increased extreme positive or extreme negative storm events. How can we link these statistical changes in storm activities to the general circulation in the atmosphere?

4.3.2 Changes in Atmospheric Energy Balance over the Storm Tracks

The vertically integrated transient eddy kinetic energy (KJ/m^2) represents the storm activity in from the perspective of general circulation at each grid point. Transient eddy kinetic energy can be given by:

$$KT = \frac{1}{2}(u'^2 + v'^2) \qquad (1)$$

Here u´ and v´ are variances in zonal and meridional winds from their temporal mean. KT Conex and Trex showed a similar pattern of maximum values of KT occurring over the North Pacific and the North Atlantic storm tracks with KT decreasing in spring (Figure 4.4). However, when we studied the differences of the long term mean of KT for Conex and Trex the difference in the state of the atmosphere between our two experiments became evident. An increase in transient eddy kinetic energy was found over the Aleutian Islands, Alaska and off the west coast of USA. Another increase was noticed over Great Britain and west coast of Europe. Over the North America, the west side of the Rockies showed an increase in KT in winter. However, a decrease in KT was found over northern Russia and the Arctic Ocean in winter. In spring the transient eddy kinetic energy increased over the North Atlantic, Eurasia, Bering Sea region and Arctic Ocean but decreased over the Aleutian Islands and North America. Thus, the differences in KT show the different response of the atmosphere in the two modeling experiments to different boundary forcings. So what are the net changes of the KT over each of the region in our experiments? For a quantitative analysis we compared the area averages of 30-year mean KT for Trex and Conex for each of the region. It was found that transient eddy kinetic energy over the North Atlantic increased by 1.5% in winter. Over the North Pacific, it increased by 1.3% for winter but decreased by 2.7% in spring. Over Eurasia, it decreased in winter by 2.5%. Over North America it increased by 1.4% in winter whereas decreased by 3.15% in spring. Over the Arctic Ocean in winter it decreased by 5.3% and in spring it decreased by 3.1%. Thus KT represents the storm activity in each grid point and by quantifying the changes in KT we found that it is consistent with our statistical

findings from PDF analysis of CAI anomalies. We know that generation of KT in the atmosphere can follow two paths: a) conversion from mean kinetic energy and b) conversion from transient eddy available potential energy [*Lorenz*, 1954; *Murakami*, 2011; *Murakami et al*., 2011]. But which path does the storm activity dominantly follows in each of the region?

For answering this question we quantified each term from the energy balance equation and set up an energy balance for our sub regions (Figure 4.5). Lorenz [1954] showed that in the energy cycle the basic variables can be divided into mean and eddy fields and considered the energy conversation among mean and eddy components of Available Potential Energy (APE) and kinetic energy (KE) [Lorenz 1954]. Murakami et al. [2011] showed that the each of the Available Potential Energy (APE) and kinetic energy (KE) can be divided into three components: mean (AM and KM), eddy (AT and KT) and interactive (AI and KI). The mean part of the energy depends on the long term mean, for example, AM depends on the long term mean of air temperature and KM depends on the long term mean wind field. The transient part of energy (AT and KT) depends on the departure of temperature or wind field from the mean air temperature or mean wind field for AM and KM respectively. Murakami et al. [2011] introduced the additional interactive term in order to accurately represent the local energy balance of a region as they showed that the conversion between the mean and eddy fields takes place through interactions between the two fields rather than direct conversion between the mean and eddy fields. This additional term represents the energy gained and lost through the interaction of mean and eddy fields of APE and KE. Apart from these energies within the

energy balance there are the generation terms: G(AM) and G(AT) and destruction terms: D(KM) and D(KT) and the rate of conversion between various forms of energy such as: C(AM,KM), C(AT,KT), C(AM,AI), C(AT,AI), C(KM,KI), C(KT,KI) and boundary fluxes: B(AM), B(KM), B(AT) and B(KT) and fluxes: AIF and KIF. The detailed equations of the energy balance of the atmosphere as used by Murakami et.al, [2011] are shown in the appendix section of this paper. Figure 4.5 shows the 30-year mean of area averaged energy terms within the energy balance equation for Trex and Conex. KT decreases in spring showing a weakening of storm activity in spring over all the regions in both Conex and Trex. From the energy cycle diagram we can see that KT can be generated via two paths: a) AM → KM → KT and b) AM → AT → KT. But among all the terms in energy balance equation, which term primarily controls the storm activity over a region? In an effort to identify the most important energy balance term for a region we did a Pearson's Correlation analysis.

We applied Pearson's correlation to the 30-year time series of area averages of these energy balance terms with time series of CAI anomaly over each of our regions (Figure 4.6). The terms with highest correlation with the storm activity expressed in terms of CAI anomalies were selected as the most important terms for the energy cycle over that region. Over the North Atlantic and North Pacific the most important role is played by the rate of conversion between AM and KM. Over Eurasia, KM in the atmosphere and conversion to KT were the dominant terms of the energy balance. Over the North America the most important role was played by the rate of conversion between AT and KT. Storm activity over the Arctic was controlled by the rate of conversion between AT

and KT. The surface boundary forcings used in Conex and Trex undergoes interaction with the complex nonlinear dynamical processes of the atmosphere and manifests a regionally variable feedback for the energy balance over the region. Thus, we identified the energy terms that drive storm activity over each of the geographical region. But how do these selected terms control the storm activity over a region? In an effort to answer this question we did a composite analysis of the most important terms to see how the dominant energy term for the region is changing between the most active phase and the least active phase of the storms.

4.3.3 Composite Analysis of the Extreme Storm Events

Based on the 30 years time series of the CAI anomalies we chose the years showing a CAI anomaly greater than ± 1 standard deviation. Then we did a composite mean of the years with the positive deviation (Conex + and Trex +) and the years with the negative deviation (Conex- and Trex-) for each of the region for Conex and Trex. The distribution of the most important energy term in positive phase and negative phase looks similar (Figure 4.7- 4.16) but on comparing the means of these extreme positive and negative years we can see many differences.

Over the North Atlantic, the conversion rate between mean available potential energy and mean kinetic energy (C(AM,KM)) was the primary term in controlling storm activity in Conex and Trex in winter and spring (Figure 4.7 and 4.8). We found higher values of C(AM,KM) over the North Atlantic area showing seasonal variability with a lower C(AM,KM) in spring. By comparing positive and the negative extreme years we can see

that there was a prominent increase in the conversion rate over the east North Atlantic and west Europe and Britain by 35 (54) W/m^2 Trex and 58 (62) W/m^2 in Conex during winter (spring). Thus, the mean vertical heat transport was controlling the storm activity over the North Atlantic region as C(AM,KM) depends on ωT, the vertical heat transport term. A comparison between Trex and Conex for positive years and negative years showed increased C(AM,KM) over the North Atlantic region. Thus, there was faster conversion between mean APE and mean KE over the North Atlantic region in Trex for both the extremes. The area averaged C(AM,KM) in Trex was higher than Conex by 25 W/m^2 in the negative extremes. So, there was an increased conversion rate between mean APE and mean KE in Trex, possibly due to increased vertical heat transport due to larger area of open water in Trex.

Over the North Pacific, the rate of conversion between mean APE and mean KE (C(AM,KM)) plays the most important role in controlling the storm activity (Figure 4.9 and 4.10). It exhibits higher values throughout the North Pacific region for both Conex and Trex showing a seasonal variation with lower values in spring. A comparison between the positive and negative years showed the highest increase over the Gulf of Alaska extending along the west coast of USA by 93(83) W/m^2 for Trex and 84 (80) W/m^2 for Conex in winter (spring). A comparison between positive years of Conex and Trex a showed decrease of C(AM,KM) by 26 W/m^2 for winter in Trex but showed an increase for spring over the Gulf of Alaska by 8 W/m^2 over the region in Trex.

Over Eurasia KM was the most important term for the storm activity for both Conex and Trex in winter and spring (Figure 4.11 and 4.12). We found a higher KM over Eurasian storm track region in the positive years but in the negative years the values over this high KM region got lowered. Seasonal variability was observed by the weakening of the KM over the region in spring. On taking the difference between positive years and negative years it was found KM increased over 30ºE to 60ºE in winter but this area of high increase shifted to 60ºE to 90ºE in spring. By examining the area averaged KM over the region, an increase in KM by $3x10^5 J/m^2$ ($2x10^5 J/m^2$) in Trex in winter (spring) was found between positive and negative extremes of the storms. So we can say that the storm activity over Eurasia was primarily controlled by the horizontal wind field over the region in winter and spring as value of KM was dependent on the magnitude of the u and v wind components and later this KM gets converted to KT. Comparing the positive years of Conex and Trex, it was found that KM showed an increase in winter by $2x10^5 J/m^2$.

Over North America the rate of conversion between AT and KT (C(AT,KT)) was the primary component of atmospheric energy balance for controlling the storm activity in both Conex and Trex (Figure 4.13 and 4.14). In winter and spring the higher values of C(AT,KT) were found to be concentrated around the Great Lakes with the values getting weaker in the negative years. A seasonal variation with higher values of C(AT,KT) in spring was also observed. A comparison between the positive and negative years showed the highest increase over the Great Lake region by 34% (20%) in winter (spring). Over North America storm activity was mainly influenced by the vertical heat transport by the

transient eddies as the value for the term C(AT,KT) are determined by vertical heat advection (ω´T´). On comparing, positive extreme of Conex and Trex it was found that C(AT,KT) decreased over the area in winter from 6.86 W/m^2 to 6.34 W/m^2.

Over the Arctic Ocean the most important term that controls the storm activity was the conversion between AT energy and KT (C(AT,KT)) for both Conex and Trex in winter and spring (Figure 4.15 and 4.16). The higher values of C(AT,KT) were located over the Chukchi Sea and Greenland Sea for Conex and Trex. It showed a seasonal variability with a reduced rate of conversion in spring. A comparison between the positive years and the negative years for Conex showed an enhanced conversion rate over the Greenland, Norwegian and Barents seas but a decreased conversion rate over the Chukchi Sea and Eurasian Arctic by 38% (15%) in winter (spring). For Trex we found an increased C(AT,KT) over the Chukchi, Greenland, Norwegian and Barents seas by 48% (38%) in winter (spring). So we can say that storm activity over Arctic Ocean is primarily controlled by vertical heat transport by the transient eddies. A comparison between positive years of Conex and Trex in winter showed maximum decrease in C(AT,KT) over the Greenland and Norwegian seas by 2 W/m^2 but there was increase over Eurasia and the Chukchi Sea by 1.5 W/m^2. For spring there was an increase over continental Eurasia and the Chukchi Sea by up to 1.5 W/m^2. For the negative years a comparison between Conex and Trex showed a decrease in C(AT,KT) over the northern Eurasia and Labrador Sea by 4 W/m^2. In spring a decrease in C(AT,KT) up to 3 W/m^2 over the east continental Eurasia was found.

The loss of sea ice over the Arctic due to the long term trend forcing resulted in larger areas of open water when there was no interannual variability of sea ice. Presence of areas of open water caused an increased vertical heat transport due to increased vertical motion over the warmer water surface. This increased vertical heat transport caused a rapid conversion of AT to KT leading to the occurrence of extreme storm events over the Arctic. The loss of sea ice and larger areas of open water affected the overlying atmospheric circulation [*Zhang et al*., 2008; *Graversen et al*., 2010; *Overland and Wang*, 2010]. The overlying circulation influenced the propagation of Rossby wave over Eurasia [*Zhang et al*., 2008; *Overland and Wang*, 2010; *Zhang et al.*, 2012]. Thus the wind field over Eurasia was affected due to the feedback from the decay of Arctic sea ice. The changes in zonal and meridional components of the horizontal wind field caused changes in KM of the atmosphere and later it got converted to KT which influenced the storm activity over Eurasia. It was found from the storm algorithm that there was decreased storm activity over Eurasia but increased extreme storm events. Thus our result was consistent with the previous findings of weakened storm activity over Eurasia in relation with the weakening westerlies over Eurasia [*Zhang et al.*, 2012]. Over the North Atlantic and North Pacific, due to an extended area of open water for the enhanced loss of sea ice in trend forcing, there was increased vertical heat transport from the open water as a result there was a faster conversion between mean APE and mean KE. The increased rate of conversion to mean KE strengthened the wind field over the North Atlantic and the North Pacific which then supported storm development.

4.4 Conclusions

The rapid decline of Arctic sea ice under the influence of global warming and the effect of the sea-ice decline on climate is a hotly debated topic in the scientific community. The loss of Arctic sea ice is composed of a long term trend superimposed with interannual fluctuations. To understand the role of the long term trend of Arctic sea ice in the Northern Hemispheric storm activity, we performed a modeling investigation for a period of January 1979 to December 2008. Our control run (Conex) was with observed sea ice forcing which includes both the inter-annual variability and a long term trend, whereas our sensitivity run (Trex) was forced with the linear sea-ice trend. We examined 6-hourly SLP output from the model by using a Lagrangian approach of storm finding and tracking, and did a detailed analysis of the energy balance of the atmosphere with respect to storm activity using a Eulerian method. The major findings are summarized as follows:

1) The declining trend of Arctic sea ice causes an overall weakening of the storm activity over the mid-latitudes and the Arctic, but an increase in extreme storm events that is defined by a criterion of extreme positive cyclone activity index anomaly.
2) The conversion rate between the transient available potential and kinetic energy C(AT,KT) over the Arctic increases due to the long-term sea-ice declining trend, supporting the increase in extreme storm events.
3) The weakening storminess over Eurasia under impacts of the declining sea ice can be attributed to the decreased mean kinetic energy due to weakened westerlies and resultant decrease in the conversion between the mean and the transient kinetic energies.

4) The conversion rate between mean available potential energy and mean kinetic energy C(AM,KM) decreases over the North Atlantic and North Pacific resulting in overall decreased storm activity but this rate of conversion increased in years with extreme storm activities.
5) The declining sea ice causes an increased rate of conversion between transient available potential energy and kinetic energy C(AT,KT) over the North America which supports the occurrence of extreme storm events.

In details, over the Arctic, the persistently declining trend of sea ice increases open water area, and surface and lower troposphere air temperature, which can decreases atmospheric stability, favoring the occurrence of convective activity and baroclinically-driven synoptic circulation. This leads to an increase in the conversion rate between AT and KT. Compared with the results from the model simulations forced by the observed sea ice, the model results forced by the declining trend of sea ice show increase in the C(AT,KT) when stronger storms occur in both simulations. The increased energy conversion rate supports the increased number of extreme storm events, which is identified in our statistical analysis.

Over the North Atlantic and North Pacific, the conversion rate between the mean APE and mean KE also increases in the sea-ice trend forced simulations in the years with stronger storm activity, compared with that in the observed sea ice forced simulations. This increase could be attributable to the increased occurrence of vertical velocity, which may reflect impacts of declined sea ice on mid-latitude atmospheric circulation. A

previous study [*Honda et al.,* 2009] suggests that reduced sea ice can trigger the downstream propagation of Rossby wave trains towards Eurasia and East Asia, altering regional westerlies and vertical circulation, and hence changes of the conversion rate between the mean available potential and kinetic energy. The increase in the conversion rate is in good agreement with our findings of increased extreme storm events over Eurasia with the declining sea ice.

An increase in extreme storm events over the high latitudes has a severe impact for human society and the natural environment. The Arctic is the center of attention for oil and other mining industries which are affected by the extratropical storms. Results from this study would help improve understanding, enhance predictive capability, and reduce future projection uncertainties of storm events over the mid-latitudes and Arctic region under the scenario of a changed Arctic climate induced by global warming forcing, which is important for policy decision-making processes.

Appendix

In our study APE and KE density in pressure coordinate system per unit mass was defined as given by Murakami et.al in 2011 as:

$$A = \frac{C_p}{2}\gamma(T - \langle\overline{T}\rangle)^2 = \frac{C_p}{2}\left(\frac{p}{p_0}\right)^{2k}\gamma(\theta - \langle\bar{\theta}\rangle)^2 \quad (4.1a)$$

$$k = \frac{u^2+v^2}{2} \quad (4.1b)$$

Where u is eastward wind, v is northward wind, p is pressure, p_0 is reference pressure (=1000hPa), T is temperature, C_p is specific heat at constant pressure, κ is ratio of universal gas constant R and C_p, θ is potential temperature and γ is an index for static stability of the dry atmosphere and is given by:

$$\gamma = -\frac{\kappa}{p}\left(\frac{p_0}{p}\right)^{\kappa}\left(\frac{d\langle\bar{\theta}\rangle}{dp}\right)^{-1} \quad (4.2)$$

Here angle brackets denote global average over a constant pressure surface and the overbar denotes the time mean operator.

Based on the division of basic variables into time mean and transient eddy, APE and KE densities are divided into three components – time mean, transient eddy and interaction components of APE and KE.

$$A = A_M + A_T + A_I \quad (4.3a)$$

$$K = K_M + K_T + K_I \quad (4.3b)$$

Where

$$A_M = \frac{C_p}{2}\gamma(\overline{T} - \langle\overline{T}\rangle)^2 \quad (4.4a)$$

$$A_T = \frac{C_p}{2}\gamma T'^2 \quad (4.4b)$$

$$A_I = C_p\gamma(\bar{T} - \langle\bar{T}\rangle)T' \qquad (4.4c)$$

$$K_M = \frac{\bar{u}^2+\bar{v}^2}{2} \qquad (4.5a)$$

$$K_T = \frac{u'^2+v'^2}{2} \qquad (4.5b)$$

$$K_I = \bar{u}u' + \bar{v}v' \qquad (4.5c)$$

Detailed expression of the energy of the terms of energy balance equations in spherical pressure coordinate system can be given as:

Generation terms:

$$G(A_M) = \gamma(\bar{T} - \langle\bar{T}\rangle)(\bar{Q} - \langle\bar{Q}\rangle) \qquad (4.6a)$$

$$G(A_T) = \gamma\overline{T'Q'} \qquad (4.6b)$$

Conversion terms from APE to KE:

$$C(A_M, K_M) = -\bar{\omega}\bar{\alpha} \qquad (4.7a)$$

$$C(A_T, K_T) = -\overline{\omega'}\overline{\alpha'} \qquad (4.7b)$$

Conversion between eddies and mean fields (APE):

$$C(A_M, A_I) = C_p\left(\frac{p}{p_0}\right)^{2\kappa}\gamma(\bar{\theta} - \langle\bar{\theta}\rangle)\nabla.\overline{\theta'u'} \quad (4.8a)$$

$$C(A_T, A_I) = C_p\left(\frac{p}{p_0}\right)^{2\kappa}\gamma\overline{\theta'u'}.\nabla(\bar{\theta} - \langle\bar{\theta}\rangle) \quad (4.8b)$$

Conversion terms between eddies and mean fields (KE):

$$C(K_M, K_I) = \bar{u}\nabla.\overline{u'\boldsymbol{u'}} + \bar{v}\nabla.\overline{v'\boldsymbol{u'}} - \frac{\tan\varphi}{a}\left(\bar{u}\overline{u'v'} - \bar{v}\overline{u'u'}\right) \qquad (4.9a)$$

$$C(K_T, K_I) = \overline{u'\boldsymbol{u'}}.\nabla\bar{u} + \overline{v'\boldsymbol{u'}}.\nabla\bar{v} + \frac{\tan\varphi}{a}\left(\bar{u}\overline{u'v'} - \bar{v}\overline{u'u'}\right) \quad (4.9b)$$

Boundary flux terms:

$$B(A_M) = C_p \left(\frac{p}{p_0}\right)^{2\kappa} \gamma \nabla . \left\{ \frac{\left(\overline{\theta} - \langle \overline{\theta} \rangle\right)^2 - \langle \overline{\theta} \rangle^2}{2} \overline{\boldsymbol{u}}' \right\} \quad (4.10a)$$

$$B(A_T) = C_p \left(\frac{p}{p_0}\right)^{2\kappa} \gamma \nabla . \left(\frac{\overline{\theta\prime^2}}{2} \overline{\boldsymbol{u}} + \frac{\overline{\theta\prime^2}}{2} \boldsymbol{u}' \right) \quad (4.10b)$$

$$B(K_M) = \nabla . \left\{ \left(\frac{\bar{u}^2 + \bar{v}^2}{2} + \Phi \right) \overline{\boldsymbol{u}} \right\} \quad (4.10c)$$

$$B(K_T) = \nabla . \left(\frac{\overline{u\prime^2} + \overline{v\prime^2}}{2} \overline{\boldsymbol{u}} \right) + \nabla . \left\{ \overline{\left(\frac{u\prime^2 + v\prime^2}{2} + \Phi' \right) \boldsymbol{u}'} \right\} \quad (4.10d)$$

So using these terms the basic equations of local energetics are:

$$\frac{\partial(AM)}{\partial t} = G(AM) - C(AM, KM) - C(AM, AI) - B(AM) + R(AM) \quad (4.11a)$$

$$\frac{\partial(AT)}{\partial t} = G(AT) - C(AT, KT) - C(AT, AI) - B(AT) \quad (4.11b)$$

$$\frac{\partial(AI)}{\partial t} = 0 = C(AM, AI) + C(AT, AI) - AIF \quad (4.11c)$$

$$\frac{\partial(KM)}{\partial t} = C(AM, KM) - C(KM, KI) - D(KM) - B(KM) \quad (4.11d)$$

$$\frac{\partial(KT)}{\partial t} = C(AT, KT) - C(KT, KI) - D(KT) - B(KT) \quad (4.11e)$$

$$\frac{\partial(KI)}{\partial t} = 0 = C(KM, KI) + C(KT, KI) - KIF \quad (4.11f)$$

Acknowledgements

We thank Dr. Uma Bhatt, Dr. Nicole Mölders and Dr. Igor Polyakov for serving on Soumik Basu's advisory committee and providing valuable suggestions and comments. We thank Dr. Peter Bieniek for assisting Soumik Basu with programming and codes. We also thank NCAR for making CAM available for conducting this research, and the Arctic Region Supercomputing Center for providing computational resources. This study is funded by through grants to the University of Alaska Fairbanks, International Arctic Research Center from the Japan Agency for Marine-Earth Science and Technology (JAMSTEC) under the "JAMSTEC and IARC Collaboration Studies" and National Science Foundation (NSF) Grant #ARC-1023592 and 1107590.

References

Bengtsson, L., K. I. Hodges, and E. Roeckner (2006), Storm tracks and Climate Change. *J. Clim.*, 19**,** 3518-3542.

Bhatt, U. S., M. A. Alexander, C. Deser, J. E. Walsh, J. S. Miller, M. S. Timlin, J. Scott and R. A. Tomas (2008), The atmospheric response to realistic reduced summer Arctic sea ice Anomalies. Arctic Sea-ice decline: Observations, Projections, Mechanisms, and Implications, *Geophys. Mono. Series,* 180: 91-110.

Blüthgen J., Gerdes R. and Werner M. (2012), Atmospheric response to the extreme Arctic sea ice conditions in 2007, *Geophys. Res. Lett.*, 39 L02707.

Collins, W. D., P. J. Rasch, B. A. Boville, J. J. Hack, J. R. McCaa, D. L. Williamson, B. P. Briegleb, C. M. Bitz, S.J. Lin and M. Zhang (2006), The formulation and atmospheric simulation of the Community Atmosphere Model Version 3 (CAM3), *J. Clim.*, 19**,** 2144-2161.

Comiso, J. C. (2003), Warming Trends in the Arctic from clear Sky Satellite Observations, *J. Clim., 16*, 3498-3510.

Francis J A and Vavrus S J (2012), Evidence linking Arctic amplification to extreme weather in mid-latitudes, *Geophys. Res. Lett.*, 39 L06801.

Graversen, R. G., T. Mauritsen, S. Drijfhout, M. Tjernstrom, and S. Martensson (2010) Warm winds from the Pacific caused extensive Arctic sea ice melt in summer 2007, *Clim. Dyn.***,** 36, 2103-2112.

Hoskins, B. J., and K. I. Hodges (2002), New Perspective on the Northern Hemisphere Winter Storm Tracks, *J. Atmos. Sci.*, 59**,** 1041-1061.

Honda M, Inoue J and Yamane S (2009), Influence of low Arctic sea ice minima on anomalously cold Eurasian winters, *Geophys. Res. Lett*., 36 L08707.

Hurrell, J. W., J. J. Hack, A. S. Phillips, J. Caron, and J. Yin (2006), The Dynamical Simulation of the Community Atmosphere Model Version 3 (CAM3), *J. Clim.*, 19**,** 2162-2183.

Hurrell, J. W., J. J. Hack, D. Shea, J. M. Caron, and J. Rosinski (2008), A New Sea Surface Temperature and Sea ice Boundary Dataset for the Community Atmosphere Model, *J. Clim.*, 21.

Lorenz, E. N. (1954), Available Potential Energy and the Maintenance of the General Circulation, *Tellus*, **7,** 157-167.

McCabe, G. J., M. P. Clark, and M. C. Serreze (2001) Trends in Northern Hemisphere Surface Cyclone Frequency and Intensity, *J.Clim.*, 14**,** 2763-2768.

Murakami, S. (2011) Atmospheric Local Energetics and Energy Interactions between Mean and Eddy Fields. Part I: Theory, *J. Atmos. Sci.*, 68, 760-768.

Murakami, S., R. Ohgaito, and A. Abe-Ouchi (2011) Atmospheric Local Energetics and Energy Interactions between Mean and Eddy Fields. Part II :An example for the Last Glacial Maximum Climate, *J. Atmos. Sci.*, 68, 533-552.

Overland, J. E. and M. Wang (2010), Large-scale atmospheric circulation changes are associated with the recent loss of Arctic sea ice, *Tellus*, 62A (2010) (1).

Petoukhov V and Semenov V A (2010), A link between reduced Barents–Kara sea ice and cold winter extremes over northern continents, *J. Geophys. Res*., 115, D21111.

Polyakov, Igor V., John E. Walsh, Ronald Kwok (2012) Recent Changes of Arctic Multiyear Sea ice Coverage and the Likely Causes, *Bull. Amer. Meteor. Soc.*, 93, 145–151.

Wu Q and Zhang X (2010), Observed forcing-feedback processes between Northern Hemisphere atmospheric circulation and Arctic sea ice coverage, *J. Geophys. Res.*, 115, D14119.

Yin, J. H. (2005), A consistent poleward shift of the storm tracks in simulations of 21st century climate, *Geophy. Res. Lett.*, 32.

Zhang, X., C. Lu and Z. Guan (2012), Weakened cyclones, intensified anticyclones and recent extreme cold winter weather events in Eurasia, *Env. Res. Lett.*.,7.

Zhang, X., J. E. Walsh, J. Zhang, U. S. Bhatt, and M. Ikeda (2004), Climatology and Interannual Variability of Arctic Cyclone Activity: 1948–2002, *J.Clim.*, 17**,** 2300-2317.

Zhang, X., A. Sorteberg, J. Zhang, R. d. Gerdes, and a. J. C. Comiso (2008), Recent radical shifts of atmospheric circulations and rapid changes in Arctic climate system, *Geophys. Res. Lett.*, 35.

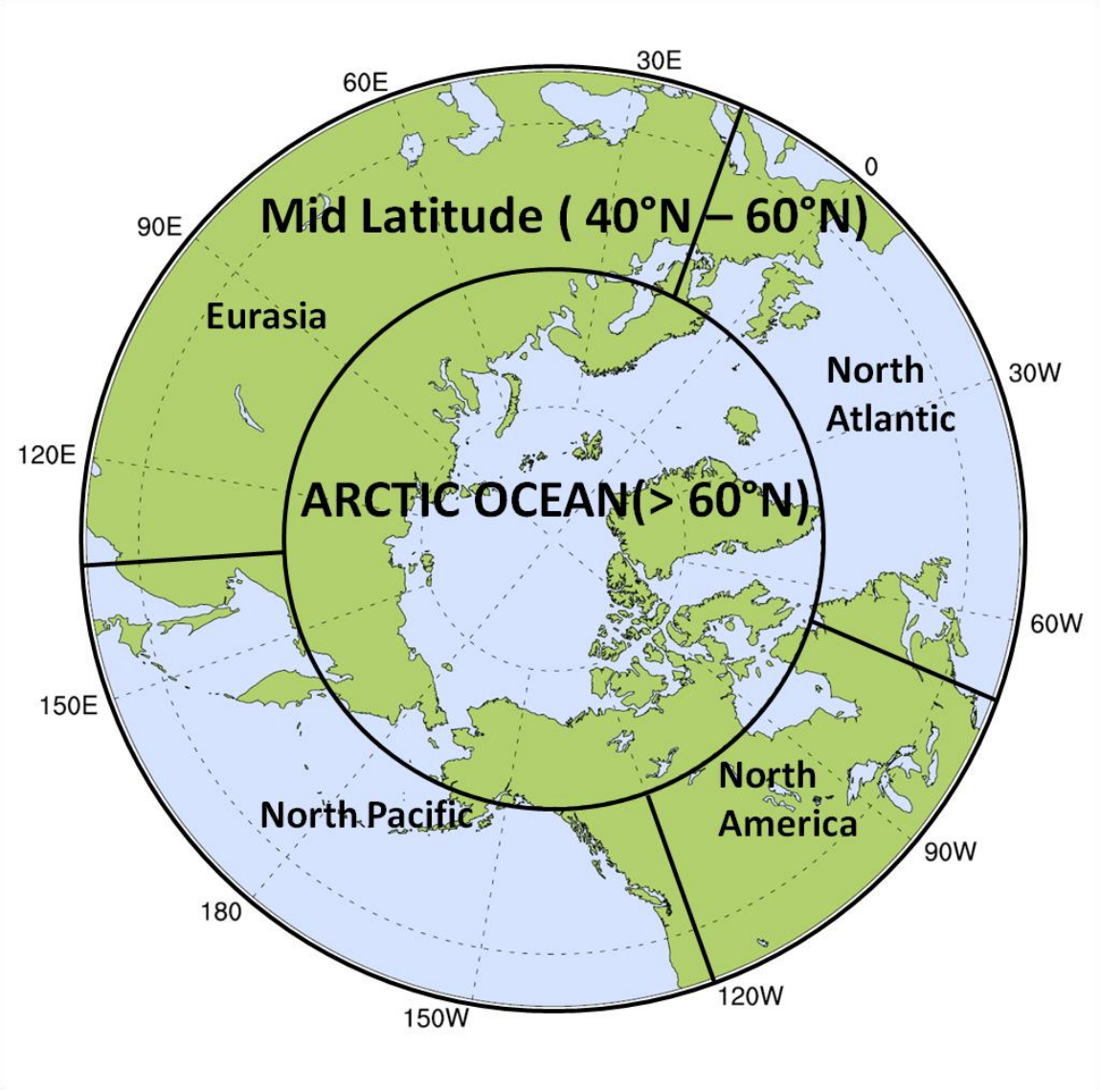

Figure 4.1 Map showing prominent storm track regions over the Northern Hemisphere: Mid-latitudes (40°N to 60°N) and Arctic Ocean (above 60°N). Mid-latitudes further divided into - North Atlantic (70°W-20°E), North Pacific (140°E-120°W), Eurasia (20°E-140°E), North America (120°W-70°W).

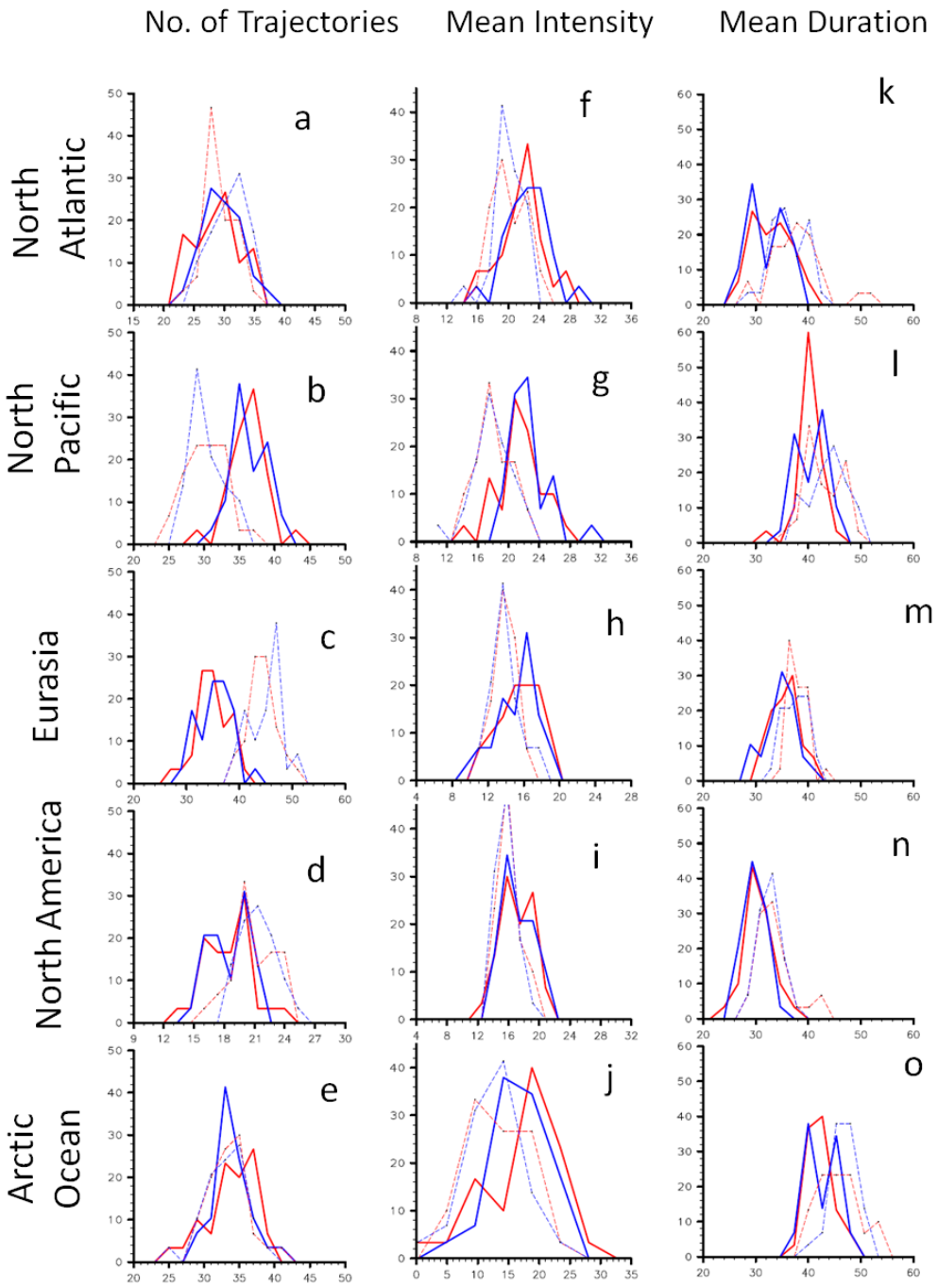

Figure 4.2 Probability Distribution Function (PDF) of number of trajectories (a-e), mean intensity (f-j) and mean duration for each of the sub regions in Trex (red) and Conex (blue) for winter (solid) and spring (dotted).

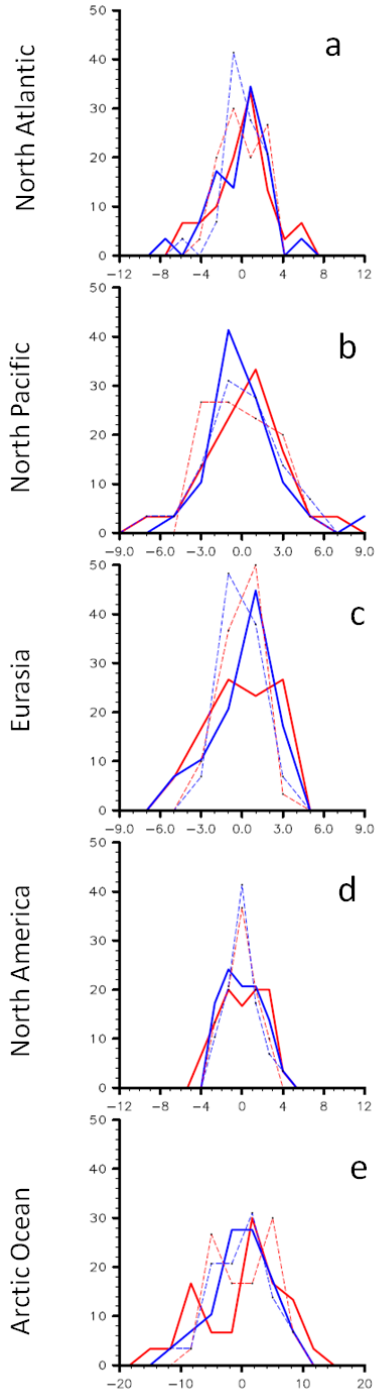

Figure 4.3 PDFs of Cyclone Activity Index (CAI) anomaly in Trex (red) and Conex (blue) in winter (solid) and spring (dotted).

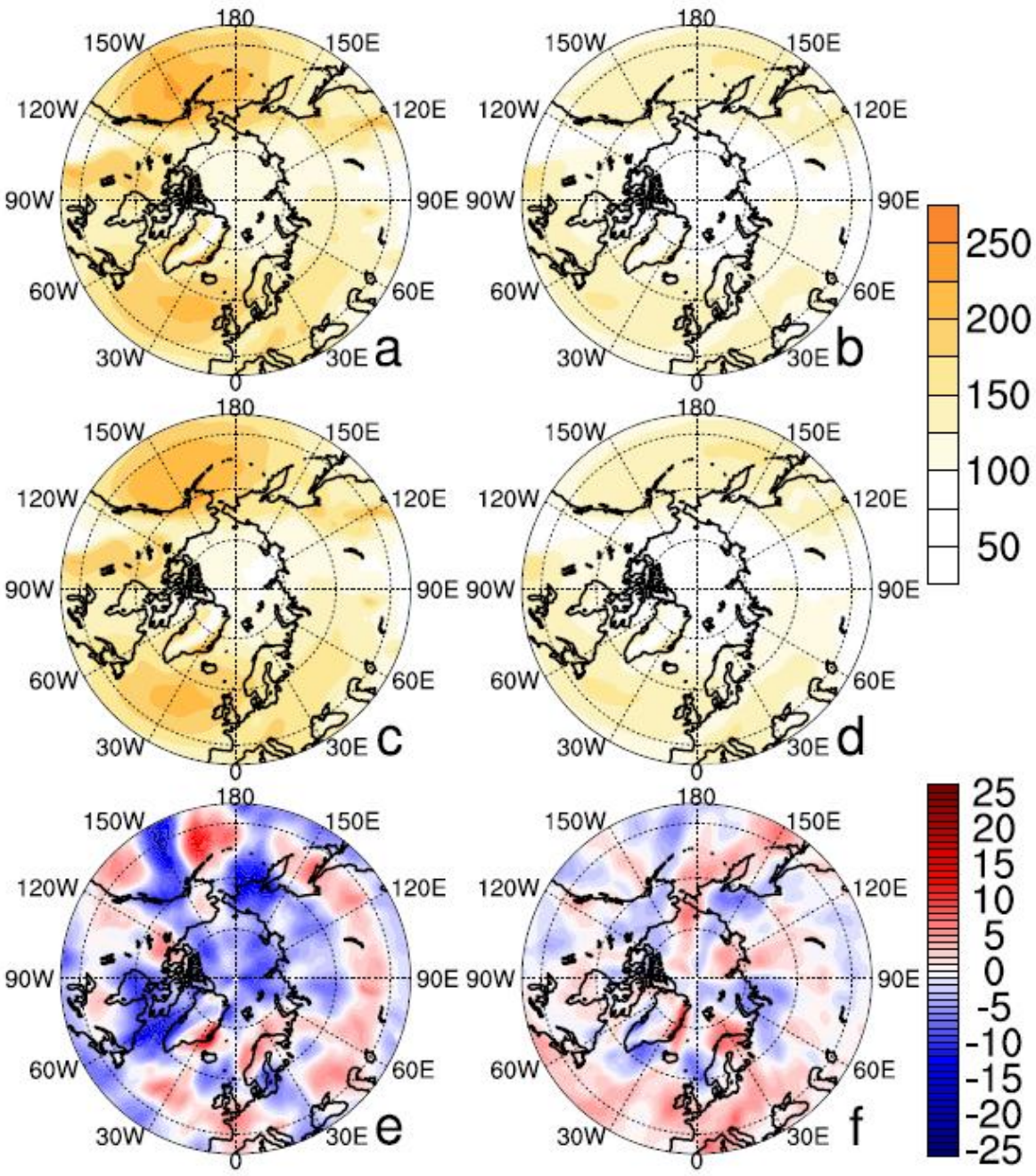

Figure 4.4 Plot shows, vertically integrated Transient Eddy Kinetic Energy (KJ/m^2) in a) winter in Conex, b) spring in Conex, c) winter in Trex, d) winter in Trex, e) Difference (Trex - Conex) in winter and f) Difference (Trex - Conex) in spring.

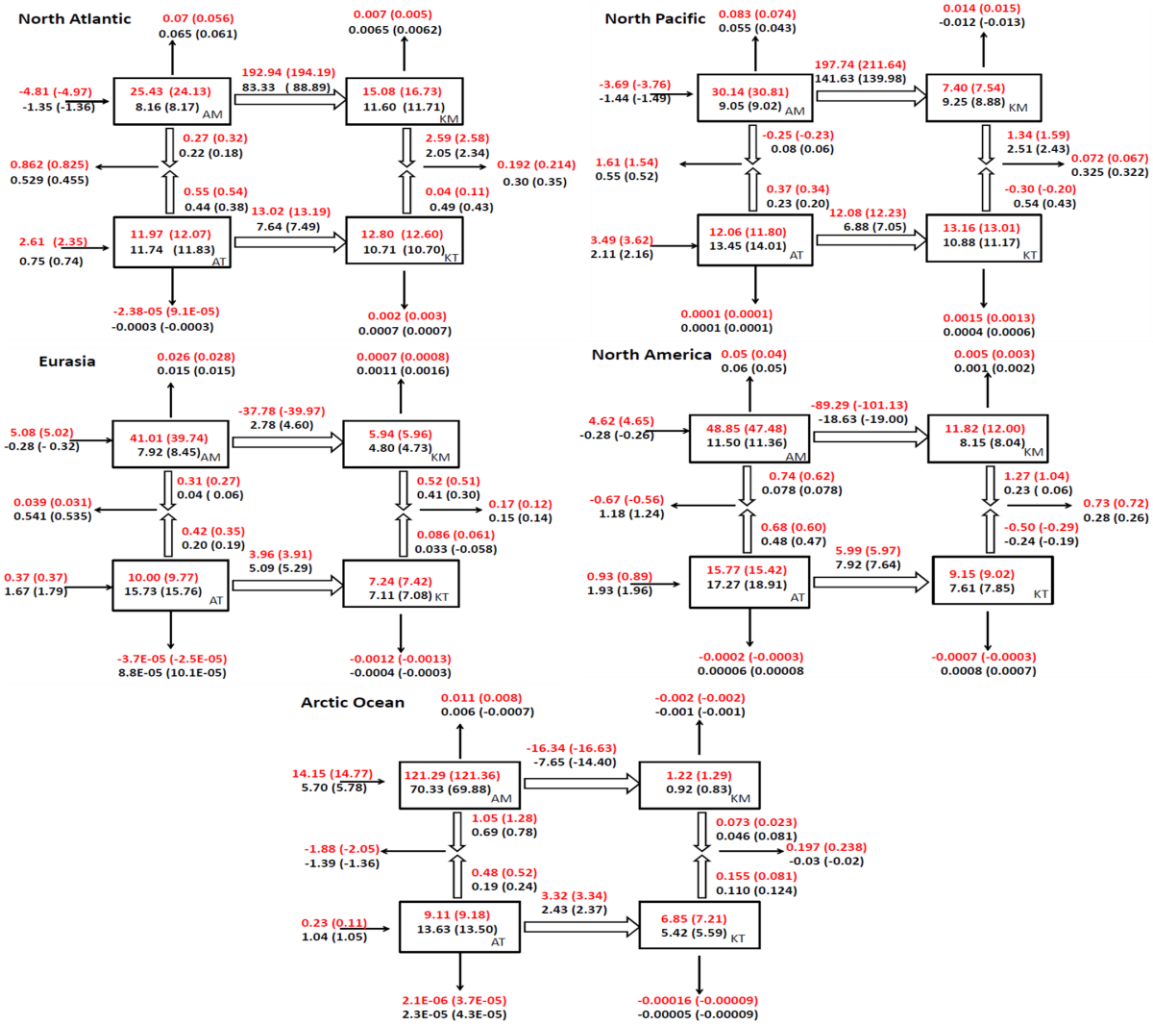

Figure 4.5 Panels showing regional energy balance diagram for each of the sub regions for winter (Red) and spring (Black) in Trex (Conex). Units of the 30 year mean of the terms within the boxes are 10^5 J/m^2 and those on the outside are W/m^2.

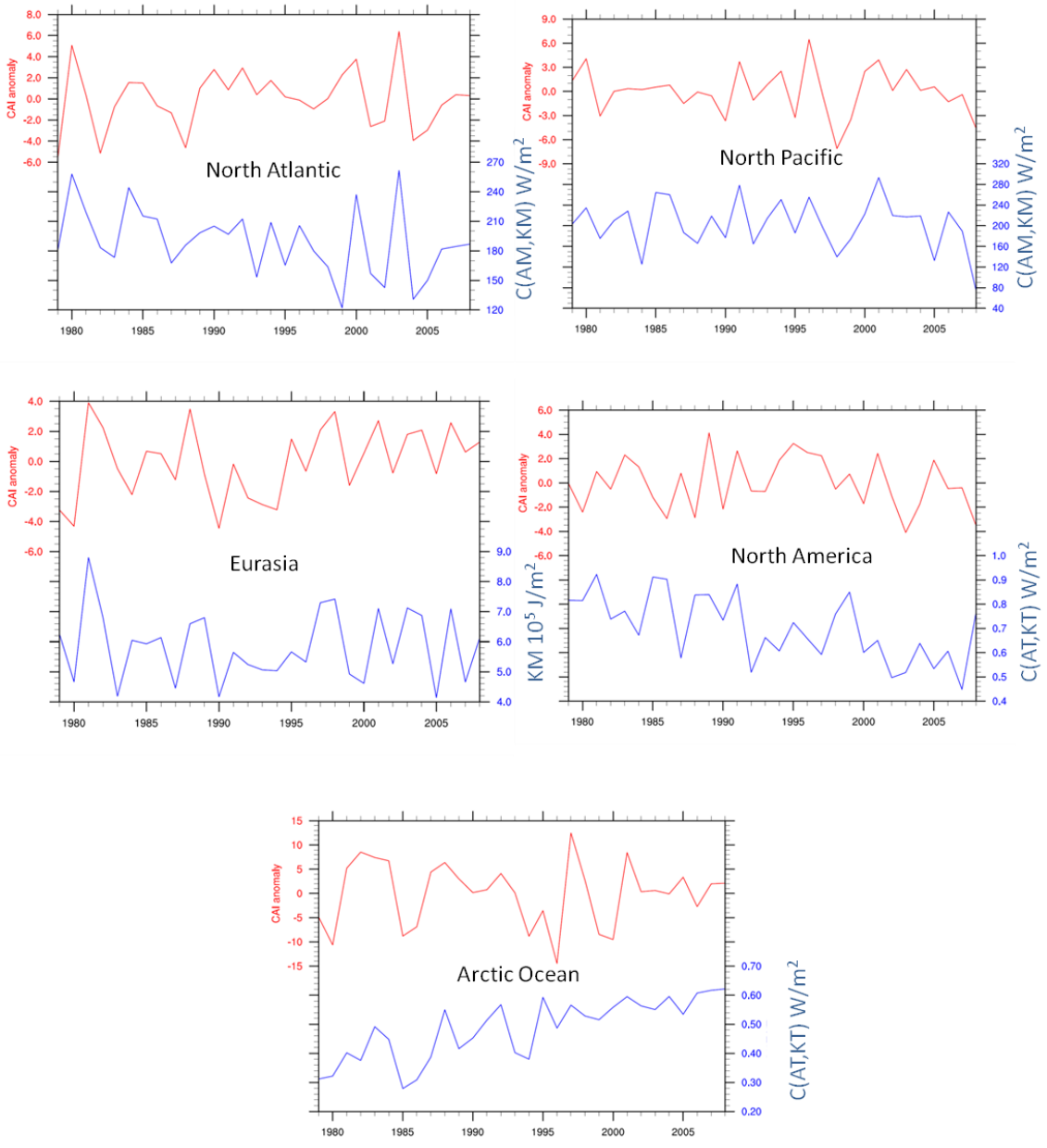

Figure 4.6 Plot shows, time series of CAI anomaly (red) and the area mean of highest co-related energy balance term (blue) for each the sub region in DJF.

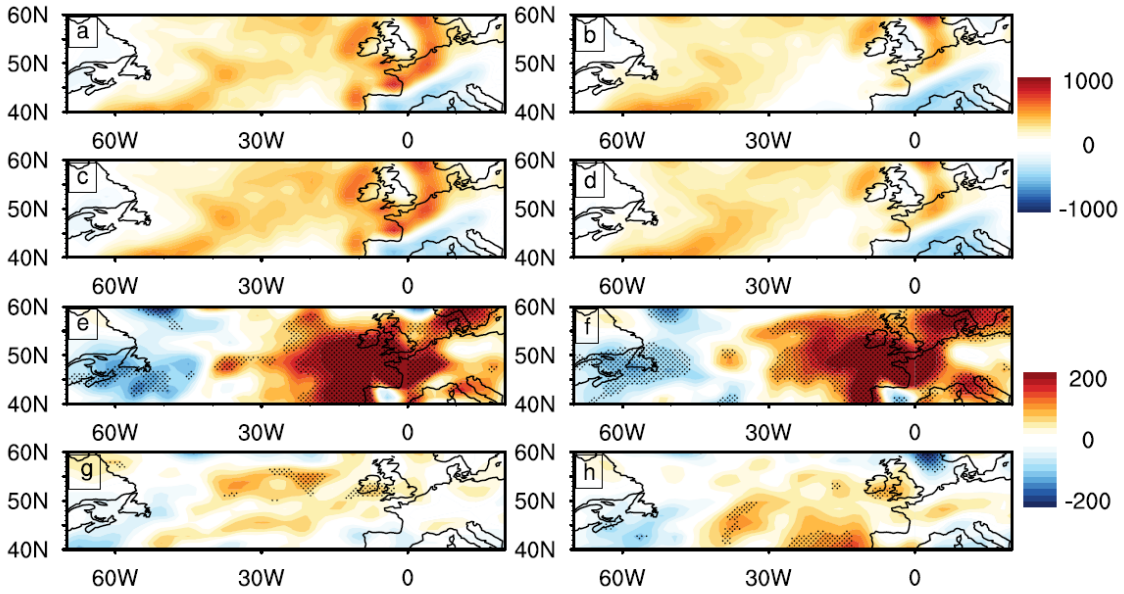

Figure 4.7 Plot showing the rate of conversion between Mean APE and Mean KE (W/m^2) over North Atlantic in winter : a) composite mean of positive years in Conex, b) composite mean of negative years in Conex, c) composite mean of positive years of Trex, d) composite years of negative years of Trex, e) Difference (Positive years of Conex – Negative years of Conex), f) Difference (Positive years of Trex – Negative years of Trex), g) Difference (Positive years of Trex – Positive years of Conex) and h) Difference (Negative years of Trex – Negative years of Conex). Dots represent greater or equal to 95% statistically significant areas.

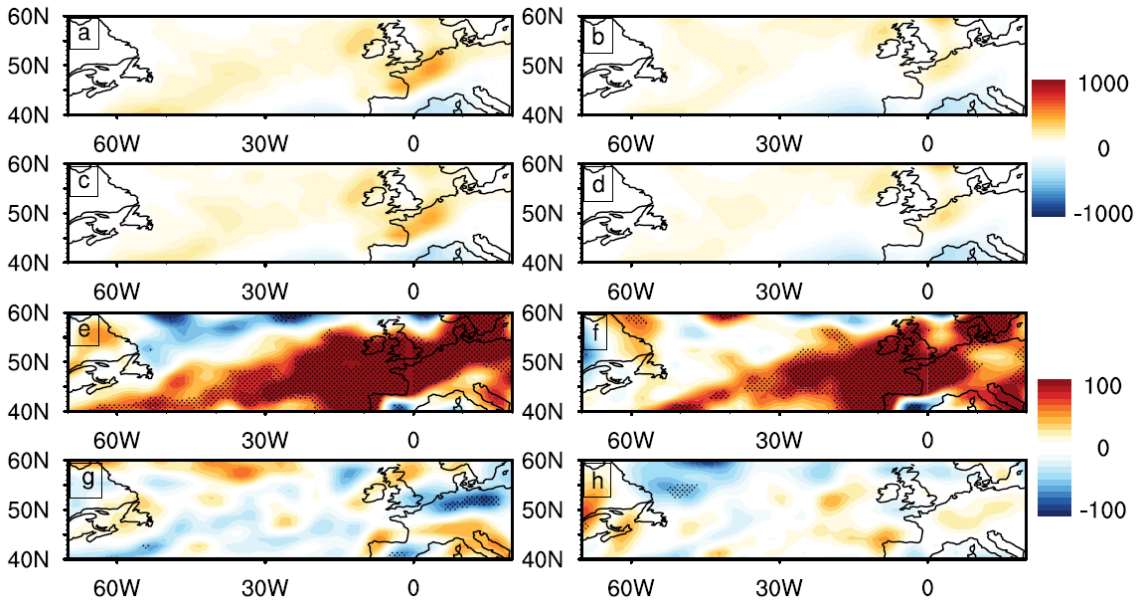

Figure 4.8 Plot showing the rate of conversion between Mean APE and Mean KE (W/m^2) over North Atlantic in spring : a) composite mean of positive years in Conex, b) composite mean of negative years in Conex, c) composite mean of positive years of Trex, d) composite years of negative years of Trex, e) Difference (Positive years of Conex – Negative years of Conex), f) Difference (Positive years of Trex – Negative years of Trex), g) Difference (Positive years of Trex – Positive years of Conex) and h) Difference (Negative years of Trex – Negative years of Conex). Dots represent greater or equal to 95% statistically significant areas.

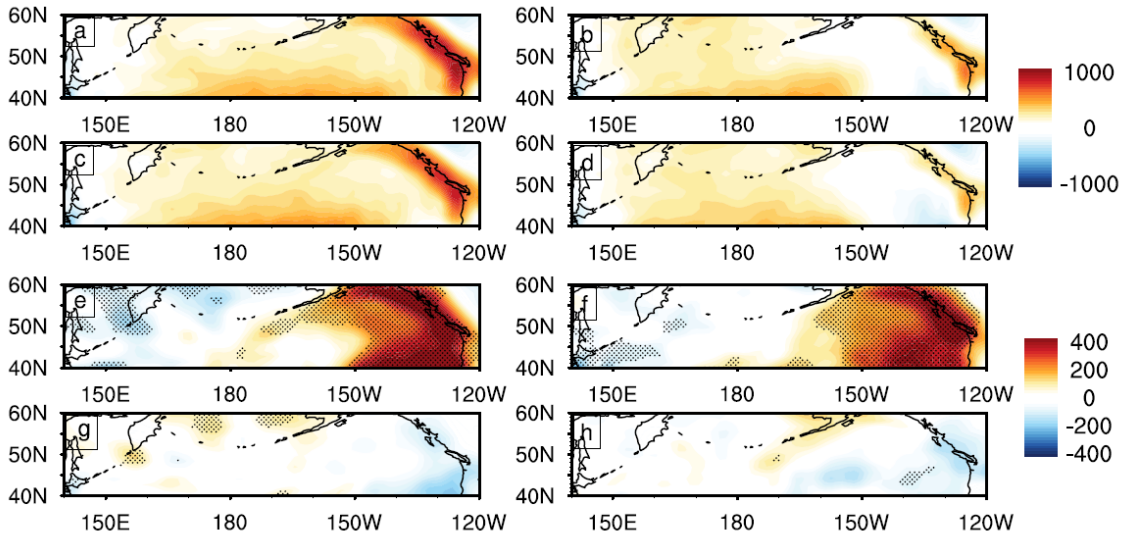

Figure 4.9 Plot showing, the rate of conversion between Mean APE and Mean KE (W/m^2) over North Pacific in winter : a) composite mean of positive years in Conex, b) composite mean of negative years in Conex, c) composite mean of positive years of Trex, d) composite years of negative years of Trex, e) Difference (Positive years of Conex – Negative years of Conex), f) Difference (Positive years of Trex – Negative years of Trex), g) Difference (Positive years of Trex – Positive years of Conex) and h) Difference (Negative years of Trex – Negative years of Conex). Dots represent greater or equal to 95% statistically significant areas.

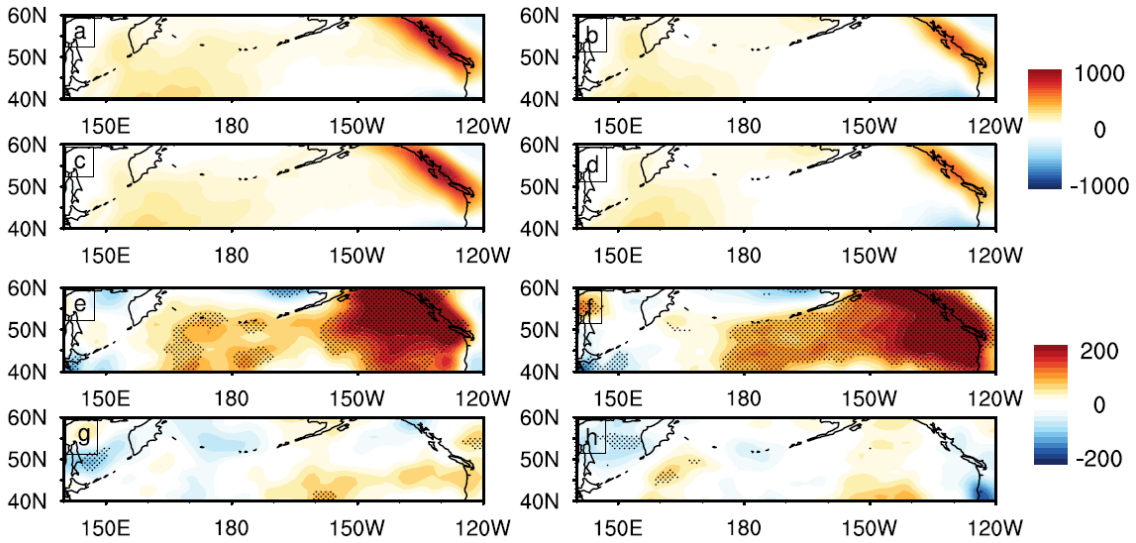

Figure 4.10 Plot showing, the rate of conversion between Mean APE and Mean KE (W/m^2) over North Pacific in spring : a) composite mean of positive years in Conex, b) composite mean of negative years in Conex, c) composite mean of positive years of Trex, d) composite years of negative years of Trex, e) Difference (Positive years of Conex – Negative years of Conex), f) Difference (Positive years of Trex – Negative years of Trex), g) Difference (Positive years of Trex – Positive years of Conex) and h) Difference (Negative years of Trex – Negative years of Conex). Dots represent greater or equal to 95% statistically significant areas.

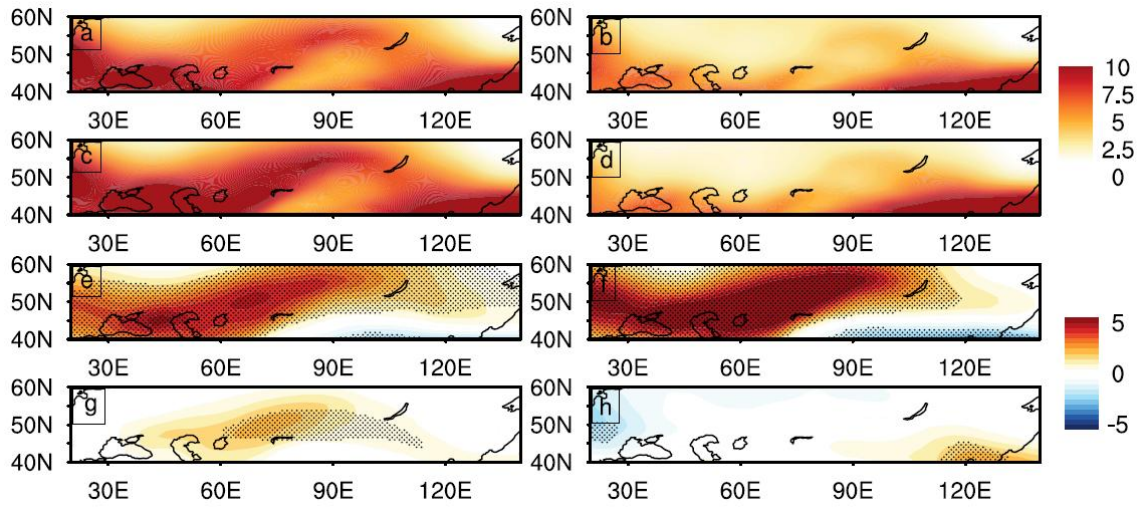

Figure 4.11 Plot showing, mean KE (10^5 J/m^2) over Eurasia in winter : a) composite mean of positive years in Conex, b) composite mean of negative years in Conex, c) composite mean of positive years of Trex, d) composite years of negative years of Trex, e) Difference (Positive years of Conex – Negative years of Conex), f) Difference (Positive years of Trex – Negative years of Trex), g) Difference (Positive years of Trex – Positive years of Conex) and h) Difference (Negative years of Trex – Negative years of Conex). Dots represent greater or equal to 95% statistically significant areas.

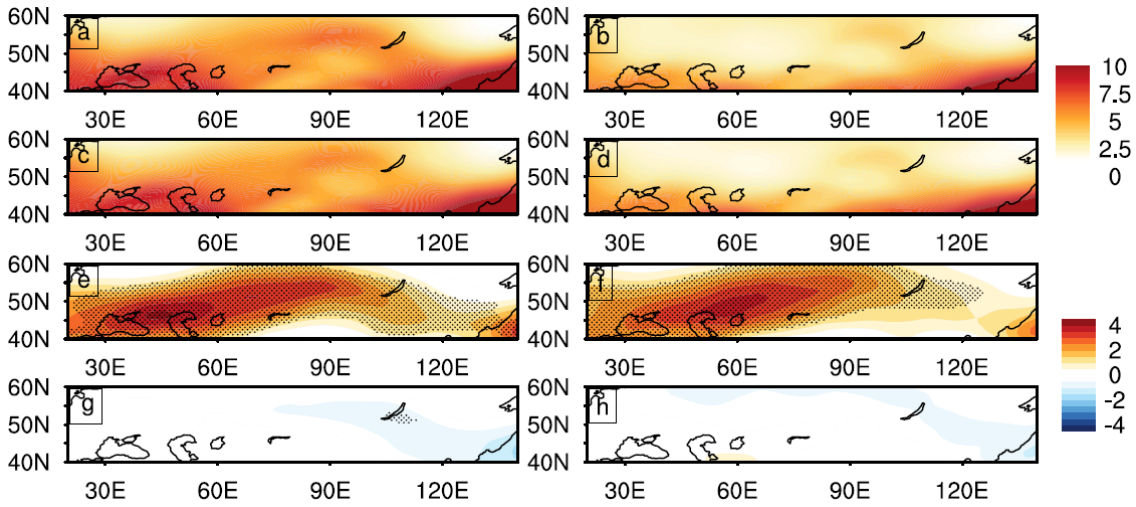

Figure 4.12 Plot showing, mean KE (10^5 J/m^2) over Eurasia in spring: a) composite mean of positive years in Conex, b) composite mean of negative years in Conex, c) composite mean of positive years of Trex, d) composite years of negative years of Trex, e) Difference (Positive years of Conex – Negative years of Conex), f) Difference (Positive years of Trex – Negative years of Trex), g) Difference (Positive years of Trex – Positive years of Conex) and h) Difference (Negative years of Trex – Negative years of Conex). Dots represent greater or equal to 95% statistically significant areas.

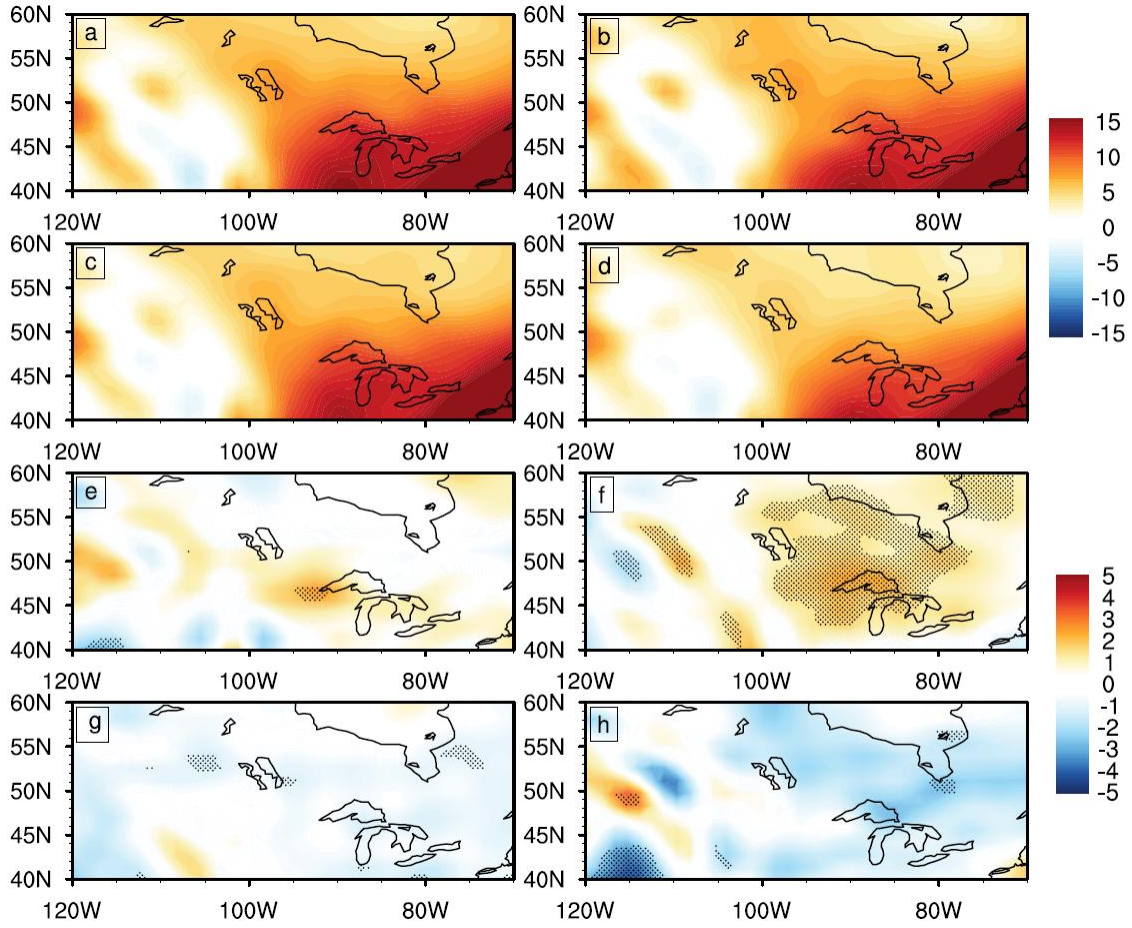

Figure 4.13 Plot showing the rate of conversion between transient eddy APE and transient eddy KE (W/m^2) over North America in winter : a) composite mean of positive years in Conex, b) composite mean of negative years in Conex, c) composite mean of positive years of Trex, d) composite years of negative years of Trex, e) Difference (Positive years of Conex – Negative years of Conex), f) Difference (Positive years of Trex – Negative years of Trex), g) Difference (Positive years of Trex – Positive years of Conex) and h) Difference (Negative years of Trex – Negative years of Conex). Dots represent greater or equal to 95% statistically significant areas.

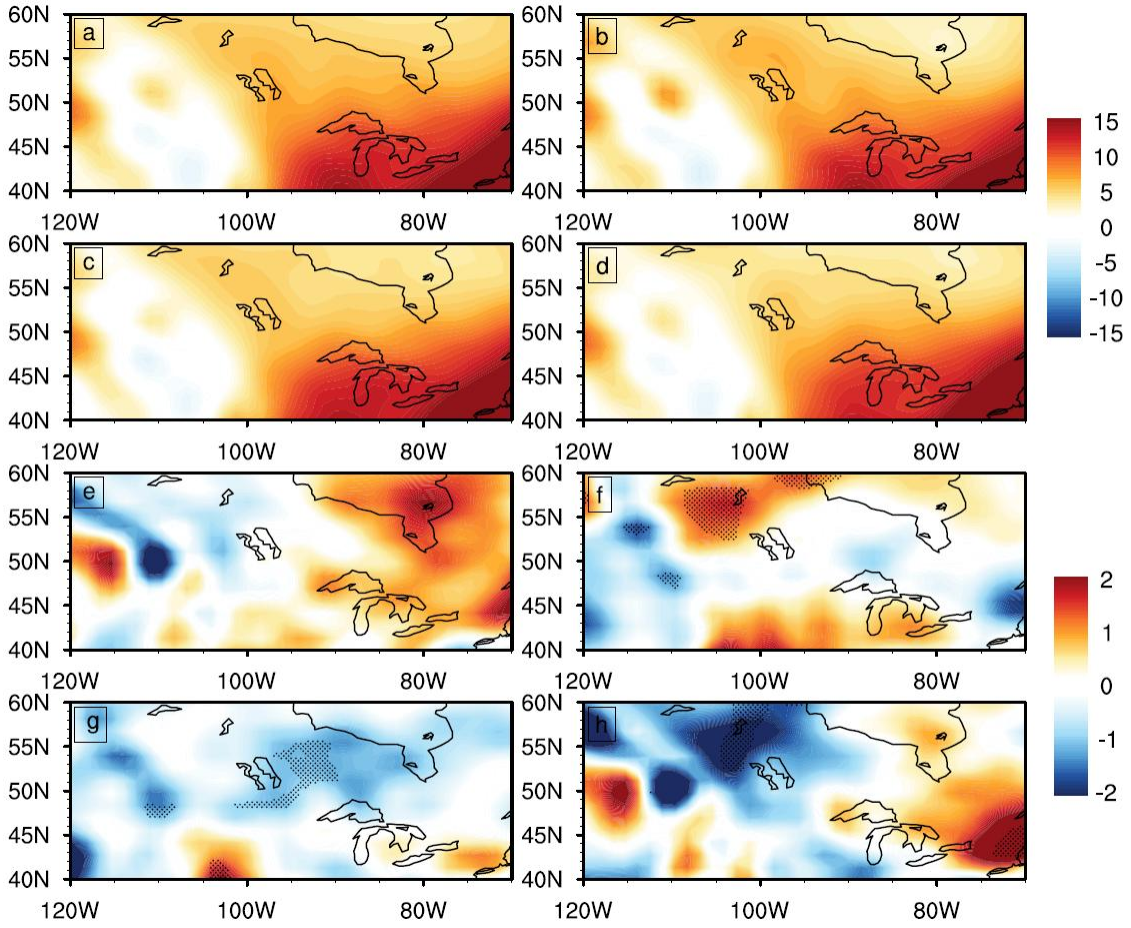

Figure 4.14 Plot shows, the rate of conversion between transient eddy APE and transient eddy KE (W/m^2) over North America in spring : a) composite mean of positive years in Conex, b) composite mean of negative years in Conex, c) composite mean of positive years of Trex, d) composite years of negative years of Trex, e) Difference (Positive years of Conex – Negative years of Conex), f) Difference (Positive years of Trex – Negative years of Trex), g) Difference (Positive years of Trex – Positive years of Conex) and h) Difference (Negative years of Trex – Negative years of Conex). Dots represent greater or equal to 95% statistically significant areas.

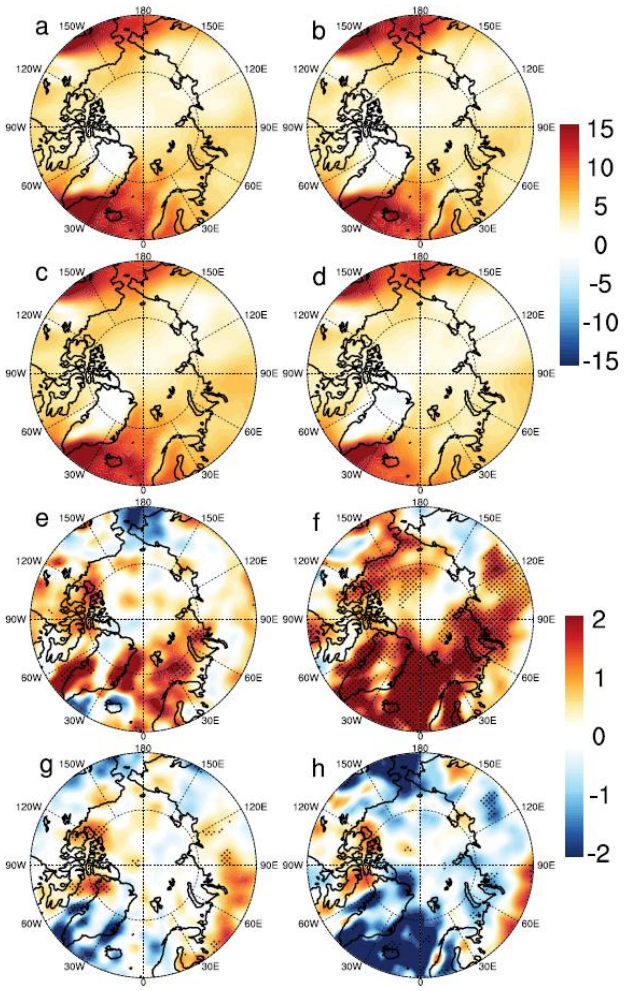

Figure 4.15 Plot showing the rate of conversion between transient eddy APE and transient eddy KE (W/m^2) over Arctic Ocean in winter : a) composite mean of positive years in Conex, b) composite mean of negative years in Conex, c) composite mean of positive years of Trex, d) composite years of negative years of Trex, e) Difference (Positive years of Conex – Negative years of Conex), f) Difference (Positive years of Trex – Negative years of Trex), g) Difference (Positive years of Trex – Positive years of Conex) and h) Difference (Negative years of Trex – Negative years of Conex). Dots represent greater or equal to 95% statistically significant areas.

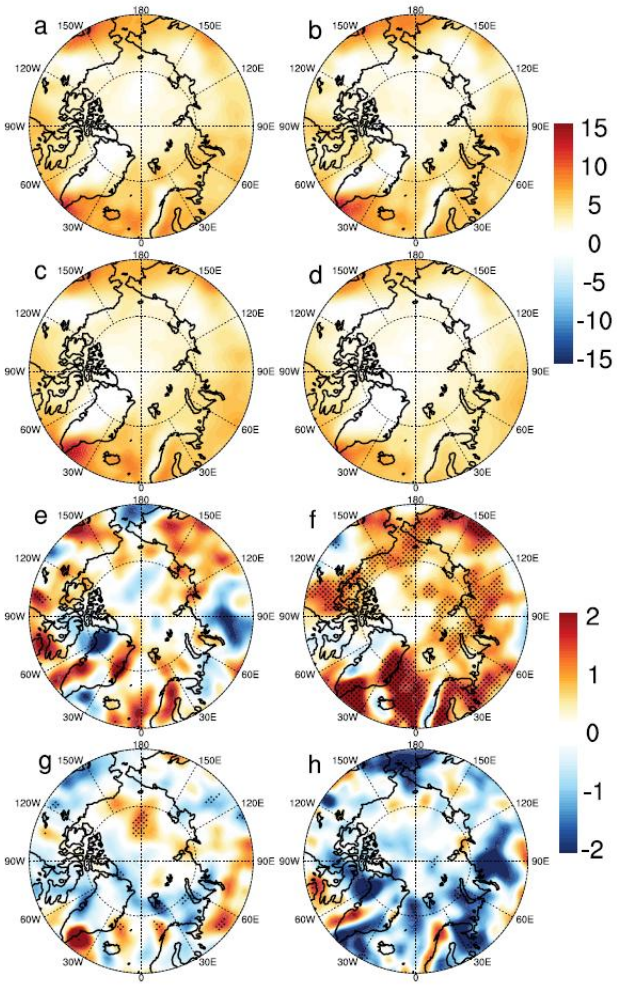

Figure 4.16 Plot shows, the rate of conversion between transient eddy APE and transient eddy KE (W/m^2) over Arctic Ocean in spring : a) composite mean of positive years in Conex, b) composite mean of negative years in Conex, c) composite mean of positive years of Trex, d) composite years of negative years of Trex, e) Difference (Positive years of Conex – Negative years of Conex), f) Difference (Positive years of Trex – Negative years of Trex), g) Difference (Positive years of Trex – Positive years of Conex) and h) Difference (Negative years of Trex – Negative years of Conex). Dots represent greater or equal to 95% statistically significant areas.

Chapter 5 Summary and Conclusions

5.1 Background and Motivation

Extratropical cyclones are associated with extreme weather events such as blizzards, gusts, flood, freezing rain etc and occur over mid- and high-latitudes. These weather events are well known for their ability to disrupt normal life by causing property and infrastructure damage and causing hazardous travel conditions. Extratropical storms are most prominent over certain geographical regions located over mid-latitudes and the Arctic and these regions are known as storm tracks. Each of these regions exhibits different temporal variability. For example, over Eurasia storms have gotten weaker with time [*Zhang et al*., 2012]. There are many gaps in our existing knowledge of changes in storm activities over the Northern Hemisphere. According to our hypothesis for this study, in addition to a warming climate these changes can be caused by anomalous surface boundary forcing such as SST or Arctic sea ice.

One of the potential anomalous surface forcing is elevated tropical Pacific SST associated with El Niño. From previous studies it was found that direct and indirect effects of the elevated tropical Pacific SST includes a southward shift of the jet stream and a southward shift and eastward extension of the storm track over the east Pacific [*Trenberth et al.*, 1993; *Hoerling*, 1994; *Straus et al*., 1997; *Zhang et al*., 1999; *Orlanski*, 2005; *Eichler et al.,* 2006; *Compo*, 2010]. But the impact of elevated tropical Pacific SST on North American storm activities has not been fully investigated. Thus, in this thesis we studied the response of winter-spring storm activities over North America to elevated tropical Pacific SSTs.

Another potential surface forcing is Arctic sea ice. Changes in Arctic sea ice impacts the atmospheric circulation and weather patterns [*Zhang et al*., 2008; *Overland and Wang*., 2010] and causes anomalous surface fluxes. But the role of Arctic sea ice in changing storm activity over the Northern Hemisphere is not fully yet understood. So in this thesis we showed the impacts of reduced Arctic sea ice on storm activities over the mid-latitudes and the Arctic and corresponding changes in surface climate parameters. Due to global warming, the Arctic Ocean is undergoing a rapid loss of sea ice. There have been no studies to distinctly identify the responses of Northern Hemisphere storm activity to the declining trend of Arctic sea ice. Thus, in this thesis we conducted a comprehensive analysis of the response of Northern Hemispheric extratropical storm activity to the long term trend of Arctic sea ice.

5.2 Key Scientific Findings and Conclusions

In this thesis we conducted an integrated evaluation of the contribution of SST and Arctic sea ice on changes in Northern Hemisphere storm activities. In order to do that we performed modeling experiments using the NCAR CAM 3.1_p2 model and analyzed 6-hourly outputs of selected variables. In our analysis we applied a storm identification and tracking algorithm [*Zhang et al*., 2004], which first identified and then tracked each storm following a Lagrangian approach and then we linked those changes in storm activity to the general circulation of the atmosphere. The key findings from our study are as follows:

1) Elevated tropical Pacific SST causes an increase in storm activity over the southern part of North America (Figure 5.1).

2) Reduced Arctic sea ice causes increased storminess over the Arctic in all seasons (except winter) whereas the storm activity decreases over the mid-latitudes in all seasons (Figure 5.2).

3) The long-term declining trend of Arctic sea ice causes an overall decrease in Northern Hemispheric storm activity but there is an increase in the extreme storm events (Figure 5.3).

In response to anomalous surface boundary forcing such as elevated tropical Pacific SST like El Niño the winter-spring storms over North American exhibit a southward shift. Elevated tropical Pacific SSTs cause a southward shift and intensification of the subtropical jet stream which favors an increased vertical wind sheer to the south of the climatological jet stream. Increased vertical wind sheer enhances baroclinicity, upper level divergence and hence supports the development of surface storms. Increased storm activity also causes an increase in the EKE over the regions located south of the climatological storm track.

Apart from SST, evaluation of another large natural forcing – changes in Arctic sea ice on Northern Hemispheric storm activities was done. The rapid loss of Arctic sea ice due to a warming climate has many consequences on climate and weather patterns. Due to the widespread impact of Arctic sea ice on global climate we studied the entire Northern Hemisphere storm activity in this experiment. In response to reduced Arctic sea ice there is increased storminess over the Arctic in contrast to a decreased storm activity over the mid-latitudes in most seasons. During a reduced Arctic sea ice condition in winter, the

storm activity decreased over the central Arctic and Eurasia. The decreased storminess associated with increased SLP (i.e. intensification of anticyclones in the central Arctic and Eurasia) causes decreases of precipitation and SAT in winter. In spring, a dramatic warming occurs over the Arctic and mid-latitudes. Anomalous sensible and latent heat fluxes in the MIZ, partially contribute to this warming. Also, decreased storminess, associated with intensified anticyclones, reduced cloud cover over the mid-latitudes results in enhanced heating from the downward shortwave radiation over the mid-latitude continents. This land-ocean temperature contrast paves the way for increased storm activity in the Arctic. The advection of heat associated with increased storminess over the Arctic also contributes to the warming. In summer, reduced Arctic sea ice causes increased storminess, increased cloud cover and decreased downward SW, increased precipitation which causes a moderate cooling over the Arctic. In fall, reduced Arctic sea ice causes increased storminess over the Arctic. The anomalous surface heat fluxes contribute to higher SAT in the MIZ. The decreased storminess causes intensification of anticyclones in association with clear sky and enhanced cooling due to outgoing LW over Eurasia.

Arctic sea ice can change due to natural variability and the long term trend. We performed a comprehensive study of the impact of the long-term declining trend of Arctic sea ice on Northern Hemispheric storm activities. In response to the declining trend of Arctic sea ice there was an overall decrease in storm activity over the Northern Hemisphere, but with increased extreme storm events. The loss of Arctic sea ice due to the declining trend causes an enlarged area of open water. The newly opened water

resulted in anomalous heating of the surface and lower troposphere which resulted in an increased convective activity and baroclinically driven synoptic circulation, leading to faster conversion between transient available potential energy (AT) and transient kinetic energy (KT) over the Arctic. The increased conversion of AT to KT resulted in an increased number of extreme storms over the Arctic in the model simulation forced by the long term trend of Arctic sea ice. There was an increased conversion rate of mean available potential (AM) and mean kinetic energy (KM) over the North Atlantic and North Pacific, which resulted in increased extreme storm events, as indicated by our statistical analysis. The declining Arctic sea ice affects the mid-latitude atmospheric circulation, which resulted in an increased vertical velocity contributing to the increased conversion between AM and KM. The reduced sea ice affects the downstream propagation of Rossby wave trains towards Eurasia and East Asia, impacts regional westerlies, vertical circulation and conversion between AM and KM. This change in conversion rate corresponds well to our finding of increased extreme storms over Eurasia with declining Arctic sea ice.

The occurrence of cyclones has significant implications for human society, properties and natural ecosystems. They also cause hazardous travel conditions contributing to huge economic impacts. Thus, in this integrated contribution of the two biggest natural forcings such as SST and Arctic sea ice it was shown that interannual variabilities like El Niño can modulate a southward shift of the storms over North America however, long term variabilities like Arctic sea ice causes increased storminess over the Arctic region with a weakened storm activity over the mid-latitude. But the long term trend of Arctic

sea ice causes decreased storm activity over middle and high latitudes with an increased occurrence of extreme storm events. Thus our modeling study provides an assessment and prediction of cyclones in the context of global warming forcing and will further facilitate the decision making processes. Careful analysis of our results will also help us to further advance our knowledge of the changes in storm activity over the Northern Hemisphere in a warming climate.

5.3 Future Work

There is a great need to study the variability of each of the major storm tracks over the Northern Hemisphere with individual details and to understand changes in dynamical processes of the atmosphere that control storm activity as each of these storm tracks has different variability over time. Storms are associated with the transport of heat and moisture across the latitudes. We have shown that increased (decreased) storm activity causes increased (decreased) precipitation and snowfall and induces changes in surface air temperature so it is important to study the changes in transport processes especially for the Arctic, which is the center of attraction for climate studies under a warming climate.

Recent studies have predicted a sea-ice free Arctic summer in the near future in conjunction with global warming. It has been observed that the growth and decay of Arctic sea ice affects the global circulation and weather patterns. So the loss of Arctic sea ice will further influence the storm activity over the Northern Hemisphere, as a result our group is currently investigating the future projections of storm activity over each of the

storm tracks under different warming scenarios such as RCP 4.5 and RCP 8.5 from the CMIP5 model simulations. A thorough investigation of future storm activities over the Arctic and mid-latitude will help us to better understand the changes and variability of extratropical cyclones at the end of the 21st century. In near future, the Arctic will be the center of attraction for oil, uranium and other mineral industries so it is important to better predict and forecast the changes in storm activity over the Arctic and the adjoining high latitudes. The rapid loss of Arctic sea ice can also lead to a loss of natural habitat for Arctic wildlife and marine life and hence can disturb the polar ecosystem.

Finally, it is necessary to develop better communication between climate science and society. It is absolutely necessary to enhance awareness of the climate science among the stake holders, policy makers, general public and industrialists as the storms affect every person and industry. This process of interactive understanding will bridge the gap between climate scientists and society as climate scientists will also have a detailed knowledge of the need of the industrialists, stakeholders and property owners.

References

Compo, G. P. (2010), Removing ENSO related variation from climate record, *J. Clim.*, *23*, 1957-1978.

Eichler, T., and W. Higgins (2006), Climatology and ENSO-related variability of North American extratropical cyclone activity, *J. Clim.*, *19*, 2076-2093.

Hoerling, M. P. (1994), Organization of extratropical transients during El Niño, *J. Clim.*, *7*, 745–766.

Orlanski, I. (2005), A new look at the Pacific storm track variability: Sensitivity to tropical SSTs and to upstream seeding, *J. Atmos. Sci.*, *62*, 1367-1390.

Overland, J. E. and M. Wang (2010), Large-scale atmospheric circulation changes are associated with the recent loss of Arctic sea ice, *Tellus*, 62A (2010) (1).

Straus, D. M., and J. Shukla (1997), Variations of midlatitude transient dynamics associated with ENSO, *J. Atmos. Sci.*, *54*, 777–790.

Trenberth, K. E., and J. W. Hurrell (1993), Decadal atmosphere - ocean variations in the Pacific, *Clim. Dyn.*, 303-319.

Zhang, X., C. Lu and Z. Guan (2012), Weakened cyclones, intensified anticyclones and recent extreme cold winter weather events in Eurasia, *Env. Res. Lett.*.,7.

Zhang, X., A. Sorteberg, J. Zhang, R. d. Gerdes and a. J. C. Comiso (2008), Recent radical shifts of atmospheric circulations and rapid changes in Arctic climate system, *Geophys.Res. Lett*., 35, L22701

Zhang, Y., and I. M. Held (1999), A linear stochastic model of a GCM's midlatitude storm tracks, *J. Atmos. Sci.*, *56*, 3416–3435.

Zhang, X., J. E. Walsh, J. Zhang, U. S. Bhatt and M. Ikeda (2004), Climatology and Interannual Variability of Arctic Cyclone Activity: 1948–2002, *J. Clim.*, 17: 2300-2317

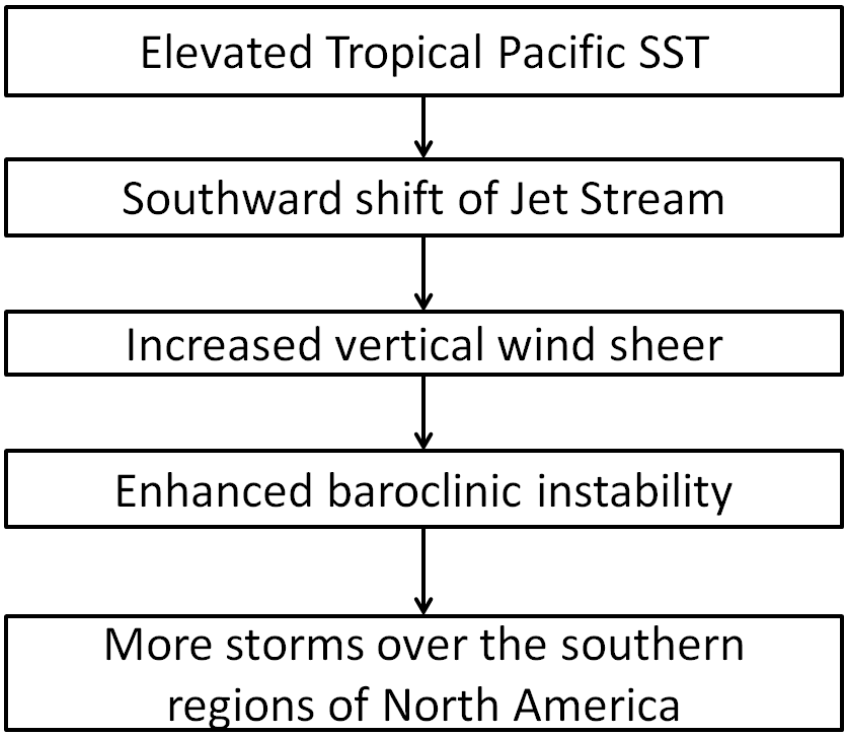

Figure 5.1 Sequence of physical processes associated with changes in storm activity over North America due to elevated tropical Pacific SST.

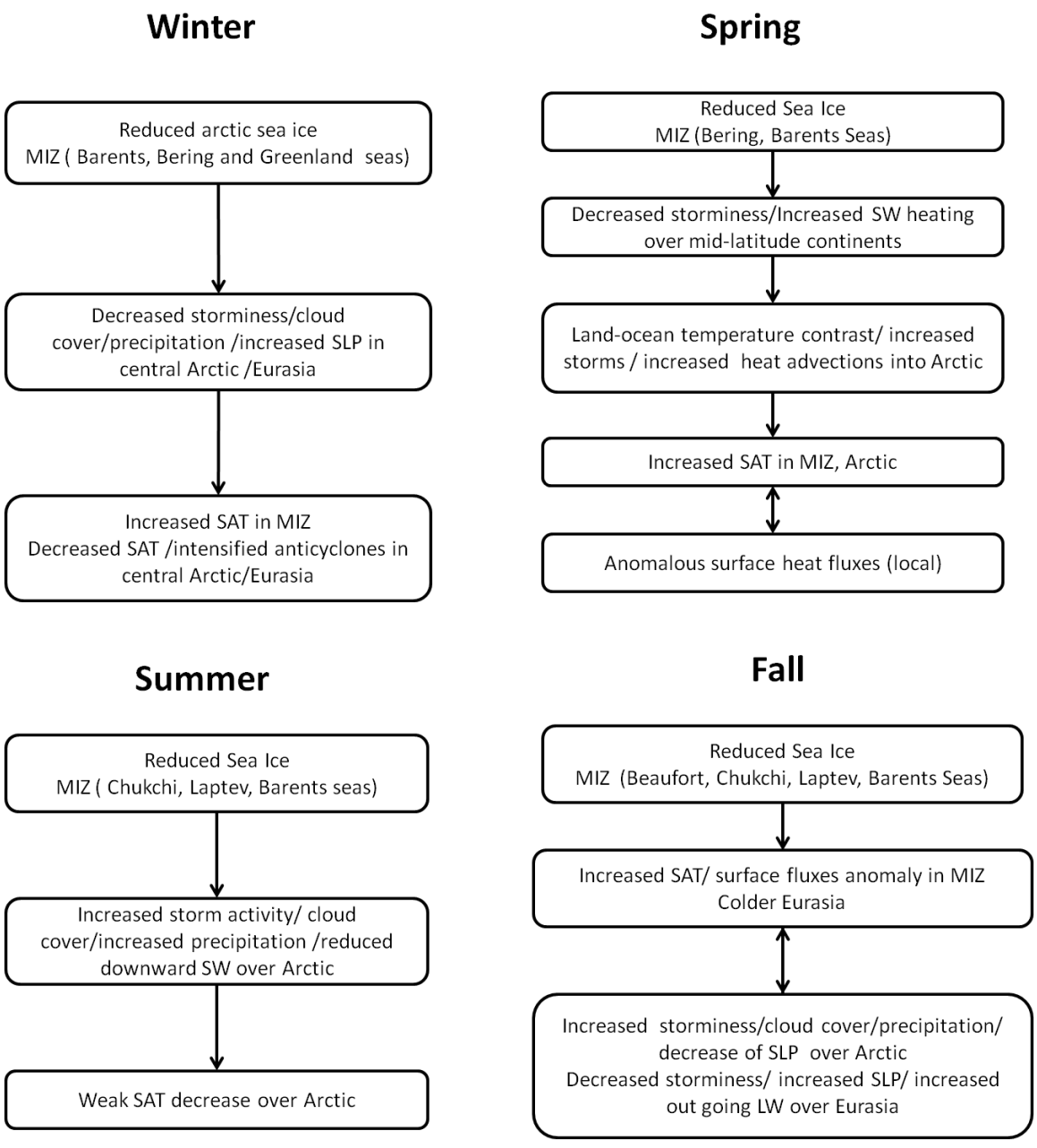

Figure 5.2 Sequence of events linking the reduced Arctic sea ice, storm activity and the most prominent surface climate changes.

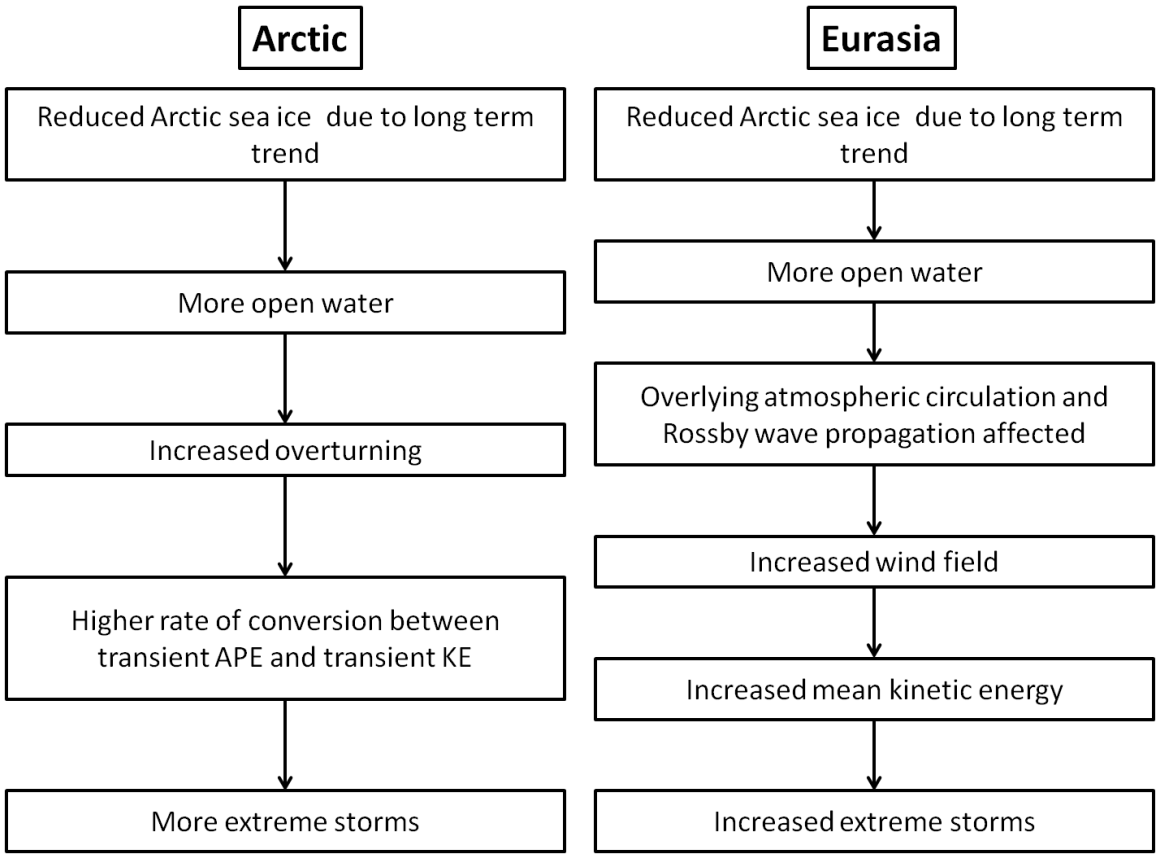

Figure 5.3 Sequence of possible mechanisms for increased extreme storm events over the Arctic and Eurasia in response to sea ice change.

Contribution to Chapters

Mr. Soumik Basu completed all studies presented in Chapter 2-4, including model configuration, experiment design and performance, data analysis, and result interpretation, and drafted and finalized the dissertation under advisement by Dr. Xiangdong Zhang. Dr. Igor Polyakov and Dr. Uma Bhatt provided constructive comments and suggestions to Mr. Soumik Basu for improving the research and dissertation, in particular Chapter 3, through the course of this Ph.D. program. Dr. Nicole Mölders also provided very helpful suggestions for completing this study.